ABSTRACT

PFEILER, TERRY WAYNE. Computational and Experimental Analyses of Bone and Adult Stem Cell Mechanobiology. (Under the direction of Elizabeth G. Loboa).

Human bone marrow and adipose derived adult stem cells have shown great promise as a source of expandable and differentiable cells for tissue engineering and regenerative medicine. However, a more complete understanding of the optimal *in vitro* culture conditions is required to create functional engineered tissue. Especially key in the context of musculoskeletal tissue is the *in vitro* generation of nascent tissue with appropriate material properties for withstanding *in vivo* loading are the combined mechanical and chemical stimuli used to culture adult stem cells.

Previous studies have shown that mechanical loading induces differentiation of human mesenchymal stem cells (hMSCs) and mesenchymal tissue into tissues such as bone, fibrous tissue, cartilage, and smooth muscle cells. More recently, human adipose derived adult stem cells (hASCs) have shown promise for similar tissue engineering applications. Fluid shear stress is believed to be one of the primary stimuli for osteocytes in the maintenance of mature bone, and tensile strain has been shown to induce the formation and repair of bone from mesenchymal tissue. However, the proper range of local stresses and strains required for stem cell-induced bone formation *in vitro* have yet to be determined.

This body of work examined the application of different methods of external loading on human adult stem cells to induce their osteogenic differentiation. Both

experimental and computational analyses were completed in order to provide a detailed understanding of cellular response to loading, and the local stresses and strains placed on cells during loading. Fluid shear stresses were applied to hASCs on and within a porous 3D scaffold to measure upregulation of osteogenic markers. Cyclic tensile strain was applied to hASCs in 2D culture and calcium accretion was quantified as a measure of osteogenic differentiation. Computational models were created to determine the range and location of different strains applied to the 2D substrate. Three dimensional finite element models were created for hMSC-seeded collagen gels subjected to cyclic tensile strain for bone tissue engineering, in order to determine the local strains most effective in inducing hMSC osteogenesis. Finally, in order to optimize the rapid creation of computational models of bone, different methods of automated finite element mesh generation were studied and validated via mechanical testing by four-point bending.

The results of this research show promising initial results for application of 3 dynes/cm^2 fluid shear stress on hASCs cultured on a novel three dimensional scaffold. In two-dimensional monolayer culture, local cyclic tensile strains of 7.7% to 20.4% were shown to induce highest calcium accretion by hASCs after 14 days. Human MSCs in three-dimensional collagen gel culture were modeled with finite element analysis and local tensile strains of 16.8% were calculated from experimental studies that upregulated BMP2 mRNA. Additionally, strains of 21.8% were shown to disrupt actin cytoskeletal alignment. Finally, a nonuniform voxel-

based finite element mesh generation was shown to accurately predict physiological strains in a long bone.

This body of work demonstrates the significance of the chemical and mechanical stimuli placed on adult stem cells during *in vitro* culture. It examines the mechanical forces necessary to induce osteogenesis of human adipose and bone marrow derived stem cells, and suggests ranges of mechanical stimuli that show promise for bone tissue engineering.

Computational and Experimental Analyses of Bone and Adult Stem Cell Mechanobiology

by
Terry Wayne Pfeiler

A dissertation submitted to the Graduate Faculty of
North Carolina State University
in partial fulfillment of the
requirements for the degree of
Doctor of Philosophy

Biomedical Engineering

Raleigh, North Carolina

2009

APPROVED BY:

_____	_____
Elizabeth Loboa Committee Chair	Albert Banes
_____	_____
Charles Finley	David Lalush
_____	
Simon Roe	

Dedication

This dissertation is dedicated to my parents Terry and Jenny and my sister Lara, for encouraging me to pursue my dreams.

Biography

Terry Wayne Pfeiler was born December 10, 1979 in Knoxville, Tennessee to parents Terry and Jenny Pfeiler. Wayne has one younger sister, Lara Pfeiler, who was born with spina bifida. Growing up with Lara and her special medical needs greatly influenced Wayne's future career plans. Wayne's primary education was in Knoxville and Chattanooga, Tennessee. Wayne graduated Hixson High School in May, 1998. The following fall, Wayne entered the University of Tennessee, Knoxville to study engineering with an academic scholarship. In May, 2002 Wayne graduated with a Bachelor of Science degree in Biomedical Engineering. Wayne continued his studies at UT Knoxville to pursue a Master of Science degree in Engineering Science under the advisement of Dr Mehran Kasra. Wayne's Masters Thesis research involved creating a nonlinear model of the human knee joint, and this degree was completed in May, 2004. In July that year, Wayne married his wife Erika in Greeneville, Tennessee. Shortly after, Wayne and Erika moved to Raleigh, North Carolina so they could both study at North Carolina State University. Wayne began his PhD program in August, 2004 under the advisement of Dr Elizabeth Loboa with the Joint Department of Biomedical Engineering at NCSU and UNC-CH. Following his PhD, Wayne is accepting a postdoctoral researcher position at Duke University in Durham with the long-term goal of teaching and conducting research at a university.

Acknowledgements

While the educational road to a PhD may have been a long one, I am very grateful that it has not been a lonely one. Time after time when I encountered difficulties in research, courses, or life in general; I found someone who was willing to point me in the right direction, offer a kind word, or maybe just go out for a beer.

First, I thank my advisor and committee chair Elizabeth Loboa for her guidance, encouragement, support, and sheer drive. Thanks for encouraging me to publish, attend conferences, and network with colleagues. Thank you to my committee members: Al Banes, Charles Finley, David Lalush, and Simon Roe. Each of you contributed to the work that is my dissertation.

Thanks to Ruwan, Carla, Seth, Audrey and Josie; my friends and fellow graduate students who shared a lab and office. Thank you Susan Bernacki and Michelle Wall for teaching me cell culture and helping me frame my experiments with the proper controls.

I am extremely thankful for my family and their support throughout my life. Mom and Dad, thanks for encouraging me to pursue whatever career path I wanted, and for always being there to talk. Thanks to my grandparents who always took an interest in whatever new thing I was working on in the lab. Finally, thank you, Erika for your support throughout our joint graduate education in Raleigh. I hope your new job in DC is everything you've hoped. So many have made a positive impact on my

life and graduate career that I could not hope to name everyone, but I hope that in some way you all know that I am grateful.

Table of Contents

List of Tables

Page

List of Figures

Page

1. Introduction

The research presented within this dissertation uses experimental stem cell culture techniques and finite element analyses to better understand the requirements for bone tissue engineering; and, to provide new tools for understanding bone *in vivo*. With the knowledge gained through this research, better protocols can be developed to synergistically apply chemical and mechanical stimuli to adult stem cells *in vitro* to optimize their osteogenesis for bone tissue engineering and regenerative medicine applications.

1.1 Background

1.1.1 Stem cells

Cells that are capable of differentiating into multiple phenotypes are referred to as stem cells. Primitive cells were recognized to exist within bone marrow in the early 20th century that could differentiate into multiple lineages of hematopoietic cells (Danchakoff 1916, Sabin et al 1936). The proliferative and regenerative capacities of these cells were later recognized, as the use of bone marrow-derived stem cells was included to regenerate additional tissues such as the spleen in irradiated mice (Cudkowicz et al 1964). Bone marrow stromal stem cells were further identified as the initiators of bone repair and regeneration (Patt and Maloney 1975, Golde et al 1980).

Through the application of chemical induction factors *in vitro*, human mesenchymal stem cells (hMSCs) are capable of differentiating different pathways into bone, cartilage, tendon, muscle and fat tissue (Bruder et al 1994, Caplan and Bruder 2001). The versatility and expandability of mesenchymal stem cells makes them very attractive for tissue engineering applications. However, the procedure used to obtain cells from a patient requires a the relatively invasive removal of bone marrow.

Human adipose stem cells (hASCs) are obtained from a patient's fat tissue and are capable of following similar differentiation pathways *in vitro* as hMSCs, under altered chemical stimuli (Estes et a 2006). In addition, hASCs may be obtained from adipose tissue beneath a patient's dermis in a far less invasive procedure (Bernacki et al 2008). However, the use of adipose stem cells for tissue engineering has not been investigated to the same extent of hMSCs.

1.1.2 Mechanotransduction

The process by which cells perceive and act upon mechanical motion and forces is called mechanotransduction. In bone, there are several proposed mechanisms that osteocytes are believed to use in osteogenic responses associated with physical stimuli such as fluid flow and cyclic strain (Riddle and Donahue 2008). Human adipose derived stem cells (hASCs) have also shown bone cell-like reactions to pulsatile fluid flow (Knippenberg et al 2005); and, investigators in our laboratory have shown that cyclic tensile strain accelerates and increases

osteogenic differentiation by mesenchymal stem cells (Sumanasinghe et al 2006) and calcium deposition by human adipose derived stem cells (Hanson et al 2009). We believe that some of the same mechanosensors likely play a role in cyclic tensile strain induced osteodifferentiation of hASCs as have been previously identified in bone and progenitor cells.

One mechanism that likely plays a role is a latent complex containing transforming growth factor-β 1 (TGF-β1) (Wells and Discher 2008, Wipff et al 2007). After being secreted into the extracellular matrix (ECM), this complex binds to cell surface integrins. The latency complex is stretch sensitive, such that when cells are surrounded by a matrix stiffer than some threshold value, cell-created traction forces cause TGF-β1 to be released. We believe that an externally applied force, such as cyclic tensile strain could also cause this latency complex to release TGF-β1. Receptors on the cell surface would then bind the free TGF-β1 and induce additional extracellular matrix deposition, latency complex formation, and structural protein formation.

Other likely stretch-related mechanotransduction mechanisms are cell surface stretch sensitive ion channels (Rubin et al 2006). These channels are normally closed, but cell surface tension causes them to open and allow ion transport across the cell membrane. These stretch-sensitive ion channels have been shown to play an important role in nitric oxide (NO) signaling in osteocytes and osteoblasts (Rawlinson et al 1996). There are two forms of nitric oxide synthase (NOS) which generate NO and have been found to play signaling roles in bone cells: inducible

nitric oxide synthase (iNOS) and endothelial nitric oxide synthase (eNOS) (van't Hof and Ralston 2001, Wimalawansa 2007). The endothelial form of nitric oxide synthase plays a critical role in down-regulating osteoclast activity (Van Epps-Fung 1994, van't Hof and Ralston 2001). However, iNOS has been found to promote Interleukin 1 beta IL-1β in bone resorption (van't Hof and Ralston 2001). In non-inflammatory conditions, osteocytes and osteoblasts express eNOS rather than iNOS (van't Hof and Ralston 2001). Nitric oxide may also inhibit protaglandins and thus bone resorption (van't Hof and Ralston 2001). Bone cells have been found to rapidly release NO following mechanical stretch (Liedert et al 2006). These studies compare well with a previous study on hMSCs by investigators in our laboratory that found no significant increase in IL-1β or TNF-α cytokine expression resulting from cyclic tensile strain (Sumanasinghe et al 2009 B).

The physiological mechanisms by which bone and progenitor cells sense mechanical forces *in vivo* can be better understood through *in vitro* experimentation. By selectively applying specific mechanical stimuli *in vitro*, it may be possible to determine the range of stimulation most effective for inducing osteogenesis of human stem and progenitor cells.

1.1.3 In vitro mechanical stimulation

In previous studies using Flexcell's TissueTrain™ system (Flexcell Int, Hillsborough, NC) that applies uniaxial cyclic tensile strain to cell-seeded Type I collagen gels, we found that the dimensions of an hMSC-seeded collagen gel

decreases significantly with time in culture (Sumanasinghe et al 2009 A). We also conducted finite element analyses of three-dimensional hMSC-seeded TissueTrain constructs, simulating mechanical loading conditions applied *in vitro* (Pfeiler et al 2008). Another study found that in cell-seeded nonwoven scaffold composites, the scaffold material initially provided the structure and mechanical strength of the construct. However, with the application of cyclic flexural strain, cells deposited extracellular matrix proteins, and increased the number of fiber-fiber bonds (Engelmayr and Sacks 2008) and increased the stiffness of their construct. We have previously shown that the magnitude of mechanical stimulation affects cell response (Sumanasinghe et al 2006, Pfeiler et al 2008). In the case of tensile strain, portions of the construct with thinner cross sections will experience increased stress. If the construct's initial material properties are homogenous, the thinner sections will also experience increased strain. Because of these factors, we can expect that cells within a cell-seeded construct with non-uniform geometry will exhibit varied responses to mechanical loading. Chapters two through four address mechanical loading of stem cells *in vitro*. In order to understand the local forces applied during *in vitro* loading, finite element analyses were conducted in chapters three and four. The next section discusses the use of finite element modeling for biomedical engineering.

1.1.4 Finite element modeling of bone

Finite element analysis is a well-established tool for determining stresses inside bone subjected to loading. However, accurate finite element simulations of *in vivo* conditions require accurate mechanical property data. Computed tomography (CT) imaging is a non-invasive technique used to gather three dimensional physiological data such as geometry and density of bone *in vivo*. These image data can be used in manual segmentation of bone to generate surfaces and create finite element models. Unfortunately, the time required to create such models is too great to allow for creation of patient-specific models for clinical applications. Therefore, several attempts to create semi-automated mesh generation methods have been undertaken with varying results since 1990 (Keyak et al 1990, Marom and Linden 1990, Les et al 1997).

Voxel-based finite element model-derived estimates of bone strength have been proven to be reasonably accurate compared to *in vitro* compressive strength (Crawford et al 2003). It has also been shown that rough gradient, material property, voxel-based models yield results comparable to geometry-based modeling (Lengsfeld et al 1998). It has been suggested that an improved method for defining the material properties of bone would be to use different equations to convert the CT Hounsfield Unit values into material properties of cortical and trabecular bone by varying both elastic modulus and Poisson's ratio (Cattaneo et al 2000). However, Wirtz *et al* claimed no correlation is found between bone density and Poisson's ratio (2000). Finally, it has also been proposed that linear or power regression equations

can be used to convert apparent density values into elastic moduli (Rho et al 1995). Considering the many applications proposed, CT imaging provides a useful method to acquire physiological information for rapid creation of finite element models of bone.

1.1.5 Computed tomography imaging

The Hounsfield Unit (HU), or CT number, is an arbitrary unit of relative x-ray attenuation, as compared to the x-ray attenuation of water. Hounsfield Units are named in honor of Sir Godfrey Hounsfeld who developed the first Computed Tomography (CT) scanner in 1972. (Jackson and Thomas 2004). CT numbers are calculated by applying a filtered back projection algorithm to x-ray attenuation values (Dhawan 2003). X-ray attenuation is the removal of x-ray photons caused by tissue absorption or scatter of the beam as it passes through the patient (Huda and Slone 2003). Within a CT image, HU relate x-ray attenuation along a spectrum compared to water, which is defined as 0 HU.

The physical property to which an HU value relates is the average density of the matter within the corresponding volume of space, determined by x-ray attenuation through the volume. Less dense substances have HU values < 0. Air is usually defined as -1000 HU and displayed as black. Substances more dense than water have HU values > 0. Bone is usually displayed in white with HU values up to +1000 (Jackson and Thomas 2004).

The HU of material x, is given by:

$$HU_x = \frac{m_x - m_{water}}{m_{water}} \times 1000$$

where μ_x is the attenuation coefficient of material x, and μ_{water} is the attenuation coefficient of water (Huda and Sloan 2003). Within a CT image or dataset, HU values describe the relative x-ray attenuation of a volume element (voxel) within the patient (Huda and Sloan 2003). Several settings on a CT machine can alter the CT numbers resulting from a scan, or the way in which the data are displayed.

Because CT numbers (or Hounsfield units) relate to the average density of a volume represented by a voxel, they are approximate. CT numbers dependent upon several factors including tube voltage used to generate the image, (Huda and Sloan 2003), the model of CT scanner used (Levi et al 1982, McCullough and Morin 1983, Birnbaum 2007), and the device's convolution kernel used to reconstruct an image (Birnbaum et al 2007).

With the advent of new types of CT scanners, comparisons have been made between the various generations. While the use of helical CT has not been found to significantly affect x-ray attenuation, differences between different multi-row CT scanners have been shown to significantly affect CT numbers in the range of 0-20 HU (Hopper et al 1997). Despite advances in technology, CT systems will continue to have technical limitations that prevent them from conveying a perfect representation of internal patient anatomy.

1.2 Objectives

The goals of this dissertation research were to study the impact of mechanical cues on adult stem cells for bone tissue engineering, to use finite element analysis to better understand those mechanical cues on cells in culture, and, finally, to develop automated techniques to build patient-specific finite element models of bone. The mechanical cues investigated for this research included fluid shear stress and cyclic tensile strain, and the cell responses analyzed were genetic expression of osteogenic proteins and calcium deposition. An automated technique to create finite element models of bone was created and uses clinical CT data for model creation and is validated through mechanical testing.

2. Pulsatile Fluid Shear Stress-Directed Differentiation of Human Adipose Stem Cells

The previous chapter introduced stem cells, the concept of mechanotransduction and some of the putative mechanisms by which adult stem cells sense external forces. In this chapter, we apply fluid shear stress to human adipose derived stem cells cultured on a novel three-dimensional scaffold material. Our goal was to apply a range of fluid shear stresses in order to determine stresses that may be most effective in triggering human adipose derived stem cell (hASC) osteogenic differentiation, and to evaluate a novel scaffold material for use in human stem cell culture.

2.1 Introduction

In regenerative medicine, three-dimensional scaffold materials are frequently used to promote cell adhesion and to provide initial structure for *in vivo* implantation. One such scaffold material which has been employed since the 1970s is polylactic acid (PLA) [Cutright and Hunsuck 1971, Kulkarni et al 1971]. PLA provides initial strength while slowly degrading after several months *in vivo* (Chawla and Chang 1985, Dejong et al 2004). The rate at which PLA degrades *in vivo* can be altered by controlling the molecular weight and crystalline structure (Chawla and Chang 1985, Pistner et al 1993). Specifically, in bone tissue engineering, it is hoped PLA as a cell-seeded scaffold will slowly degrade as cell-mediated *de novo* bone forms in its place.

Human adipose-derived adult stem cells (hASCs) have proven to be a promising source of differentiating cells for tissue engineering and regenerative medicine (Tholpady et al 2006). The relative ease of harvesting adipose tissue versus bone marrow-derived stem cells also provides benefits for the patient (Parker and Katz 2006). Human adipose-derived stem cells, (hASCs) have been shown to exhibit reactions to pulsatile fluid flow similar to those of bone cells (Knippenberg et al 2005). Despite some differences, such as hASC responsiveness to certain growth factors as compared to hMSCs, hASCs are able to differentiate into several lineages including osteogenic and chondrogenic (Bunnell et al 2008).

Osteocytes *in vivo* are believed to respond to stimulations such as fluid flow and cyclic strain by upregulating osteogenic processes (Riddle and Donahue 2008).

Evidence suggests that the ability of bone to remodel in response to loading is due in part to the ability of bone and bone-lining cells to sense fluid flow through the lacunar-canalicular system (Burger et al 1995, Klein-Nulend et al 1995).

The magnitude of fluid shear stimulation has been shown to modulate cell response. Pulsatile fluid flow-induced shear stress of 5 dynes/cm^2 has been shown to cause an increase in nitric oxide synthesis by chicken osteocytes (Klein-Nulend et al 1995) and shear stresses of 7 dynes/cm^2 to cause an increase prostaglandin E2 production (Ajubi et al 1996). Modeling of fluid flow in bone has predicted the peak *in vivo* shear stresses applied to cells under physiological loading to be between 8 and 30 dynes/cm^2 (Bonewald 2006).

Previous studies have demonstrated that osteogenesis is linked to upregulation of several genes. Bone morphogenetic protein 2 (BMP2) and Runt-regulated transcription factor 2 (RUNX2) have been linked to osteoblast differentiation and activity *in vivo* (McCarthy et al 2000, Lee et al 2000, Halvorsen et al 2001). Mesenchymal stem cells have been shown to upregulate expression of Type I collagen, alkaline phosphatase, and osteocalcin under osteogenic conditions *in vitro* (Halvorsen et al 2001, Jaiswal et al 2000, Oreffo et al 1999, Frank et al 2002).

The purpose of this study was to determine if a novel high surface area scaffold material is suitable for three-dimensional cell culture of hASCs and to examine the effects of varied magnitudes of pulsatile fluid flow on hASC osteogenesis of human adipose-derived stem cells. We hypothesized that the

scaffold material would serve as a viable platform for hASC culture and that pulsatile fluid flow would induce osteogenic differentiation, as evident through hASC viability, proliferation, and upregulation of genes indicative of osteogenesis. To test our hypothesis, we analyzed the scaffold material, verified hASC viability following culture on the scaffolds, and perfused scaffolds with 3, 6, and 9 dynes/cm^2 of pulsatile fluid shear for one hour in complete growth medium.

2.2 Methods

2.2.1 Scaffold creation

A high surface-area fabric was created at NCSU using hydro-entangled fibers created from poly-lactic acid (PLA) and a proprietary water-dispersible sulfo-polyester (EastONE, Eastman Chemical, Kingsport, TN). Briefly, the fibers were extruded with a PLA core and EastONE sheath. The extrusion die formed a PLA core cross section roughly approximating an asterisk, surrounded by EastONE. Fibers were then hydro-entangled to form a fabric which was heat-set using a laminator at 100°C and 4 meters per minute. The fabric was then washed twice in 90°C deionized water to remove EastONE. Individual scaffolds were then cut to 18 mm diameter circles (Fig 2.1) and sterilized under ultraviolet light for 4 hours per side in a biosafety cabinet.

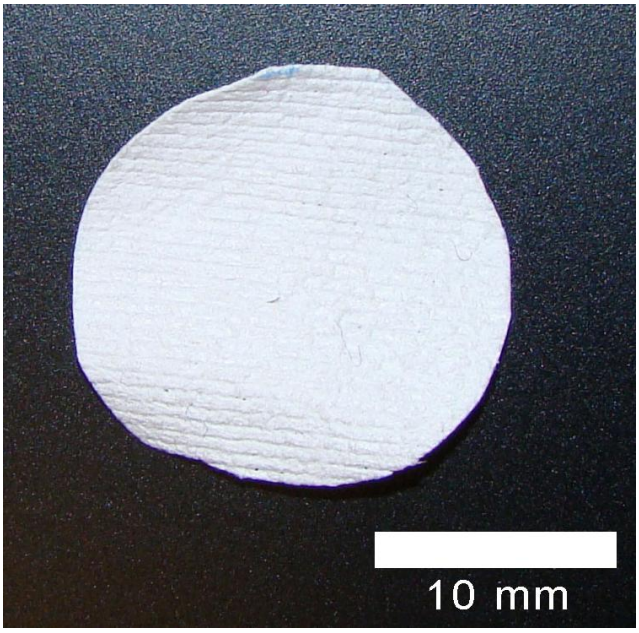

Figure 2.1. Individual cell culture scaffold cut from washed fabric sheet.

2.2.2 Scaffold structure

In order to confirm scaffold microstructure, sample scaffolds were freeze – fractured in liquid nitrogen and plasma-coated with gold. Samples were then imaged using scanning electron microscopy (model JSM6400F JEOL, Peabody, MA). Scaffold surface topology and cross section were imaged at varying magnifications from 30x to 6000x. Measurements of fibers thickness and scaffold cross section were made using the Revolution™ software package (4pi Analysis Inc, Durham, NC) calibrated to SEM magnification.

In order to calculate the required volumetric flow rates through the scaffold material, average pore size was measured. Briefly, the scaffold material was immersed in Silwick oil of 20.1 dynes/cm viscosity, then a capillary flow porometer, (model CFP-1100-AX; Porous Materials Inc, Ithaca, NY) was used to apply an increasing air pressure across the fabric to force oil from the scaffold pores. The amount of air flow was measured throughout the ramped air pressure, and mean pore diameter was calculated using the associated manufacturer's software (Porous Materials). Triplicate measurements were made on different sections of fabric.

2.2.3 Cell culture

One second-passage hASC cell line (36 year old female of mixed ethnicity) was plated in T-75 flasks at 100,000 cells per flask, cultured in 25 ml complete growth medium (CGM) containing fetal 10% bovine serum by volume, 4 mM L-glutamine, 0.05 units/ml penicillin, and 0.05 ug/ml streptomycin. A complete medium

change was performed twice weekly and flasks were kept in cell culture incubators maintained at 100% humidity, 37°C and 5% CO_2 until passaging at 70% confluency (6 days in culture). Third passage hASCs were then seeded onto 18 mm diameter circular scaffolds using 25,000 cells suspended in 50 ul CGM per scaffold side, for a total of 50,000 cells per scaffold, and placed in 6-well suspension culture plates. After allowing 30 minutes for cell attachment within an incubator, 3 ml of CGM was added to each well. Acellular control scaffolds were also maintained in CGM.

2.2.4 Fluid shear application

After three days in culture, the hASC-seeded three-dimensional scaffolds were mounted within a fluid shear system with all assembly performed within an incubator maintained at 37°C and 5% CO_2 (Fig 2.2). To supply fluid for stimulation, a media reservoir was attached with gas-permeable tubing (Cole-Parmer, Vernon Hills, Illinois) to a distribution manifold (Tissue Growth Technologies, Minnetonka, MN). From the manifold, individual lines of impermeable PharMed® tubing (Cole-Parmer) were loaded through a MasterFlex model L/S 7519-25 peristaltic pulsatile pump head-cartridge system (Cole-Parmer) and connected to a second length of gas-permeable tubing. Tubing lines were attached to each flow chamber, and discharge tubing lines were routed to collection tubes. Sufficient CGM was added to the media reservoir bottle in order to supply one hour of fluid shear flow for each set of samples. Tubing was temporarily disconnected at the flow chambers while medium was primed through the tubing to reach the flow chambers. Human ASC-

seeded scaffolds were then individually loaded into four fluid shear chambers (Tissue Growth Technologies) (Figs. 2.3, 2.4). Flow rates appropriate to apply the desired shear rates were calculated using scaffold area and experimentally-determined scaffold pore geometry using the following two equations:

$$V = \frac{t \cdot r0}{2 \cdot m} \quad (1)$$

$$Q = A * V \quad (2)$$

In equation 1, V was average fluid velocity through pores, t was fluid shear, r0 was pore radius, and m was kinematic fluid viscosity. In equation 2, fluid flow rate (Q) was determined by pore area (A) multiplied by average velocity (V). The appropriate flow rates to induce shear stresses of 3, 6, or 9 dynes/cm^2 (Table 2.1) were entered into the pump controller and four scaffolds were simultaneously stimulated for one hour. Unstimulated control scaffolds were also kept in the incubator for one complete cycle.

Table 2.1. Fluid flow rates applied to hASC-seeded scaffolds

Desired shear stress (dynes/cm^2)	Applied fluid flow rate (ml/min)
3	0.2
6	0.4
9	0.6

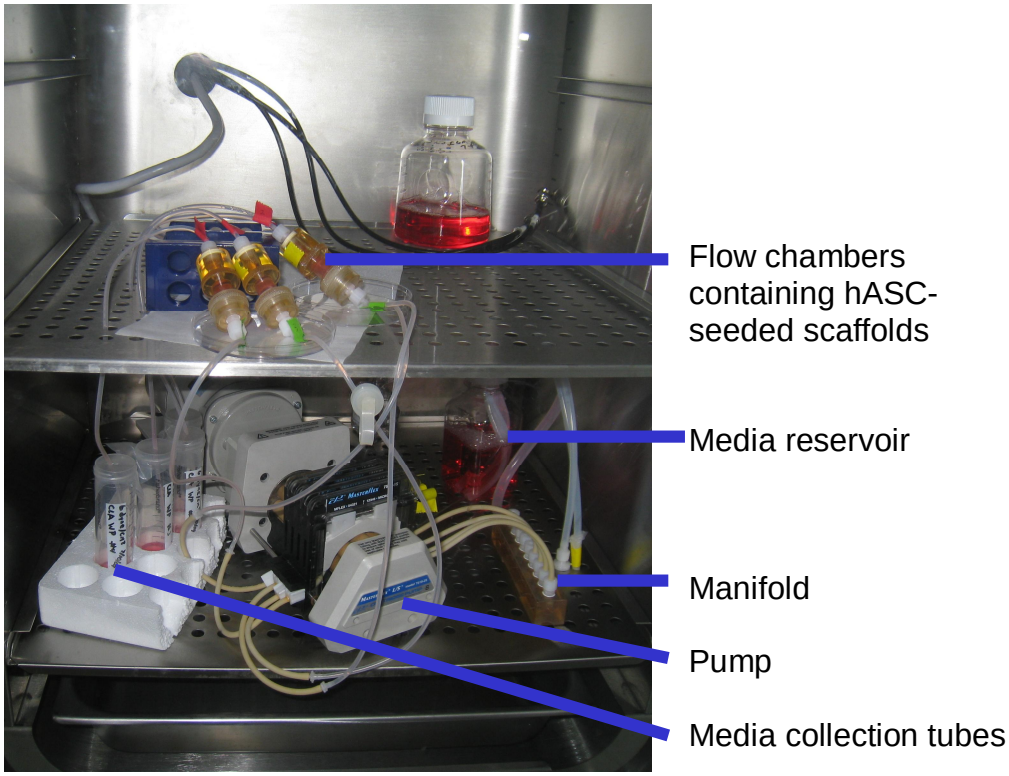

Figure 2.2. Complete pulsatile fluid shear system within cell culture incubator.

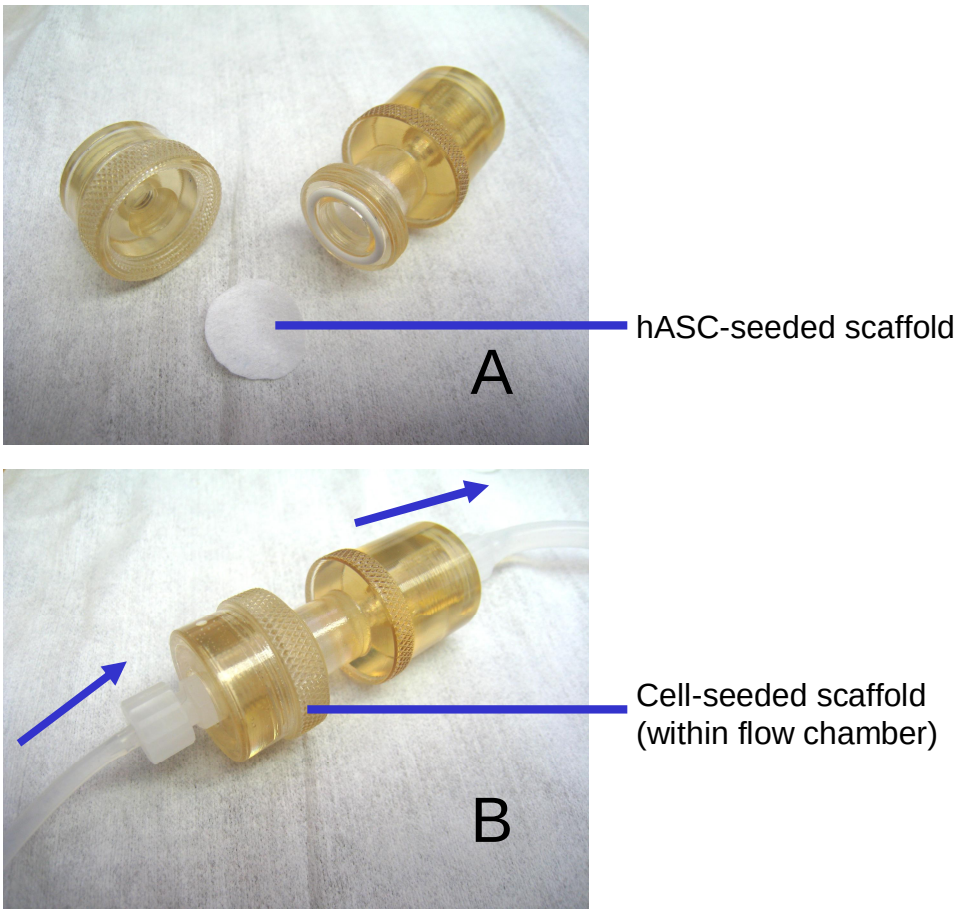

Figure 2.3. Detail of fluid shear bioreactor chamber. A) Unassembled chamber, B) Assembled chamber with gas-permeable tubing attached. Arrows indicate direction of fluid flow.

Figure 2.4. Flow chambers housing hASC-seeded scaffolds during pulsatile fluid flow stimulation. Fluid flow occurred in an upward direction from green to red labels.

2.2.5 Cellular viability

Following application of fluid shear for one hour, one scaffold from each experimental condition was washed twice with phosphate buffered saline, stained with the LIVE/DEAD® Cell Viability Kit (Invitrogen, Carlsbad, CA), and imaged using confocal microscopy (Zeiss model LSM 710) with the Zeiss ZEN 2008 software package (Carl Zeiss Microimaging Inc, Thornwood NY). Viable cells were

fluorescently labeled green and dead cells red. Three-dimensional image datasets of each hASC-seeded scaffold were created from 2D images taken at a vertical spacing of 3.5 microns and a scanning depth of 50 microns.

2.2.6 Real-time PCR

Following one hour of exposure to pulsatile fluid shear stress, hASC-seeded scaffolds were removed from fluid flow chambers, immersed in cell lysis buffer, flash-frozen in liquid nitrogen and then stored at -80°C. After obtaining all stimulated specimens, samples were thawed on ice and total RNA was isolated using an RNeasy® Mini kit following manufacturer's protocol for mammalian cells (QIAGEN, Valencia, CA). Total RNA quantity and purity were determined via spectroscopy, model ND-1000 (Thermo Fisher Scientific, Wilmington, DE). Following quantification, 50 ng of RNA obtained from each stimulated hASC-seeded scaffold was used to create cDNA libraries with a SuperScript III reverse transcriptase kit using oligo(dt) primers and following manufacturer's protocol (Invitrogen). Complimentary DNA libraries were then measured with spectroscopy to determine quantity and quality.

Real-time reverse transcriptase polymerase chain reaction (PCR) was performed in quadruplicate with 100 ng of cDNA per reaction tube using an ABI Prism 7000 real-time thermocycler and TaqMan® Gene Expression Master Mix (Applied Biosystems Inc, Foster City, CA). Expression levels of target genes Bone morphogenetic protein 2 and Runt-regulated transcription factor 2 were measured and fold change was normalized to the endogenous control glyceraldehyde-3-

phosphate deyhydrogenase (GAPDH). Target genes studied were bone morphogenetic protein-2 (BMP-2), and runt-related transcription factor 2 (RUNX2). All PCR primer sets were purchased from Applied Biosystems.

The $2^{-\Delta\Delta C}{}_{T}$ method (Livak and Schmittgen 2001) was used to calculate fold change in gene expression. Briefly, an amplification threshold was determined for each gene, and the number of PCR cycles (CT) to reach that threshold was calculated for each PCR reaction. Average Ct values for each gene were calculated, and the difference between average CT for target genes and the endogenous control were calculated as ΔCT for each target gene. Next a standard error of the mean (SEM) was calculated for CT values for each gene, and a CT standard error (s) was calculated as the vector sum of the target gene SEM and the endogenous control SEM. The ΔΔCT value for each target gene was calculated as the difference between the control condition (no flow) target gene ΔCT and the stimulated target gene ΔCT values. Finally, relative quantification of target genes were calculated as $2^{-(\Delta\Delta CT)}$ with error bars extending to $2^{-(\Delta\Delta CT \pm s)}$. In such a representation, error bars indicate a range of possible fold change values as determined by the SEM of CT values. Statistical analysis was performed using one-way ANOVA on $2^{-\Delta CT}$ values for each fluid shear stress condition, as recommended for comparative PCR (Livak and Schmittgen 2001).

2.3 Results

2.3.1 Scaffold structure

Scanning electron microscopy yielded several images that confirmed the desired high-surface area of the fibers (Figs 2.5-2.8). The average fabric thickness was determined to be 284 ± 3.84 um (Fig 2.9, 2.10). Cross section measurements showed a range of fiber widths from 5.4 um to 12.6 um (Average 8.15 ± 0.56 um) (Fig 2.8), with individual protrusions on the order of 3 um long and 0.9 um wide.

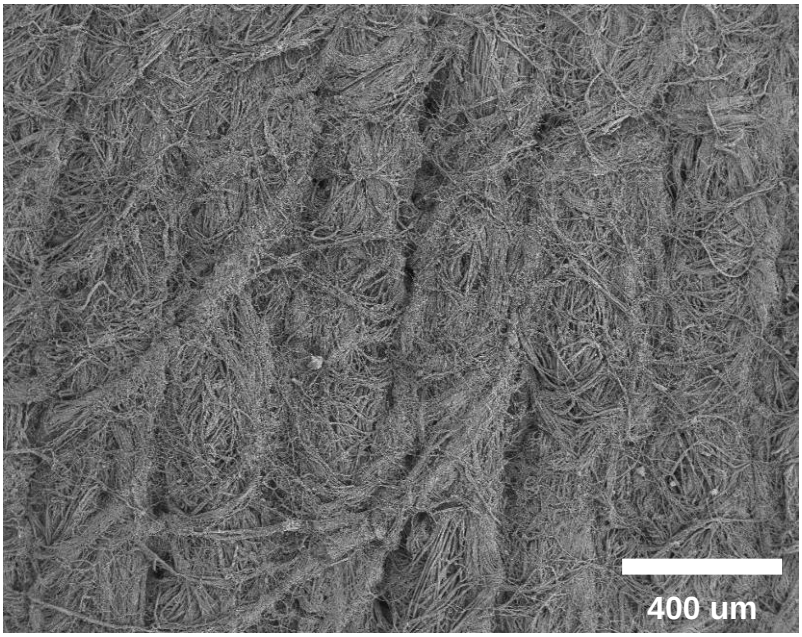

Figure 2.5. Surface topology at 30x magnification.

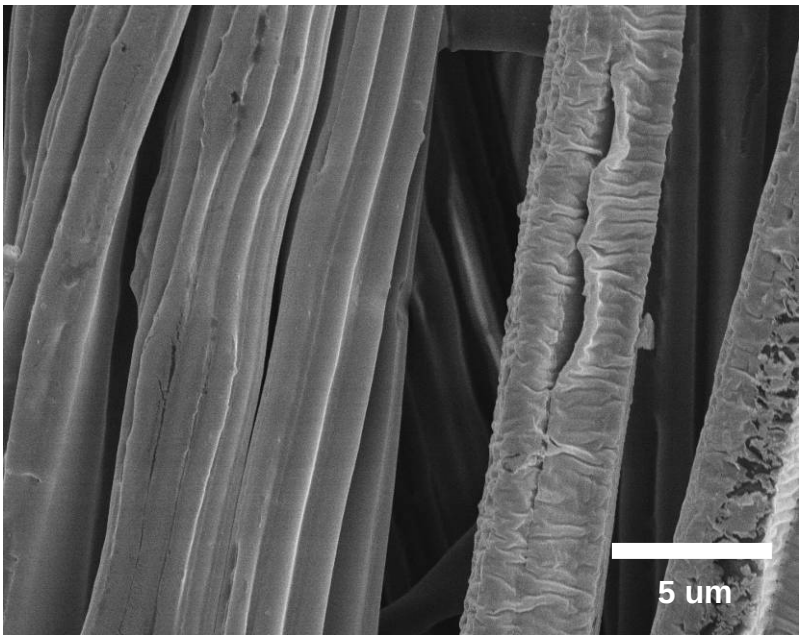

Figure 2.6. Surface detail at 5000x magnification.

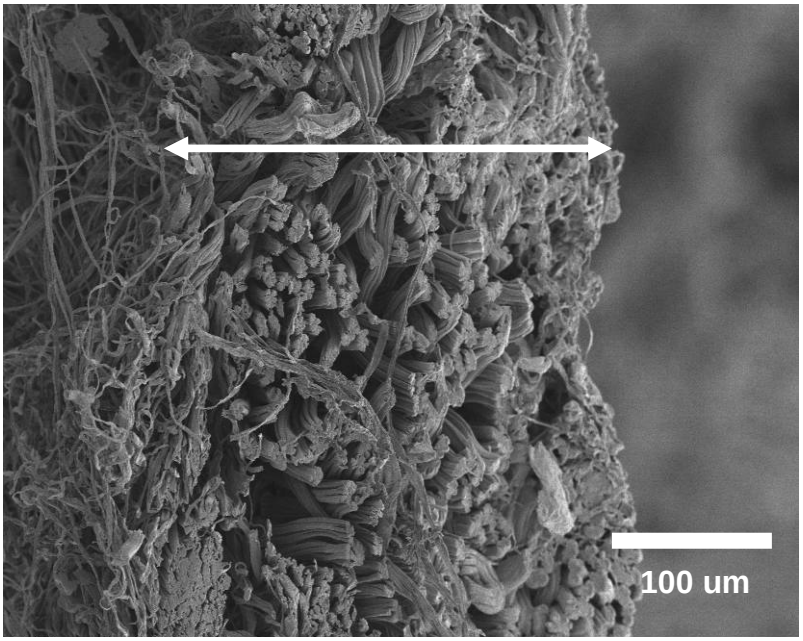

Figure 2.7. Scaffold thickness detail at 250x magnification. Arrow indicates thickness measurement.

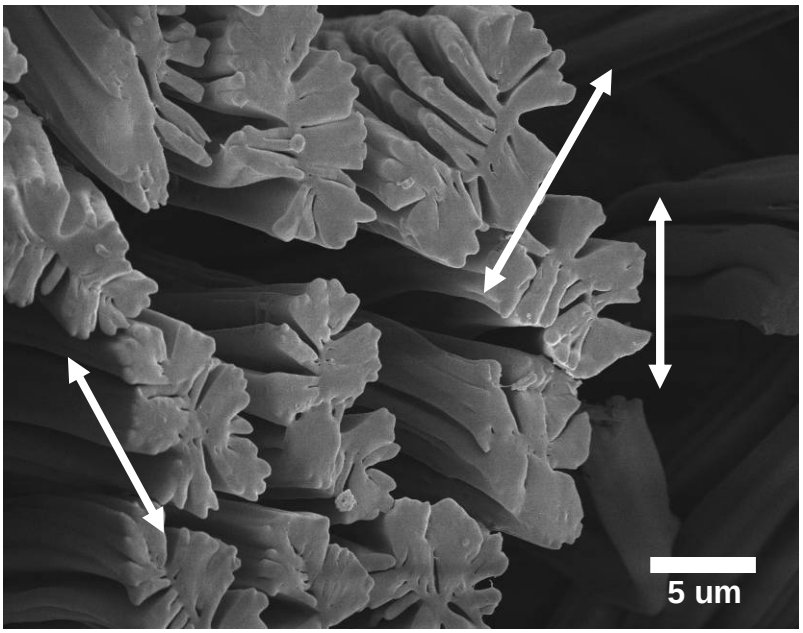

Figure 2.8. Cross section detail of multi-lobal fibers at 3000x magnification. Arrows indicate fiber diameter measurements.

Capillary flow porometry was performed on scaffold fabric samples in triplicate to measure average pore size. All samples exhibited a very similar power law relationship between pore diameter and applied air pressure of $y = 8.341\ x^{-1}$ (Fig 2.9). Average pore size was measured to be 5.01 ± 1.23 um in diameter. The overall range of pore diameters was 1.25 um to 102.16 um. The distribution of pore diameters was strongly weighted near the average diameter (Fig. 2.10).

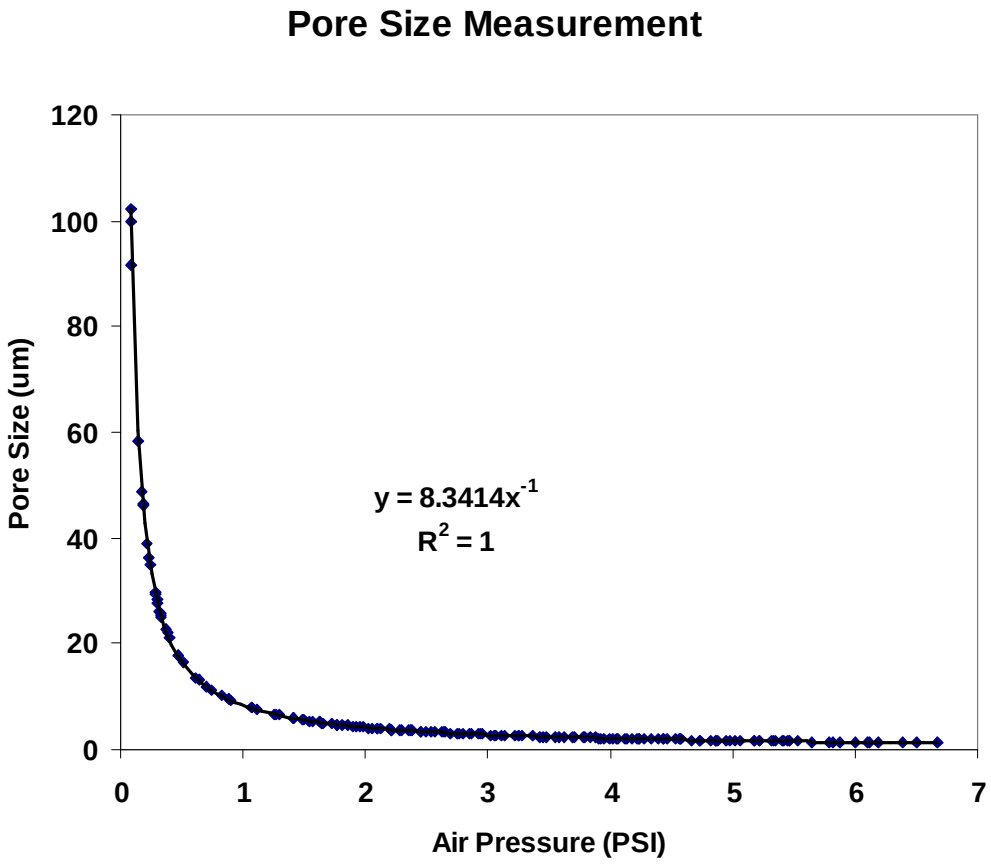

Figure 2.9. Range of pore sizes calculated versus applied air pressure during capillary porometry measurement.

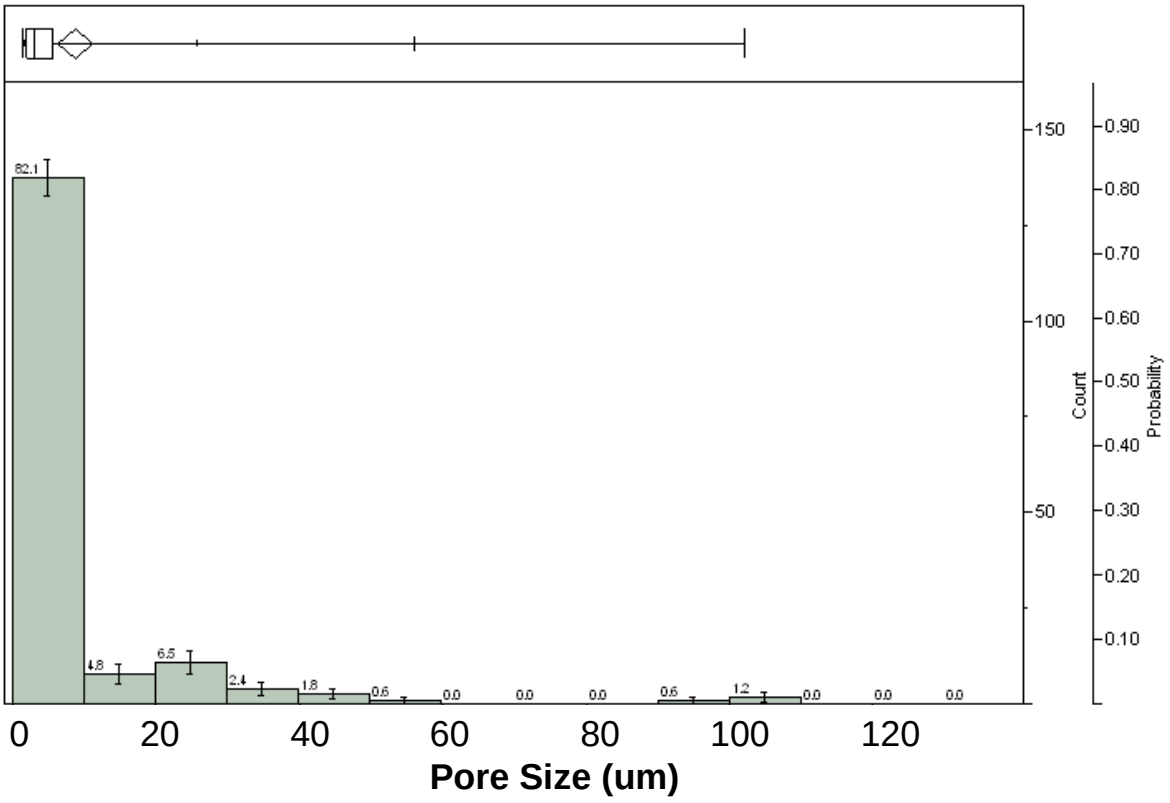

Figure 2.10. Distribution of measured pore diameters.

2.3.2 Fluid shear bioreactor

No leakage was evident at the flow chambers or any tubing connections throughout the period of fluid shear stress application. Collection tubes showed equal medium volumes following stimulation, confirming that an equal volume of medium was supplied to each scaffold.

2.3.3 Cellular viability

After one hour of pulsatile fluid flow, confocal microscopy showed live hASC distribution across all scaffolds, regardless of fluid shear applied (Fig 2.11). Fluorescently-labeled dead cells (red) were present in very few fields of view, and at minimal numbers compared to viable cells. The non-stimulated control scaffolds (Fig 2.11, A) appeared to show a slightly greater number of total cells than pulsatile flow stimulated scaffolds (Figs 2.11, B, C, D). However, there was no appreciable difference in total number of cells between stimulated scaffolds.

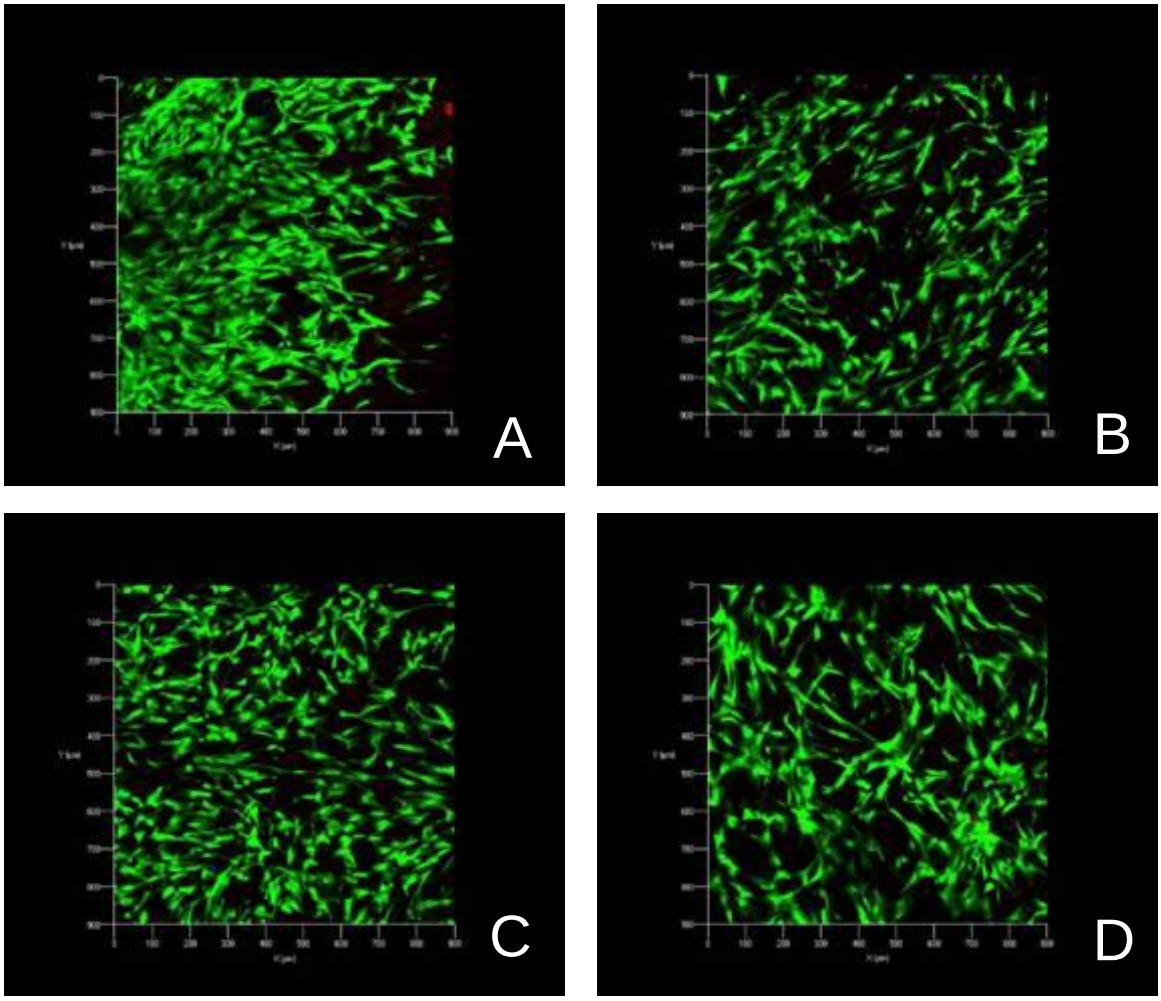

Figure 2.11. Confocal microscopy images of hASC-seeded scaffolds following one hour of pulsatile flow. A: Non-stimulated control, B: 3 dynes/cm^2, C: 6 dynes/cm^2, D: 9 dynes/cm^2. Lives cells stained green and dead cells stained red.

2.3.4 Effect of fluid shear on BMP-2 and RUNX2 mRNA expression

Real-time PCR was performed to determine the expression of BMP2 and RUNX2 mRNA relative to the endogenous control GAPDH for each experimental group. Relative to the unstimulated control, there were no measurable increases in BMP2 mRNA expression due to applied fluid shear stresses of 3, 6, or 9 dynes/cm^2.

However, the hASC-seeded scaffolds stimulated at 3 dynes/cm^2 exhibited significantly higher RUNX2 mRNA expression than non-stimulated controls ($p<0.01$), (Table 2.2 and Fig 2.12). There were slight increases in average fold change for 6 and 9 dynes/cm^2 conditions, though not at a significant level.

Table 2.2. Relative fold change in hASC expression of RUNX2 mRNA.

Applied fluid shear (dynes/cm^2)	RUNX2 mRNA expression
0	1 (0.697 - 1.435)
3*	2.301 (1.834 - 2.887)
6	1.14 (0.914 - 1.423)
9	1.694 (1.366 - 2.101)

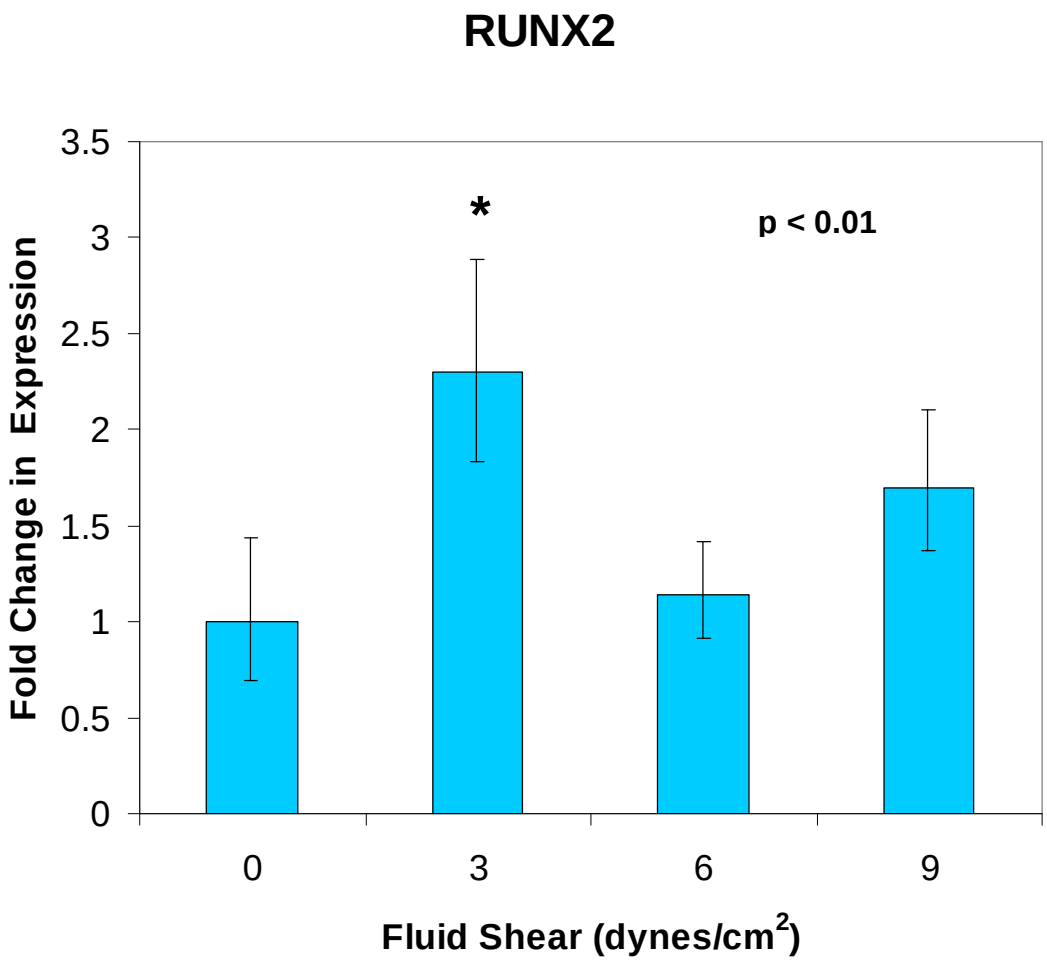

Figure 2.12. Fold change in expression levels of RUNX2 mRNA in hASCs exposed to 3, 6, and 9 dynes/cm2 of pulsatile fluid shear stress for one hour. The non-stimulated control is indicated as zero fluid shear. Results are presented as average fold change ± standard error of the mean.

2.4 Discussion

Successful bone tissue engineering with adipose-derived adult stem cells requires a combination of appropriate chemical and mechanical cues. To help provide a better understanding of the proper mechanical cues, we investigated the application of pulsatile fluid flow to hASCs cultured on a novel three dimensional scaffold. We examined scaffold microstructure through scanning electron microscopy and capillary flow porometry, we cultured hASCs on the scaffold material for three days, applied pulsatile fluid flow through the scaffold at 3, 6, and 9 dynes/cm^2, verified cell viability, and performed real-time PCR to examine mRNA expression of the osteogenic bone markers BMP2 and RUNX2.

The novel fabric presented in this study proved to be a promising scaffold material for cell culture of hASCs. After 3 days in culture, nearly all hASCs remained viable on the non-stimulated controls. Additionally, cellular adherence to the scaffold was shown to be sufficient to withstand up to 9 dynes/cm^2 of shear stress for a large majority of cells. The porous structure of the scaffold may allow for greater cell in-growth if cells are cultured for an extended time, or seeded at a higher cell density. Additionally, the bioreactor flow chambers used in this study were very successful as compared to previous flow perfusion bioreactors examined in our laboratory. No leaking occurred at any tubing connections and the flow chambers allowed for rapid insertion and removal of scaffolds, decreasing the likelihood of cell death due to scaffold drying.

There was a significant increase in mRNA expression of RUNX2 in hASCs exposed to fluid shear stress of 3 dynes/cm^2 ($p<0.01$). RUNX2 is an early marker for osteogenic differentiation and it is likely that the hASCs were able to respond to the one hour stimulation used in this study. A previous study by Knippenberg et al (2005) found increased mRNA expression of cyclooxygenase-2 by adipose derived stem cells exposed to one hour of 6 dynes/cm^2 pulsatile fluid flow. However, in that study cells were exposed to osteogenic differentiating media conditions.

This was an initial study to investigate the mechanobiological response of hASCs to three pulsatile fluid shear stresses at one time point. These results should be used in future studies that expand the variables such as culture duration, target genes examined, and incubation following application of fluid shear. The one hour stimulation duration used in this experiment may not have reached a stimulation threshold for hASCs to upregulate BMP2, which would explain the lack of any observable results for BMP2 expression over experimental controls. This study did not apply chemical differentiation factors such as dexamethasone, and future studies will examine the interplay between a combination of chemical and mechanical cues. The range of pore diameters for the novel scaffold material used in this study means the range of fluid shear stresses applied to hASCs would extend beyond the average fluid shear stresses of 3, 6, and 9 dynes/cm^2.

In summary, we have validated the use of a novel three dimensional high-surface area PLA scaffold for use in three-dimensional cell culture and as a porous substrate for a fluid shear bioreactor. We found an increase in the osteogenic

marker RUNX2 by hASCs after one hour exposure to 3 dynes/cm^2. Results of this study also suggest that hASCs are responsive to pulsatile fluid shear in three dimensional culture.

2.5 Summary

Providing the proper mechanical stimulation to engineered tissue replacements is a key concern in tissue engineering of musculoskeletal tissues. One promising technique to induce differentiation of adult stem cells is the application of fluid shear stress. Studies in our laboratory have previously examined cyclic tensile strain as a means to induce osteogenesis of human mesenchymal stem cells, as measured by genetic expression of osteogenic markers and calcium deposition. In this study, we sought to expand our stimulation methods and examine short term fluid shear stress applied to hASCs cultured on a novel porous scaffold. We hypothesized that the application of pulsatile fluid shear to hASCs would upregulate expression of the osteogenic markers BMP2 and RUNX2 in the absence of chemical differentiation supplements. Human adipose stem cells were cultured on and within a novel porous three-dimensional PLA scaffold for three days and then subjected to one hour of pulsatile fluid flow at 0, 3, 6, or 9 dynes/cm^2. Live/Dead staining revealed that cells remained viable and adherent to scaffolds following fluid shear stimulation. RT-PCR results showed that BMP2 expression was unchanged, but RUNX2 expression was upregulated in hASCs stimulated at 3 dynes/cm^2. This is the first study to examine the effects of pulsatile fluid shear stress at various rates on human adipose stem cells cultured on a three-dimensional scaffold and shows upregulation of RUNX2 following one hour of stimulation at 3 dynes/cm^2 of fluid shear stress.

3. Effects of Varied Tensile Strains on Calcium Production by Human Adipose-Derived Adult Stem Cells

The previous chapter examined pulsatile fluid shear stress as a form of mechanical stimulation to trigger differentiation of human adipose derived adult stem cells. In that study, we found that adipose stem cells are differentially responsive to ranges of pulsatile fluid shear stresses. In this chapter, we expand upon the idea of differential cellular response by applying a range of magnitudes of cyclic tensile strain as another form of mechanical stimulation. We are interested in determining what strain range may be most effective in inducing osteogenesis as measured by calcium accretion by human adipose derived adult stem cells.

3.1 Introduction

Previous studies have shown that mechanical loading induces differentiation of human mesenchymal stem cells (hMSCs) and mesenchymal tissue into tissues such as bone, fibrous tissue, cartilage, and smooth muscle cells (Ignatius et al 2004, Altman et al 2002, Campbell et al 2006, Carter et al 1998, Kelly et al 2005, Park et al 2004). Studies by investigators in our lab have shown that cyclic tensile strain, even in the absence of osteogenic differentiating medium (i.e. hMSCs maintained in growth medium alone), promotes osteogenic differentiation of bone marrow-derived hMSCs when seeded in 3D type I collagen matrices (Sumanasinghe et al 2006).

Obtaining hMSCs involves a painful procedure to remove bone marrow from the donor or patient. As a result, hASCs have become a focus of study for engineered tissue constructs, due to their relative ease of harvest and abundance as compared to mesenchymal stem cells. Studies in our lab and others have shown that hASCs present a phenotype similar to hMSCs (Gronthos et al 2001, Zuk et al 2002, Wickham et al 2003, Hanson et al 2008). Additionally, hASCs have been shown to possess the potential for use as progenitor cells for mesenchymal tissue such as bone. (Zuk et al 2001, De Ugarte et al 2003, Wall et al 2007, McCullen et al 2007, Tapp et al 2009).

Results of another study by the investigators suggested that cyclic tensile strain (CTS) above a certain threshold range (~12% global CTS) may damage the actin cytoskeletal network of hMSCs, and hamper osteogenesis (Pfeiler et al 2008). However, strains in the range of ~10% global CTS promote osteogenesis of hMSCs

by upregulating bone morphogenetic protein 2 (BMP-2) (Sumanasinghe et al 2006). We believe that a similar trend of an “optimal” strain range may be observed with hASCs. A recent pilot study by investigators in our lab suggests that certain magnitudes of global cyclic tensile strain in the range of 10% may accelerate osteodifferentiation and increase calcium accretion by hASCs cultured in osteogenic differentiating medium (Hanson et al 2008).

The purpose of this study was to correlate calcium accretion by hASCs to the magnitude of cyclic tensile strain to which they were exposed. To accomplish this, a combination of *in vitro* experiments and finite element analysis were used. We hypothesized that finite element analysis would predict different magnitude strains on regions of a Bioflex membrane exposed to 10% global cyclic tensile strain for which hASCs accreted disparate quantities of calcium. To test our hypothesis, we quantified calcium deposition of three hASC cell lines exposed to 4 hours/day of 10% global cyclic tensile strains for 14 days. We also created a nonlinear finite element model of a Bioflex well, simulating 10% global strain, and calculated the strains across the well diameter.

3.2 Methods

3.2.1 Cell culture

Human ASC cell lines from three donor patients (Table 3.1) were isolated under an IRB-approved protocol (IRB: 04-1622). Each cell line was verified to accrete calcium under osteogenic culture conditions following isolation. Third passage hASCs were plated on 35 mm diameter Bioflex culture plates (Flexcell Intl, Hillsborough, NC) and 6-well static tissue culture plates at an initial density of 50,000 cells per well. Cells were cultured in complete growth medium (CGM) which was changed twice weekly until hASC monolayers reached confluency. Upon reaching 100% confluency, complete growth medium was changed to osteogenic differentiating medium (ODM) which contained 0.1 uM dexamethasone, 10 mM beta glycerol phosphate, and 50 uM ascorbic acid and a cyclic tensile strain regimen was begun for each Bioflex plate. The strain regimen consisted of 10% cyclic tensile strain at 1 Hz for 4 hours per day for 14 days.

Briefly, the Bioflex bioreactor system worked by cyclically applying a vacuum under a flexible silicone rubber membrane. The membrane is pulled downward and to each side of a low-friction loading post. The portion of the membrane contacting the top surface of the loading post experiences nearly uniform uniaxial strain in the horizontal direction. But in order to understand the strain profile across the entire well diameter, the unsupported regions to each side of the loading post were also considered in this study. Partial media changes were performed twice weekly. To

provide conditioned media, 2 ml of ODM was replaced with fresh ODM, which allow cell-expressed signaling chemicals to remain in each well.

Table 3.1. Patient specimen information

Cell Line	Age	Gender	Ethnicity	Tissue Source
A	36	F	other	Abdominoplasty
B	44	F	other	Liposuction
C	49	F	Caucasian	Abdominoplasty

3.2.2 Calcium quantitation

Following completion of the 14-day strain regimen, three wells from each cell line were rinsed with phosphate-buffered saline and aspirated dry. Each well membrane was marked at the left and right edges along the strained axis and cut from the Bioflex^{TM} plate with a surgical scalpel. After removing the silicone rubber wells from each plate, each well was placed in a 100 mm diameter culture plate resting on a 1:1 scale cutting template (Figure 3.1).The well membrane was then cut along the strained diameter as marked into top and bottom halves. Using the cutting template as a guide, each top half was then sectioned into a strip of dimensions 35 mm by 5 mm. These strips were cut into ten equally sized rectangles of 3.5 mm by 5 mm. Each rectangle was then placed in a 1.5 ml microcentrifuge tube and

submerged in 0.5 ml of 0.5 N HCl. These tubes were incubated at 4°C overnight on a rotating table to dissolve calcium accreted by cells. The calcium-containing supernatant fluids were used in the colorimetric Calcium LiquiColor® assay (Stanbio Laboratory Boerne, TX). Samples from each square were pipetted in triplicate into a clear 96-well plate and read with a Magellan microplate reader (Tecan Group Ltd. Männedorf, Switzerland) to quantify calcium concentration in the sample and calculate mass of calcium accreted by hASCs on each rectangle.

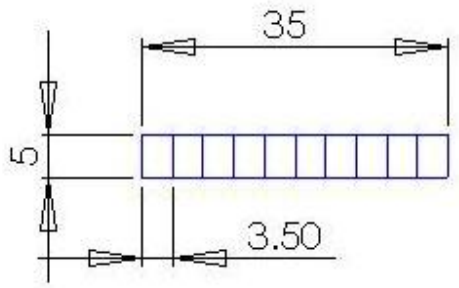

Figure 3.1. Cutting template for sectioning Bioflex wells.

3.2.3 Cell quantitation

The bottom halves of three strained wells from each cell line were sectioned into ten rectangles per well membrane, as described above. These rectangles were added to microcentrifuge tubes and immersed in 0.5 ml of a cell lysis solution containing papain (Sigma-Aldrich Corp. St. Louis, MO). Tubes were sealed and maintained at 40°C for 8 hours, then centrifuged to remove cellular debris. The supernatant from each tube was collected and used in a DNA assay. This assay

used the fluorescent Hoescht 33258 dye (Invitrogen Corp. Carlsbad, CA) to selectively stain double-stranded DNA in each sample. Fluorescence was quantified using a Magellan microplate reader. DNA concentration was calculated via fluorescence of experimental samples against a standard curve of known DNA concentrations. Average calcium accretion per cell was calculated along the strained axis for each hASC cell line.

3.2.4 Finite element modeling

The dimensions of the Bioflex wells and Arctangle™ loading post were measured and used to create a three dimensional model. A large displacement linear elastic contact model was created in ABAQUS CAE 6.7-5 simulating a one-quarter section of a Bioflex well membrane strained against the loading post. Appropriate boundary conditions were added for symmetry and a vacuum pressure load was placed on the membrane (Figure 3.2). Material properties of the flexible membrane were previously determined through mechanical testing. From this model, in-plane strain was calculated along the strained diameter.

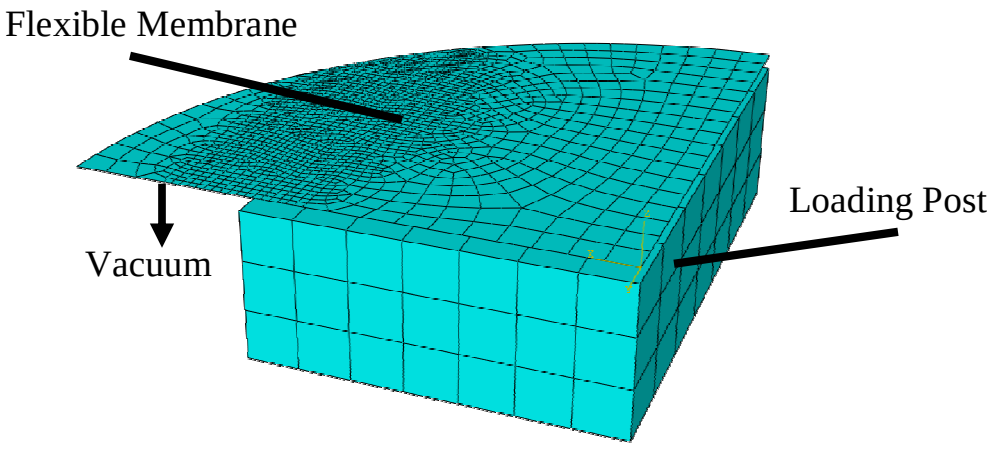

Figure 3.2. Finite element mesh of Bioflex membrane and Arctangle loading post.

3.3 Results

3.3.1 Calcium visualization

In general, Alizarin Red S staining indicated lowest levels of calcium accretion at the centers of the wells (Fig. 3.3). The edges at each end of the strained diameters showed higher calcium accretion. A roughly symmetric staining pattern was observed for all wells along the strained horizontal axis.

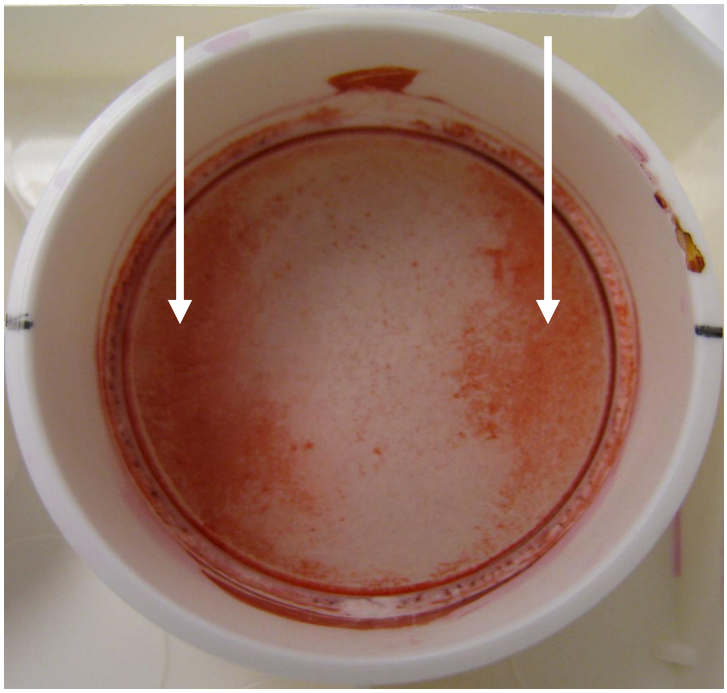

Figure 3.3. Alizarin Red S staining allowing for visualization of calcium accretion. Arrows indicate areas of greater calcium mineral, as evident by darker red staining.

3.3.2 DNA quantitation

DNA data were used to normalize calcium accretion. Cellular DNA ranged from 19.3 ng to 69.6 ng per membrane section (Fig. 3.4). This equates to 2900 to 10500 cells per membrane section. There was no clear trend across cell lines relating cell number to membrane strain.

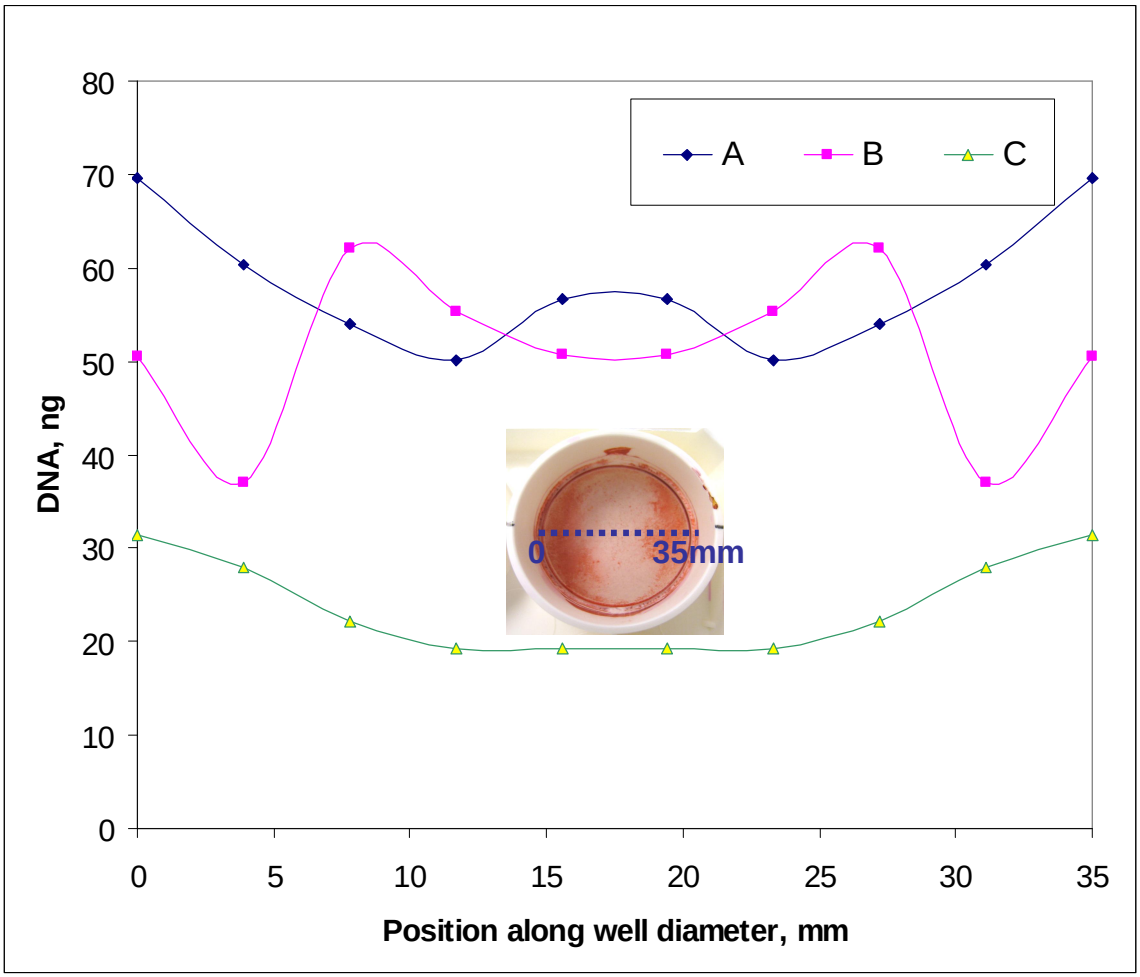

Figure 3.4. DNA content measured along well strained diameter for hASC lines from donors A, B and C, determined experimentally. Inset shows Alizarin Red S stained well with strained axis labeled from 0 to 35 mm.

3.3.3 Calcium quantitation

Calcium accretion per cell varied from 0.02 ng to 1.2 ng for the three hASC lines along the diameter of the strained well (Fig. 3.5). The calcium accretion distribution trend was shaped similarly for each cell line; however each exhibited a different magnitude of calcium accretion.

3.3.4 Finite element analysis

In-plane tensile strains varied along the diameter of the strained well from 4.3% to 36.4% (Fig. 3.6). The highest strain occurred 3.2 mm from the well edge, corresponding to an unsupported portion of the membrane that is pulled down with each vacuum cycle. The lowest strain occurred at the well edge constrained from motion.

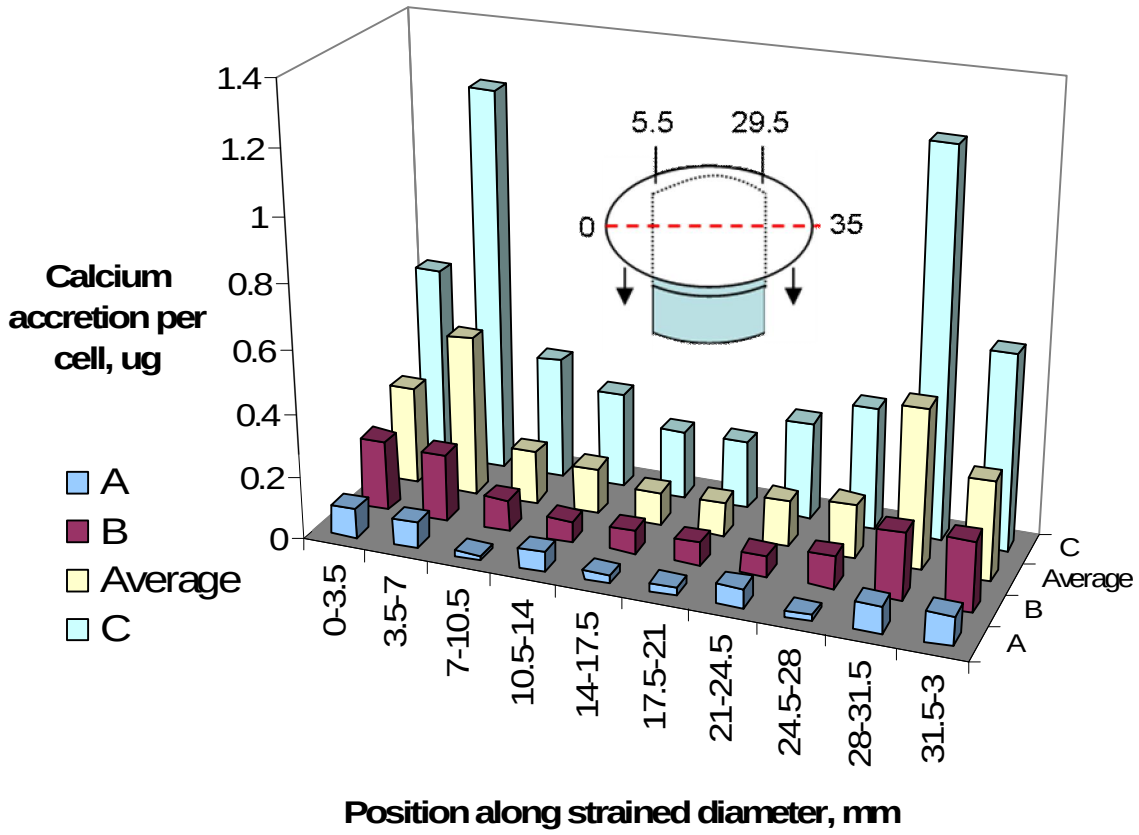

Figure 3.5. Calcium accretion per cell for three hASC lines from donors A, B and C along strained well diameter, determined via LiquiColor assay. Inset depicts membrane and loading post, strained diameter shown in dashed red.

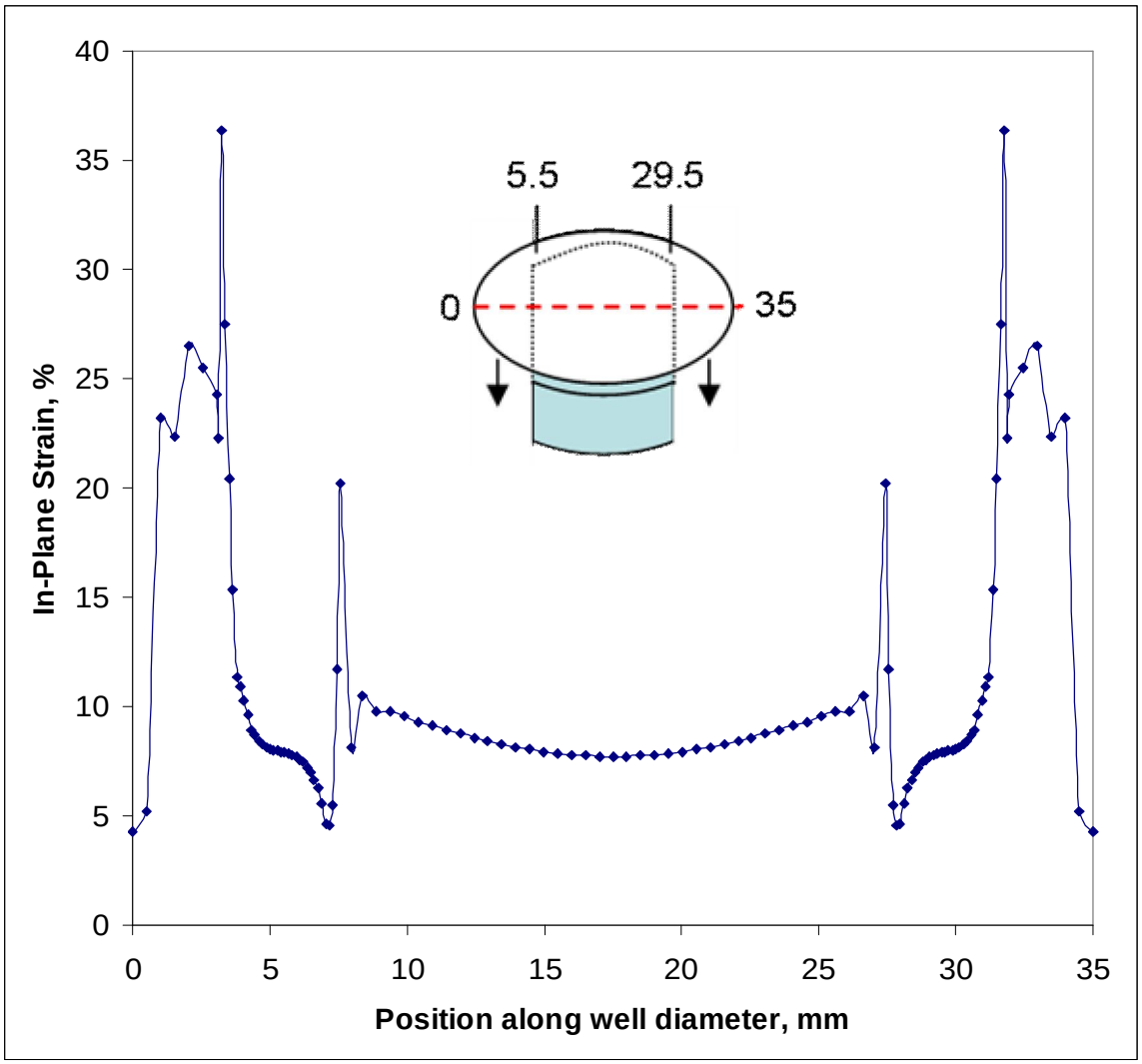

Figure 3.6. In-plane strain vs. position along strained well diameter, determined by finite element analysis. Inset depicts membrane and loading post, strained diameter shown in dashed red.

3.4 Discussion

Calcium is the primary mineral constituent of bone and osteoblast accretion of calcium is a key component of bone formation. Furthermore, the presence and quantity of calcium can be used as a metric in order to verify hASC differentiation down an osteoblast pathway. The purpose of this study was to quantify hASC calcium accretion in response to varying levels of tensile strain. Three hASC lines were cultured in osteogenic differentiating medium for 14 days and exposed to 10% global cyclic tensile strain. Calcium mineral and hASC DNA were quantified in discrete sections along the strained well diameters and finite element analysis was conducted to calculate local strains resulting from 10% global strain at each location within the well.

The lowest levels of calcium mineral accretion occurred at the centers of each flexible well along the strained diameter, corresponding to an in-plane strain of 7.7% to 8.2%. Two-thirds of total calcium accretion occurred in the two sections closest to each well edge. These sections experienced tensile strains ranging from 4.7% to 36.4% and an average of 12%. The highest calcium accretion occurred in the section directly above the loading post edge where FEA calculated strains ranged from 6% to 20%. The in-plane strain determined via FEA varied significantly across the strained well diameter. This was due to the significant deformation that occurred as vacuum pressure deformed the membrane to each side of the loading post. The central portion of the membrane supported by the loading post experienced a fairly

constant strain between 7.7% and 10.5%, and corresponded to the lowest calcium accretion across the strained diameter.

One notable observation made during the pilot phase of this study was that the hASC cell lines used in this study were less adherent to the Bioflex well membranes than hMSCs previously studied in our lab. This caused the hASC monolayer to detach from the membrane in sections of higher strain magnitudes. This problem was solved in large part by altering the experimental protocol to use conditioned media, instead of complete medium changes. It is believed this change prevented the cell monolayer from over-drying during medium changes, and also added the benefit of allowing cell-signaling molecules to remain within the culture medium.

This study highlights the sensitivity of hASC calcium accretion to varying levels of tensile strain and the importance of considering mechanical load for bone tissue engineering using hASCs. This experiment was designed to determine the range of strains most effective for inducing calcium accretion by hASCs *in vitro*. With the identification of the appropriate strains, plans can be made to move this research toward clinical applications using patients' own adipose-derived adult stem cells *in vitro* to create *de novo* bone for critical defect repair.

3.5 Summary

Human adipose derived stem cells are promising for use in tissue engineering, and offer certain advantages over other cell types due to the relative ease in harvesting adipose tissue from patients. It has been established previously that hASCs are responsive to chemical and mechanical signals applied *in vitro*. However, the combined *in vitro* culture conditions that lead to functional tissue require greater understanding. In this study, three hASC cell lines were cultured on two-dimensional flexible membranes and exposed to a range of magnitudes of local cyclic tensile strain. Experimental analyses were performed to determine areas of the membrane where hASCs accreted highest levels of calcium. Next, a nonlinear contact finite element model was created to determine the local strains experienced by hASCs during cyclic tensile strain. Mechanical property and geometry data used in the model were obtained experimentally. Through finite element analysis, it was determined that maximum calcium accretion occurred at a tensile strain range between 7.7% and 20.4%. These results compare well with another study in our lab discussed in the following chapter that determined the strain magnitude most effective for inducing hMSC osteogenesis in three-dimensional culture.

4. Finite Element Modeling of 3D Human Mesenchymal Stem Cell-Seeded Collagen Matrices

The previous study examined the impact of cyclic tensile strain on human adipose stem cells cultured in two dimensions. We found that the range of strain applied to cells impacted their magnitude of calcium accretion. In this study, we now apply a finite element approach to model human bone marrow-derived mesenchymal stem cells cultured within three dimensional collagen gel constructs. These constructs are modeled at two different times in culture, under two different culture medium conditions, and exposed to two different global magnitudes of cyclic tensile strains. Our goal was to determine the local strains the cells within these constructs to attempt to explain the different levels of osteogenic differentiation observed *in vitro*.

4.1 Introduction

Functional bone tissue engineering for large critical defects remains an elusive goal in restorative medicine. Key to *in vitro* generation of nascent tissue with appropriate material properties for withstanding *in vivo* loading are the combined mechanical and chemical stimuli used to culture cells. Previous studies have shown that mechanical loading induces differentiation of human mesenchymal stem cells (hMSCs) and mesenchymal tissue into tissues such as bone, fibrous tissue, cartilage, and smooth muscle cells (Ignatius 2004, Altman 2002, Campbell 2006, Carter 1998, Kelly 2005, Park 2004). We have previously shown that cyclic tensile strain, even in the absence of osteogenic differentiating medium (i.e. hMSCs maintained in growth medium alone), promotes osteogenic differentiation of bone marrow-derived hMSCs when seeded in 3D type I collagen matrices (Sumanasinghe 2006). The cyclic tensile strains that were applied to hMSCs *in vitro* in that study (10% and 12%), however, were much greater than the strains bone typically experiences under physiological conditions (0.09% to 0.21%) (Mikić 1995, Hillam 1996, Burr 1996).

This study focused on engineered three dimensional hMSC-seeded collagen constructs cultured in TissueTrain (Flexcell Int. Hillsborough, NC) culture plates. The TissueTrain system has been used in previous studies to impart mechanical stimuli to a variety of cells in three-dimensional culture (Garvin 2003, Qi 2006), and to investigate the effects of cyclic tensile strain on osteogenic differentiation of hMSCs. In brief, the system works by drawing a vacuum against a rubber membrane, which

in turn pulls two anchors in tension. Between the anchors, a linear cell-seeded collagen matrix is created so that cyclic uniaxial tension may be applied (Fig. 4.1).

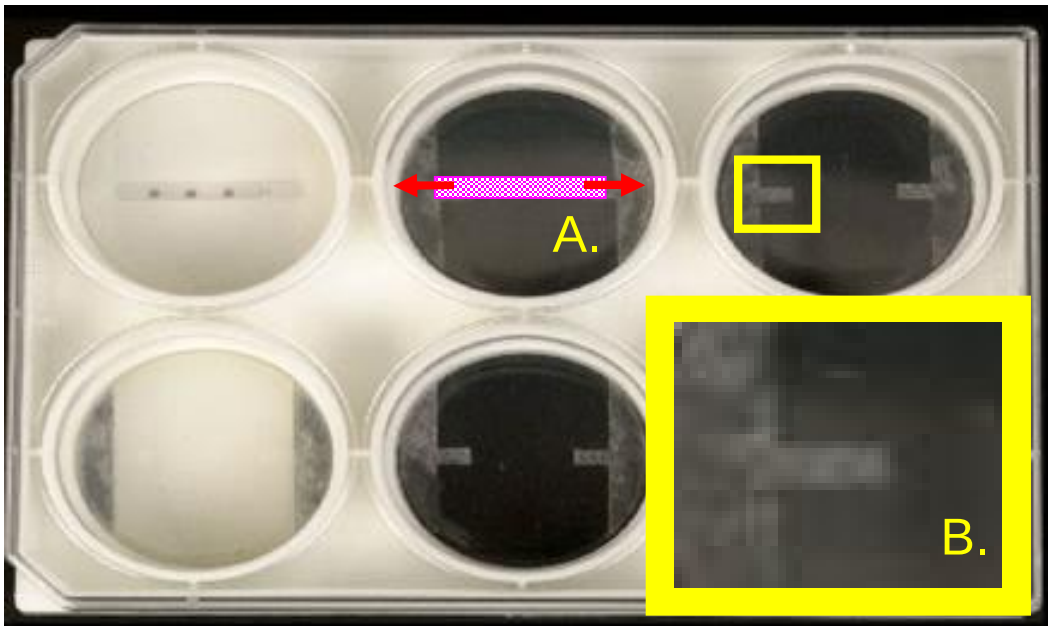

Figure 4.1. TissueTrain culture plate: A. Illustration of MSC-seeded collagen gel set between anchors and direction of uniaxial tensile strain. B. Detail of nylon nonwoven anchor.

A previous study in our laboratory examined bone morphogenetic protein-2 (BMP-2) expression in 10% and 12% cyclically strained 3D hMSC-seeded collagen matrices at 7 and 14 days as compared to unstrained controls using the Tissue Train system. The results of that study showed that matrices exposed to cyclic tensile strain increased BMP-2 expression in the absence of osteogenic growth

supplements; however differences existed between apparently similar 10% and 12% strain levels with 10% cyclic tensile strain leading to a greater increase in BMP-2 expression than 12% cyclic tensile strain (Sumanasinghe 2006 A).

As a biomaterial and engineered tissue scaffold, collagen has been modeled in numerous finite element analysis (FEA) studies. Two-dimensional FEA has been used to quantify forces exerted by corneal fibroblasts on a surrounding collagen matrix (Roy 1999). FEA has also been used to predict differentiation and repair of cartilage surrounding injuries (Cullinane 2003). Two-dimensional models have been created to simulate extension of prealigned collagen gels. (Chandran 2007). Collagen fiber alignment has been predicted during compaction in cell-seeded tissue equivalents (Ohsumi 2008). To our knowledge, no previous study has addressed the local stress and strains within cell-seeded collagen gel matrices cultured under cyclic tensile strain using three dimensional FEA.

The goal of the present study was to use finite element analysis to simulate the hMSC-seeded collagen matrices under the mechanical loading conditions in which they were grown in culture. We hypothesized that local strains experienced by cells within the matrices would differ from the global strains applied by the bioreactor, and these local strains would change with time in culture. To investigate this hypothesis, we created finite element models of the three-dimensional hMSC-seeded collagen gels in an attempt to answer the following questions: 1. What are the local stress and strain fields experienced by cells within the three-dimensional collagen gels? 2. How do the local stress and strain fields vary at different time

points in culture? 3. What may be the difference between 10% and 12% applied global cyclic tensile strain that causes a significant difference in expression of BMP-2?

4.2 Methods

4.2.1 Mechanical testing

Eleven nonwoven Nylon mesh specimens (Cerex Advanced Fabrics Cantonment, FL) were tested in tension to determine the elastic modulus of the Cerex anchor of the TissueTrain (Flexcell Int., Hillsborough, NC) device (Fig. 4.1 B). The mesh material consists of spunbond Nylon 0.09 mm thick with a basis weight of 0.60 ounce per square yard which was stamp cut to dog bone shaped test specimens. The cross sectional area of each sample was determined by averaging measured width at three locations and multiplying it by the manufacturer-provided thickness. Previously unstrained specimens were incubated in phosphate buffered saline (PBS) for one hour then tested in tension using an EnduraTEC ELF 3200 (Bose, Minnetonka, MN) under ramp displacement control at 0.05 mm/sec (0.2% strain/sec) to 150% of maximum strain experienced by constructs when strained within the TissueTrain bioreactor. A 500 gram load cell was used to record the resulting forces. Elastic modulus was calculated by averaging the stiffness data from the linear portions of the stress-strain histories for each specimen.

Linear elastic moduli data of unstrained, 10%, and 12% axially strained hMSC-seeded collagen matrices cultured in either complete growth or osteogenic media were previously determined experimentally after 7 or 14 days through similar mechanical testing (Sumanasinghe 2007). In brief, Young's moduli and failure stresses of the hMSC-seeded collagen constructs were determined one day after completing culture strain regimen by applying a 0.5% per second constant strain rate

to a 10 mm central section of each matrix until failure using a 500 gram load cell with a force resolution of 0.03 g.

4.2.2 Actin staining

At 14 days in culture, actin morphology and alignment were visualized by staining the hMSC-seeded collagen matrices with Alexa 594 phalloidin (Molecular Probes, Eugene, OR). Matrices were rinsed twice in PBS and fixed for 30 minutes with 10% neutral-buffered formalin. After fixing, matrices were rinsed twice in PBS then incubated in buffer consisting of 0.2% Triton X-100 with 0.5% bovine serum albumin in PBS for 30 minutes. Matrices were then stained with 1ug/ml phalloidin in buffer for 20 minutes while protected from light. Following staining, matrices were rinsed twice with PBS and imaged at 10X magnification using fluorescence microscopy (Leica Microsystems Inc., Bannockburn, IL).

4.2.3 Finite element modeling

Previous studies have shown that mesenchymal tissue and type I collagen gel scaffolds initially have a linear elastic response under physiological loading frequencies (Loboa 2004, Roeder 2002). Therefore, the matrices were modeled as isotropic, linear elastic materials based on these studies and previous mechanical testing results from our laboratory (Sumanasinghe 2007).

In the present study, finite element models were designed and solved using ABAQUS CAE version 6.4-3 (ABAQUS, INC. Providence, RI). A total of eight

axisymmetric models, each representing one-half of the hMSC-seeded collagen gel at different time points, strain levels, and in either osteogenic or growth medium (Fig. 4.2), were constructed using geometry and material property data obtained experimentally (Table 4.1) and a Poisson's ratio of 0.49. Other studies have modeled type I collagen and hMSCs with Poisson's ratios near 0.49 or 0.50 (Simha 1999, Zhang 2005, Darling 2008). Models in the present study simulated hMSC-seeded collagen gels cultured in either osteogenic differentiation or complete growth medium, and exposed to 10% or 12% cyclic tensile axial strain, after 7 or 14 days time in culture. The shaft of each matrix was approximated with an elliptical cross section using width and thickness data taken in a previous study (Table 4.1) (Sumanasinghe 2008). In that study, the width and thickness data were taken by imaging the constructs in two planes and using Scanflex image analysis software (Flexcell, Hillsborough, NC), and mechanical property data were determined using the same technique described above for nonwoven Nylon anchors.

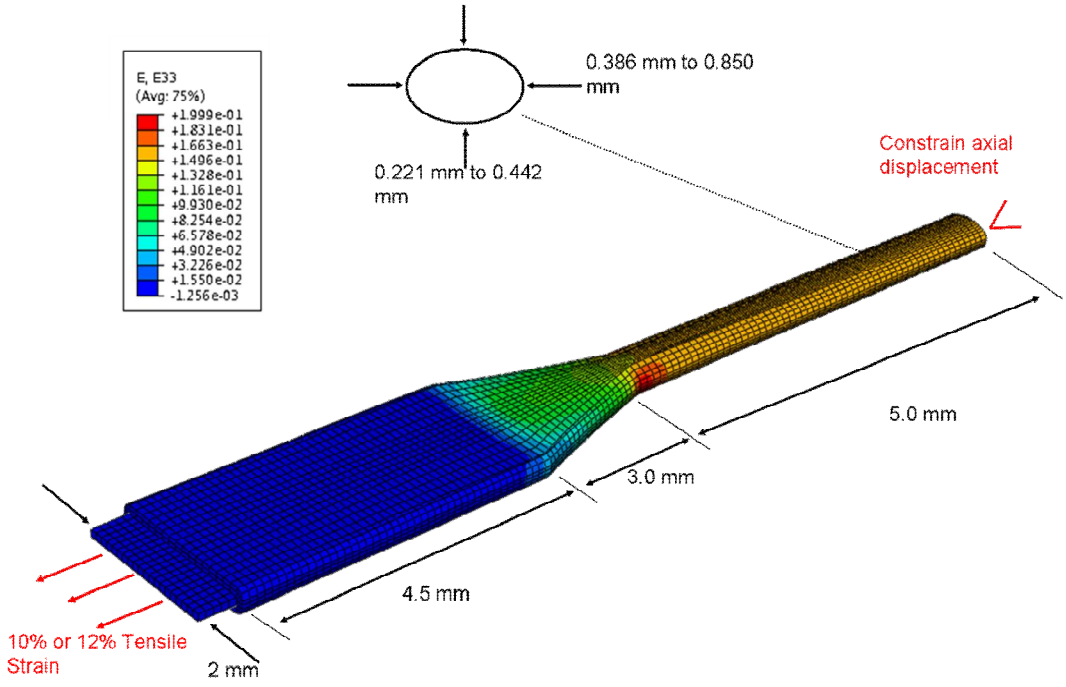

Figure 4.2. Representative example of matrix geometry with embedded anchor and boundary conditions. Detail shows shaft cross section. Shading illustrates strain resulting from matrix loading. Model shown is globally strained at 10% at 7 days in culture with osteogenic differentiating medium.

Table 4.1. Elastic Moduli and geometry of hMSC-seeded collagen gel matrices measured with respect to medium type (CGM: complete growth medium, ODM: osteogenic differentiating medium), time in culture and global cyclic tensile strain (Sumanasinghe 2007).

Medium	Time	Strain, %	E, kPa	Width, mm	Thickness, mm
CGM	7 days	10	469.24	0.6133	0.3205
		12	736.57	0.5724	0.2984
	14 days	10	2356.07	0.3756	0.2212
		12	1670.40	0.4118	0.2354
ODM	7 days	10	615.25	0.8498	0.4426
		12	493.04	0.7064	0.3456
	14 days	10	1339.20	0.6655	0.3897
		12	984.88	0.6310	0.3318

Average widths of the elliptical sections ranged from 0.386 mm to 0.850 mm and average thicknesses ranged from 0.221 mm to 0.442 mm. The anchor-attachment zone of the hMSC-seeded collagen gel was modeled to follow the anchor geometry with a small surrounding thickness (Fig. 4.3). The shaft was joined to the anchor attachment zone by lofting. One anchor was created for each model using geometry measurements taken from a TissueTrain plate (Flexcell Int.). An embedding constraint was used to attach the anchor into the matrix. The model was loaded by constraining axial motion at the midsection and applying a 10% or 12% tensile deformation to the end of the anchor.

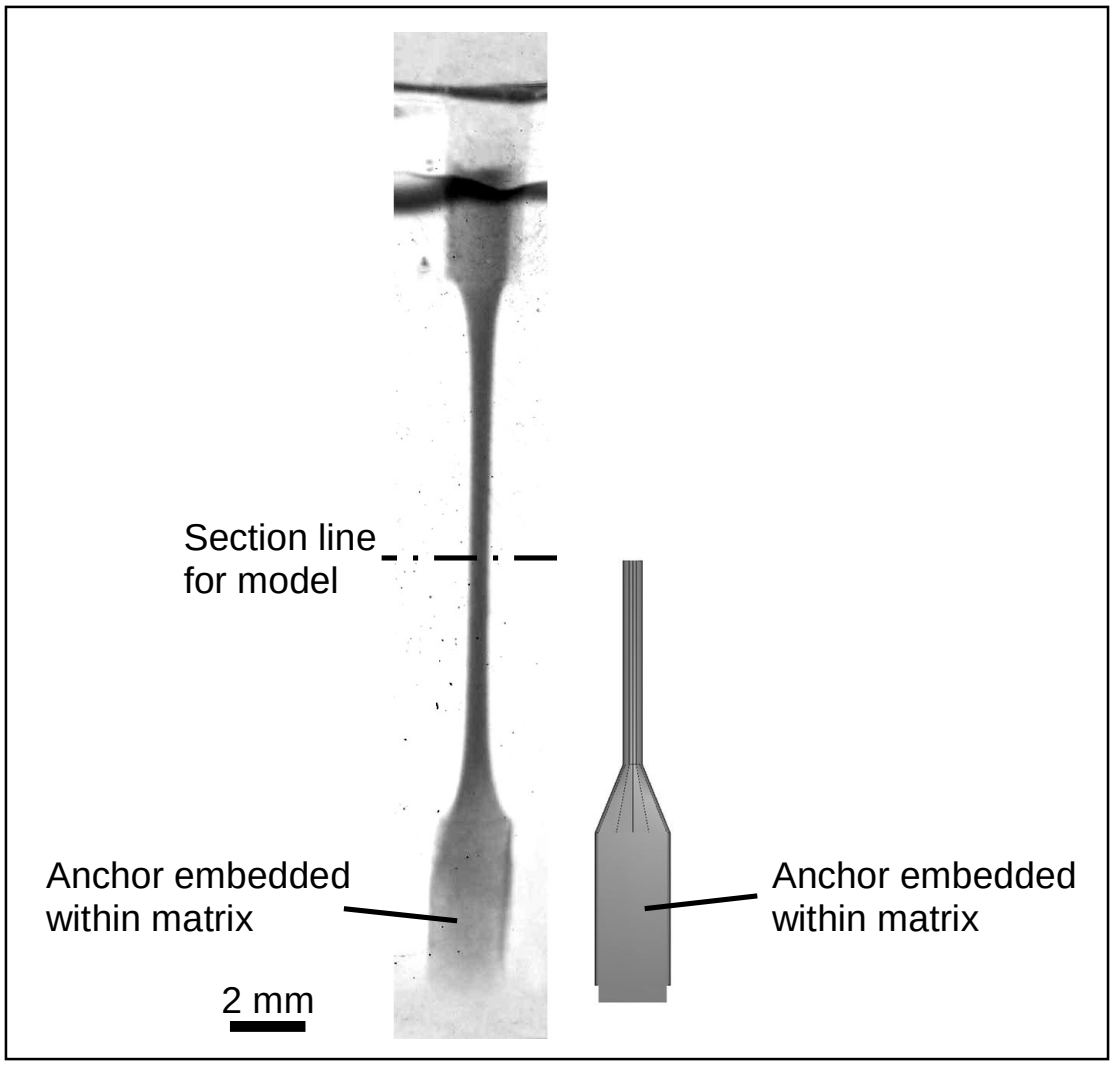

Figure 4.3. Comparison of representative hMSC-seeded collagen matrix on left with axisymmetric finite element model on right.

Each completed model consisted of approximately 15,000 hexahedral elements. A linear static solution was conducted and stress and strain fields were recorded for each model. The reaction forces on the anchors necessary to achieve each strain were also recorded.

4.3 Results

4.3.1 Mechanical testing

Eleven nonwoven nylon mesh specimens had an average stiffness of 16.3 MPa with a standard deviation of 3.6 MPa. All specimens exhibited linear stress-strain relationships to the applied displacements (Fig. 4.4). The data from one specimen were not included due to inadequate nylon fiber mesh density, which led to immediate rupture.

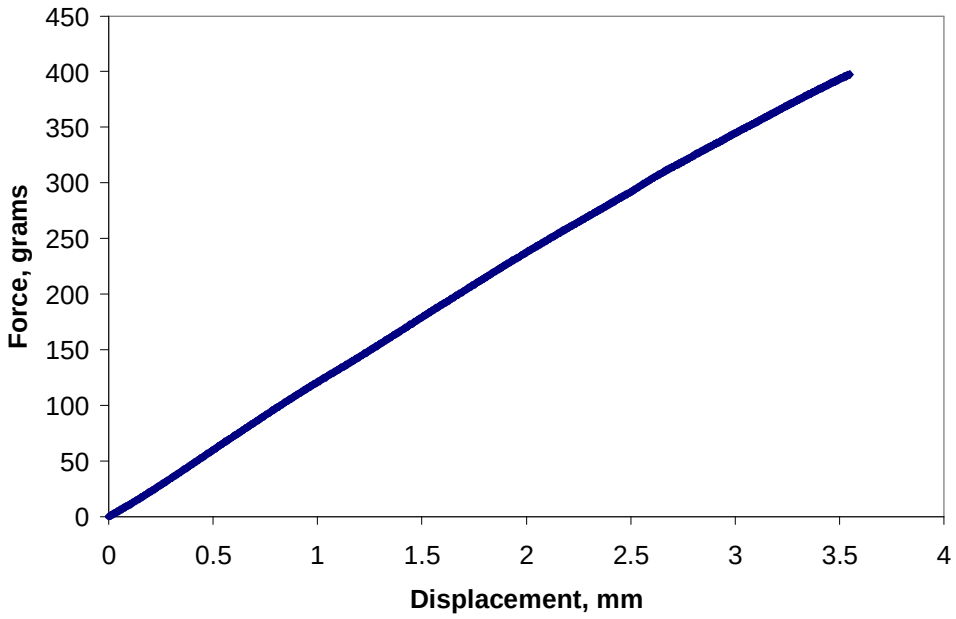

Figure 4.4. Representative example of linear response to loading during mechanical testing of nylon nonwoven mesh anchors.

4.3.2 Cytoskeleton staining

Representative images taken near the center of the hMSC-seeded collagen gels appeared to show increased number of actin fibers and more consistent actin organization in matrices globally strained at 10% (Fig. 4.5 A, C) compared to 12% (Fig. 4.5 B, D). Fiber alignment in the applied strain direction (horizontal) also appeared to be more consistent in matrices globally strained at 10%.

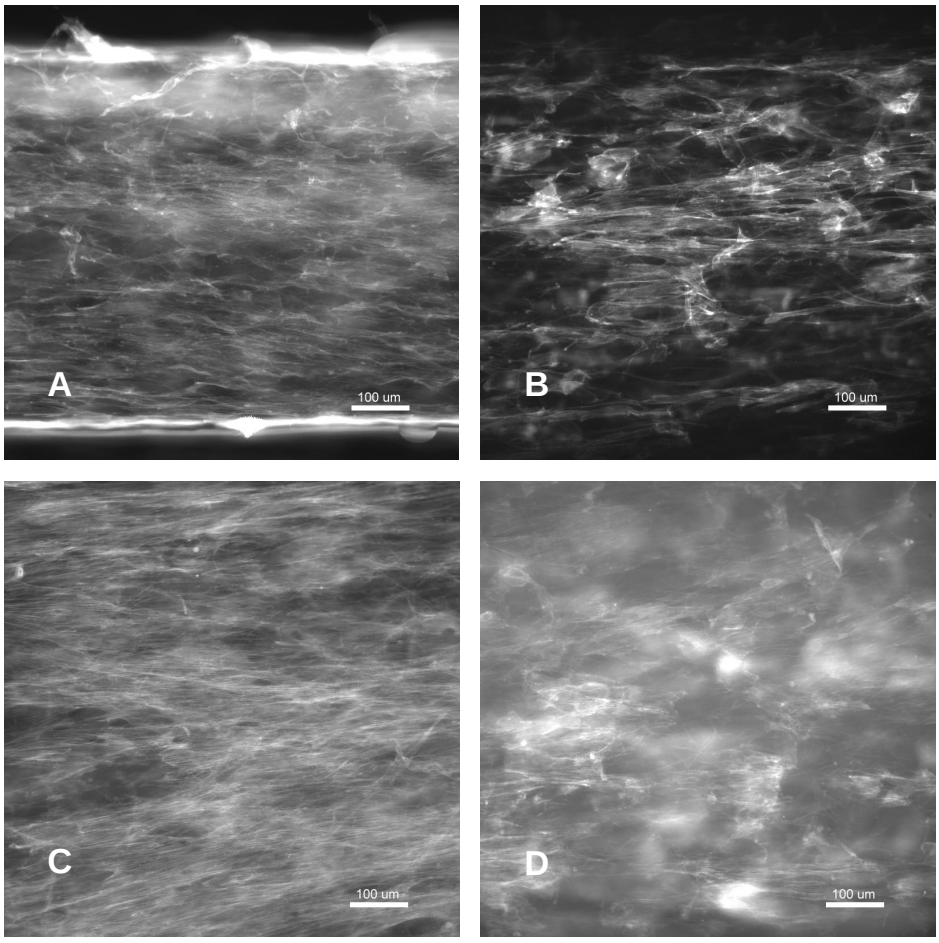

Figure 4.5. Actin filaments within matrices stained with Alexa 594 phalloidin. Matrices globally strained at 10% (A and C) and 12% (B and D). Matrices cultured in complete growth medium (A and B) and osteogenic differentiation medium (C and D).

4.3.3 Axial strain

The strain magnitudes were highest within the central contracted portion of the matrices, gradually decreasing with the increase in cross section to the anchor, and lowest in the portion overlapping the anchors (Fig. 4.6). All models indicated local strains higher than the applied global strains within the central portions of the matrices. Depending on the specimen type being modeled, the increase in local strain over global strain varied from 6.4% to 9.8%. The greatest increase of 9.8% over applied strain was found in the 14 day matrix strained globally at 12% (local strain = 21.8%) while cultured in complete growth media (Fig. 4.6 A). The lowest increase of 6.4% over applied strain was found in the 7 day matrix globally strained at 10% (local strain = 16.4%) cultured in osteogenic differentiation media (Fig 4.6 B).

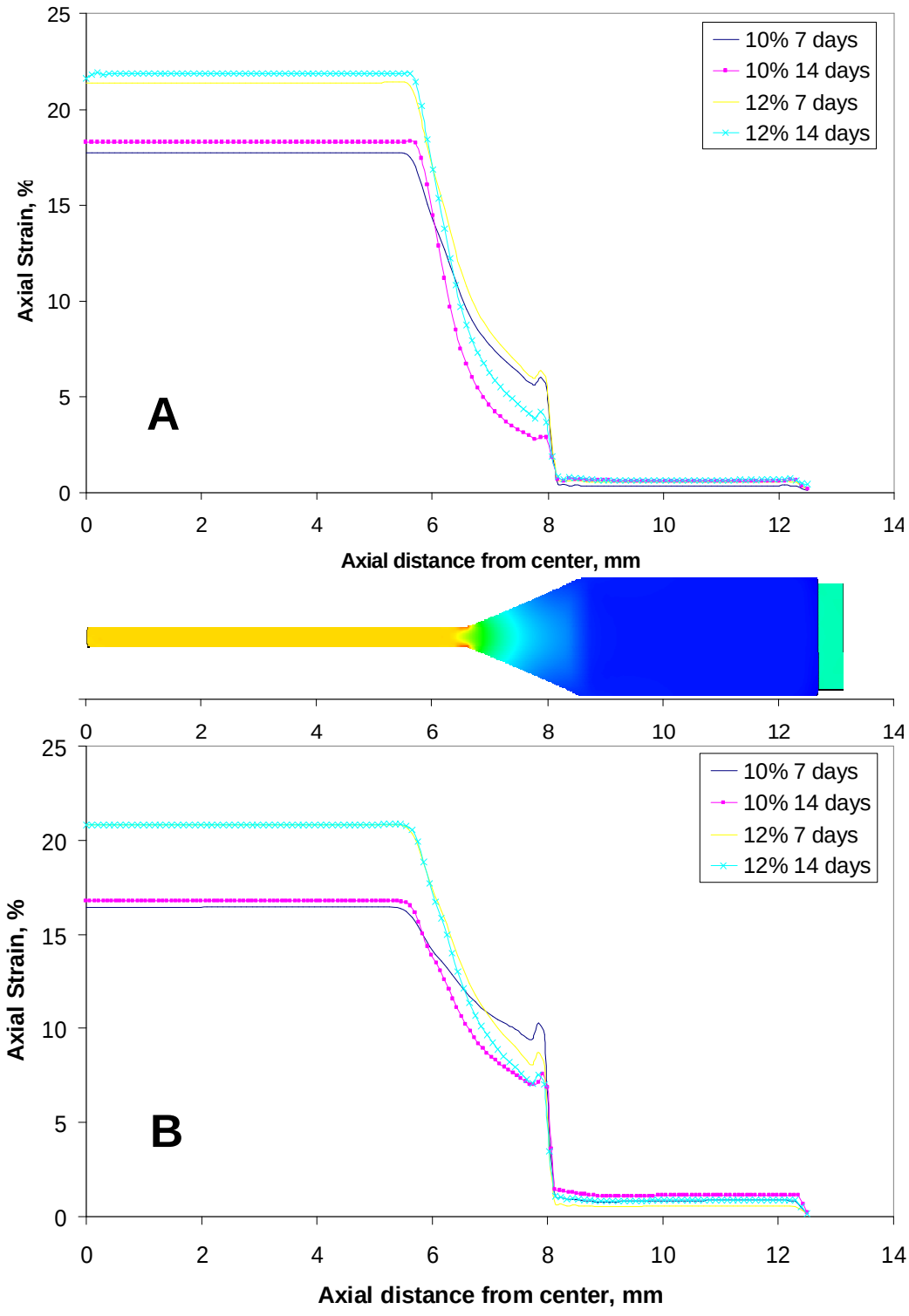

Figure 4.6. Axial strain as a function of distance from center of matrices cultured in A) complete growth medium and B) osteogenic differentiating medium.

4.3.4 Axial stress

Stress fields followed a similar distribution to the strain fields described above (Fig. 4.7). The stress experienced by the central portion of the matrices varied from 83.2 KPa in the model representing a 7 day matrix globally strained at 10% cultured in complete growth medium (Fig. 4.7 A) to 430 KPa as indicated in the model of a 14 day matrix globally strained at 10% cultured in complete growth medium (Fig. 4.7 A).

4.3.5 Axial displacement

Axial displacements were linear through the central contracted portions of the matrices (Fig. 4.8). As the model stiffness increased through the greater cross section near the anchor, the change in displacement decreased. The portions of each model where the collagen gel overlapped the anchors exhibited much stiffer behavior than the rest of the model.

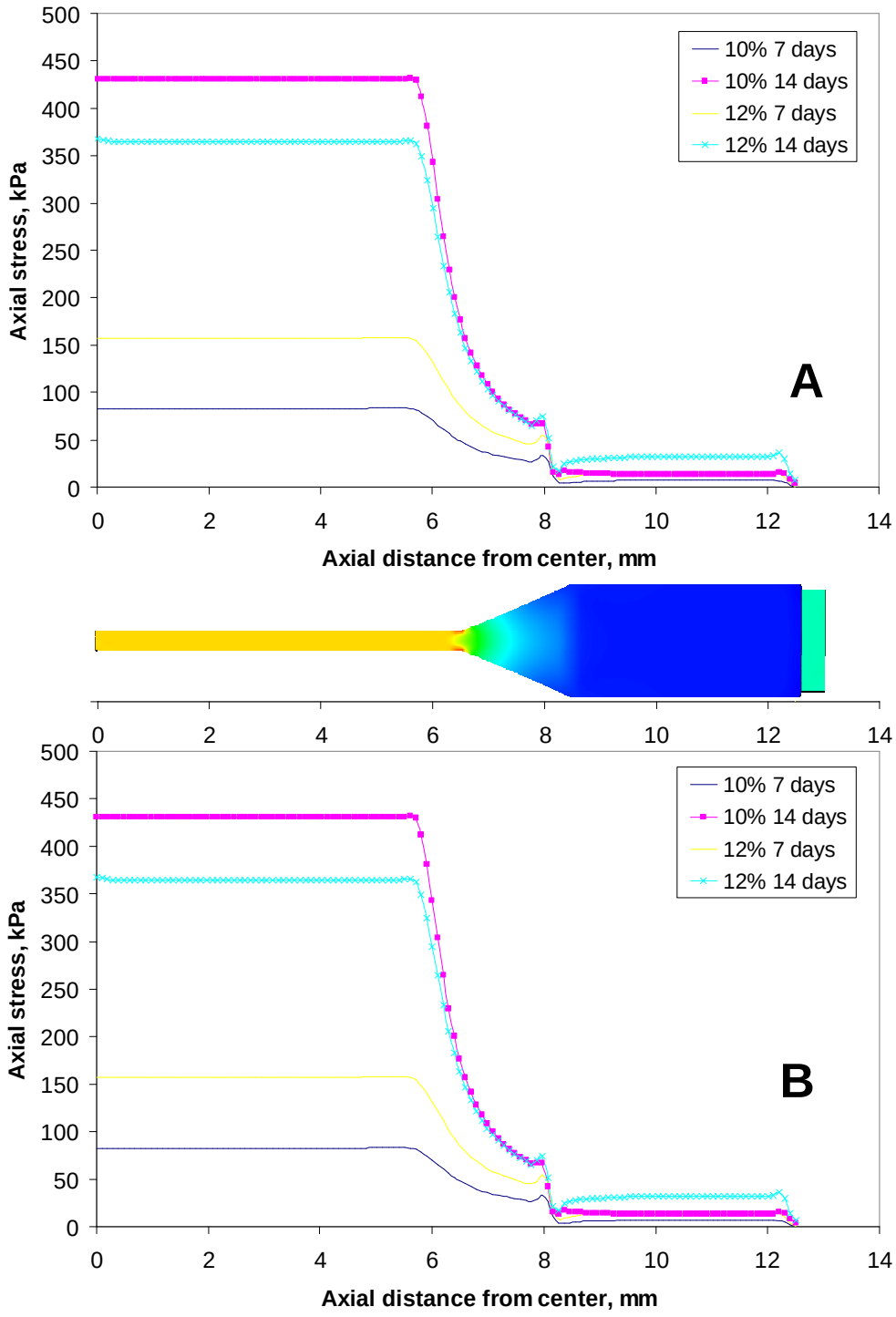

Figure 4.7. Axial stress as a function of distance from center of matrices cultured in A) complete growth medium and B) osteogenic differentiating medium.

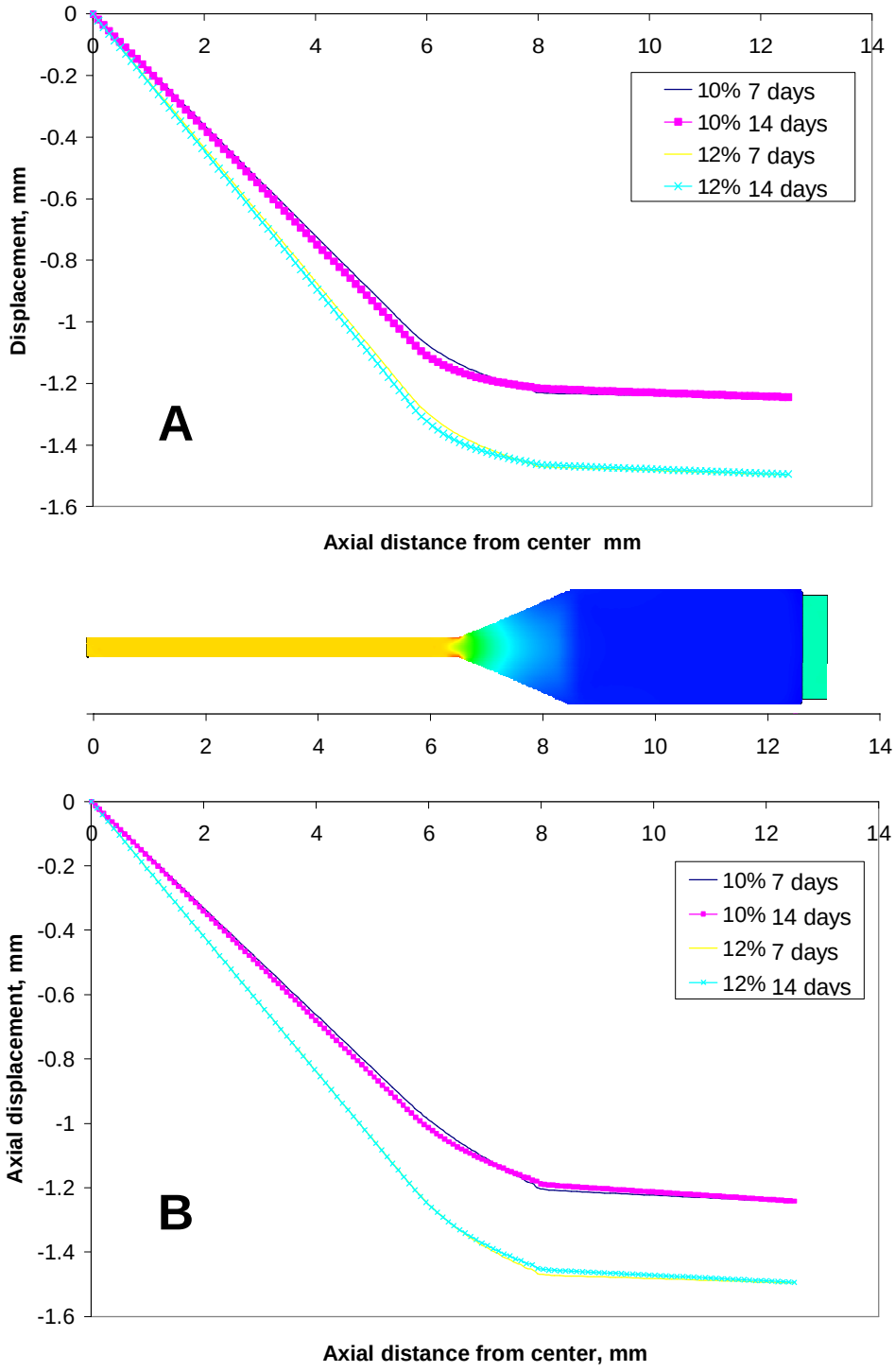

Figure 4.8. Axial displacement as a function of distance from center of matrices cultured in A) complete growth medium and B) osteogenic differentiating medium.

4.3.6 Effect of culture duration

Axial strain increased only marginally within the central section of all models from 7-day to 14-day hMSC-seeded collagen matrices (Table 4.2). Axial stress within the central contracted portion increased in models of matrices cultured in complete growth medium from day 7 to day 14 (Table 4.2). The greatest increase was within the 10% globally strained matrices cultured in complete growth media. The lowest increase in stress was indicated by the models of the 12% globally strained matrices cultured in osteogenic differentiation media.

Table 4.2. Summary of finite element model results in center of cell-seeded construct by medium type, time in culture and global applied strain. CGM: Complete growth medium; ODM: Osteogenic differentiating medium.

Medium	Time	Global Applied Cyclic Tensile Strain, %	Average Local Axial Strain, % (St Dev)	Average Local Axial Stress, kPa, (St Dev)
CGM	7 days	10	17.7 (0.03)	83.2 (0.1)
		12	21.4 (0.01)	157.5 (0.3)
	14 days	10	18.3 (0.02)	430.4 (0.1)
		12	21.8 (0.04)	365.1 (0.5)
ODM	7 days	10	16.4 (0.08)	101.2 (0.3)
		12	20.8 (0.06)	224.8 (0.1)
	14 days	10	16.8 (0.0003)	102.6 (0.2)
		12	20.8 (0.04)	205.2 (0.2)

4.4 Discussion

In the present study, we created 3D finite element models to determine the local stress and strain fields experienced by hMSCs cultured in 3D collagen matrices and exposed to global cyclic tensile strains of 10% and 12%. We have previously shown that these apparently similar magnitudes of cyclic tensile strain result in distinctly different responses by hMSCs in 3D collagen gels with respect to BMP-2 mRNA expression, matrix contraction, nuclear morphology and orientation, and tensile properties of hMSC-seeded collagen gels (Sumanasinghe 2006, 2007 2008,). In the present study, the local strains varied with axial location in all models. The greater stiffness of the nylon nonwoven anchors caused stress shielding of the surrounding portion of the more compliant hMSC-seeded collagen matrix. This resulted in the remaining portion of the hMSC-seeded collagen matrix between the anchor tips experiencing an increased strain.

The 14 day models yielded higher axial stresses than 7 day models representing equivalent global strains and medium types, although the change was less for specimens cultured in osteogenic differentiating media as compared to complete growth media. The increases in stress from 7 day models to 14 day models were due in large part to decreases in cross sectional area. The 14 day specimens cultured in complete growth media had smaller cross sectional areas than the 14 day specimens cultured in osteogenic differentiating media. The smaller matrix area contributed to the increased stress. The actin fibrillar network appeared to be more diffuse and have more densely concentrated aggregates in the 12%

global strain matrices (Fig. 4.5 B, D) compared to the 10% global strain matrices(Fig. 4.5 A, C), which appear to have greater fibrillar density and alignment in the axial strain direction. This difference may be due to actin cytoskeleton damage that appears to occur in the 12% global strain matrices (Fig. 4.5 B, D). It is possible that local strains resulting from the 12% global strain may be above a threshold that the hMSCs can tolerate without damage, in light of the encouraging experimental results from the 10% global applied strain matrices, which exhibited a significantly higher fold change in expression of BMP-2 over unstrained controls (Sumanasinghe 2006). A connection between mechanical stretch and rat MSC F-actin filament arrangement has been previously reported (Qi 2005). Work by other investigators suggests that actin filament bundles affect overall cell mechanical properties (Deguchi 2006). Such a strain threshold would need to be confirmed with experimental analyses quantitating F-actin content and morphology.

Another large component affecting the local stress and strain fields was the effect the hMSCs had on cross section of the collagen matrix as a result of matrix contraction by the cells. As cells exert traction forces on their environment, the substrate or 3D matrix surrounding them is compacted (Harris 1987, Tranquillo 1992, Choquet 1997, Sumanasinghe 2008). With longer times in culture, the hMSCs continued to reorganize and compact the collagen matrix, causing the volume, thickness, and width to decrease. In three of the eight models, the predicted axial stress experienced by matrices in culture was greater than the failure stress levels reported previously during mechanical testing (specifically 430, 157, and 365 kPa

model stress as compared to 171, 124, and 195 kPa failure stress for cell seeded collagen gels cultured in complete growth medium subjected to 10% strain for 7 days, and 12% axial strain for 7 and 14 days respectively) (Sumanasinghe 2007). This was likely due to variations in methods by which the failure stress was calculated in the previous experimental studies and this study. The previous experimental studies measured cross-sectional area of the hMSC-seeded collagen matrices in an unstrained condition. When mechanical testing was conducted, the engineering failure stress was calculated based on the area of the initial unstrained cross-section. The finite element models created in this study decreased in cross-section as strain was applied due to Poisson effects, and the axial stress reported was based on the changing geometry.

As illustrated by the difference between 7 day and 14 day time points (Table 4.2), the global applied strains of 10% and 12% did not create consistent stresses within hMSC-seeded collagen matrices throughout the culture duration. It is possible that the hMSCs deposited collagen or calcium within the matrix that might have caused the stiffness of the matrix to increase. Some studies have also shown mechanical strain increases stiffness of cell-seeded collagen gels (Shearn 2007, Sumanasinghe 2007) while another found no significant increase (Nirmalanandhan 2007). Mineralization was not verified in this study. In a bioreactor system without feedback such as the one investigated here, this straining method could lead to a decrease in the local strain experienced by cells. Another study found effective increases of 10% to 20% over prescribed strains on two-dimensional, biaxial BioFlex

(Flexcell, Int) culture plates which use similar rubber membrane substrates (Thompson 2007).

A limitation of this study is that the mechanical property and geometry data used in the models were taken from bone marrow-derived hMSCs from a single donor. It is possible that other cell lines may exhibit different results, as the amount of mineral or collagen deposited by hMSCs within the matrices may vary. It should also be noted that this study modeled hMSC-seeded collagen matrices in the linear elastic range of displacement, due to the applied cyclic strain frequency of 1 Hz. Another study used much longer loading durations and found viscoelastic properties of both cell-seeded and acellular type I collagen gels matrices when held in tension for one hour (Karamichos 2006). This difference in material response of collagen gels is expected, due to the significant difference between loading frequencies used in the two studies.

In this study, we simulated 3D hMSC-seeded collagen gel matrices through 3D finite element modeling. We applied geometry and material property data previously determined experimentally to create models of matrices at 7 and 14 days cultured in complete growth medium or osteogenic medium and subjected to 10% or 12% global tensile strain. These models were used to determine the local stresses and strains within the matrices at 7 and 14 days. We also suggest that damage to the actin fibrillar network may occur at strains above 10% which may inhibit expression hMSC of BMP-2 mRNA.

This study emphasizes the importance of understanding the relationship between global strains applied by a bioreactor and local strains experienced by cells in culture. Transitioning from one bioreactor system to another or between different cell types requires an understanding of this strain relationship in order to achieve desired results. As the use of mechanical stimulation becomes increasingly common to a multitude of cell types in culture, a more complete understanding of the effective loading applied to cells in culture should enhance experimental results.

4.5 Summary

As with hASCs, the use of human mesenchymal stem cells (hMSCs) in tissue engineering is attractive due to their ability to extensively self-replicate and differentiate into a multitude of cell lineages. It has been experimentally established that hMSCs are influenced by chemical and mechanical signals. However, the combined chemical and mechanical *in vitro* culture conditions that lead to functional tissue require greater understanding. In this study, finite element models were created to evaluate the local loading conditions on bone marrow derived hMSCs seeded in three dimensional collagen matrices exposed to cyclic tensile strain. Mechanical property and geometry data used in the models were obtained experimentally from previous studies in our laboratory (Sumanasinghe et al 2009 A, 2009 C) and from mechanical testing. Eight finite element models were created to simulate three-dimensional hMSC-seeded collagen matrices exposed to different levels of cyclic tensile strain (10% and 12%), culture media (complete growth and osteogenic differentiating), and durations of culture (7 and 14 days). Through finite element analysis, it was determined that globally applied uniaxial tensile strains of 10% and 12% resulted in local strains up to 18.3% and 21.8%, respectively. Model results were also compared to experimental studies in an attempt to explain observed differences between hMSC response to 10% and 12% cyclic tensile strain.

5. Semiautomated Finite Element Mesh Generation Methods for a Long Bone

The previous studies applied experimental and computational analyses to cell culture *in vitro*. We determined ranges of strains and forces that stem cells are differentially responsive to for inducing osteogenesis. In this study, we now move closer to a clinical application by examining finite element mesh generation methods for creating patient specific models using noninvasive computed tomography imaging. We are interested in evaluating the effectiveness of three different mesh generation techniques for estimating strains of a bone under physiological loading conditions. After creating these models, a mechanical testing of a bone is used to experimentally validate the computational results.

5.1 Introduction

Noninvasive data acquisition methods, such as computed tomography (CT) imaging, have become useful tools for assisting physicians with surgical planning of complicated orthopaedic procedures. However, these imaging methods do not provide detailed data about material properties of bone and other tissues. Such information would be useful to surgeons during presurgical planning of more complicated procedures. Reconstructive surgery, such as distraction osteogenesis, often involves numerous complicated and painful procedures. The time and expense required to correct injuries could be decreased if a more complete understanding of the patient was available to surgeons. Preoperative planning using finite element models derived from CT imaging data could provide such patient specific information for complicated reconstructive procedures (Remmler et al 1998).

Finite element analysis is a well established tool for determining stresses inside bone subjected to hypothetical loading conditions. However, an accurate finite element simulation of *in vivo* conditions requires proper physiological data. CT imaging is a useful method to gather three dimensional physiological data such as geometry and density of bone *in vivo*. This image data can be used in manual segmentation of the bone to generate idealized surfaces for creating finite element models. However, the time required to produce models by this method is prohibitively high to yield patient-specific results. Since 1990, numerous attempts to create semi-automated mesh generation methods have been undertaken with varying results (Keyak et al 1990, Marom and Linden 1990, Les et al 1997).

It has been shown by Crawford *et al*. (2003) that voxel-based, finite element model-derived estimates of bone strength were reasonably accurate compared to *in vitro* compressive strength. Lengsfeld *et al*. (1998) showed that rough gradient, material property, voxel-based modeling yielded results comparable to geometry-based modeling. Cattaneo *et al*. (2000) suggested that an improved method for defining the material properties of bone was to use different equations to convert the CT Hounsfield Unit values into material properties of cortical and trabecular bone by varying both elastic modulus and Poisson's ratio. However, Wirtz *et al* claimed no correlation had been found between bone density and Poisson's ratio (2000). Rho *et al* suggested using linear or power regression equations to convert apparent density values into elastic moduli (1995). The uniform voxels that make up such finite element models lead to interesting challenges.

One inherent limitation with voxel-based modeling is the jagged contours that result along the surface of the model. Camacho *et al* presented an automated element reshaping method to smooth the jagged contours of a three dimensional voxel-based mesh, which slightly improved surface stress prediction (1997). Other smoothing techniques have been reported for contact problem analysis that required user interaction to specify planes of contact within the model (Grosland and Brown 2002). In order to automate the creation of finite element models based on CT image data, user interaction should be minimized. To address this concern, the focus of this study is to develop a semi-automated mesh generation method to build a computational model that can be used to accurately simulate the response of bone

in four-point bending without mesh smoothing. We hypothesize that such a model with nonuniform material properties could more accurately simulate bone than a uniform elastic modulus geometry-based model.

5.2 Methods

5.2.1 Specimen isolation

One left radius, 181.2 mm in length, was harvested from a 25 kg adult mongrel dog obtained from the North Carolina State University Veterinary School farm. The subject had been euthanized due to shelter overpopulation and the radius was harvested on the same day from the cadaver. The radius was scanned in air with a third generation CT system (GE Sytec Sri 3000, GE Medical Systems, Milwaukee, WI), and the resulting image data were utilized in finite element mesh generations of the same radius. The canine radius was stored at -20 C until mechanical testing was conducted.

5.2.2 Mechanical testing

The same left canine radius imaged by CT was mechanically tested to determine strains in the bone while undergoing four-point bending. Mechanical testing was performed similarly to previous studies (Carter et al 1981, Turner and Burr 1993). Briefly, the bone was thawed to room temperature, and the midshaft diaphysis was scraped clean of soft tissue to allow proper bonding of strain gages. The bone was kept hydrated with phosphate-buffered saline throughout preparation and testing. Three uniaxial strain gages (5.6 mm wide, 13.22 mm axial length; Vishay Micro-Measurements Raleigh, NC) were applied around the periphery of the midshaft diaphysis on medial, lateral and caudal sides (Fig. 5.1). Each strain gage was fully encapsulated with preattached lead wires. This helped avoid electrical

interference from the saline solution. Gage bonding was conducted following a procedure suggested (Vishay 1992): After soft tissue was removed, a bonding catalyst and cyanoacrylate were used to apply strain gages to the bone.

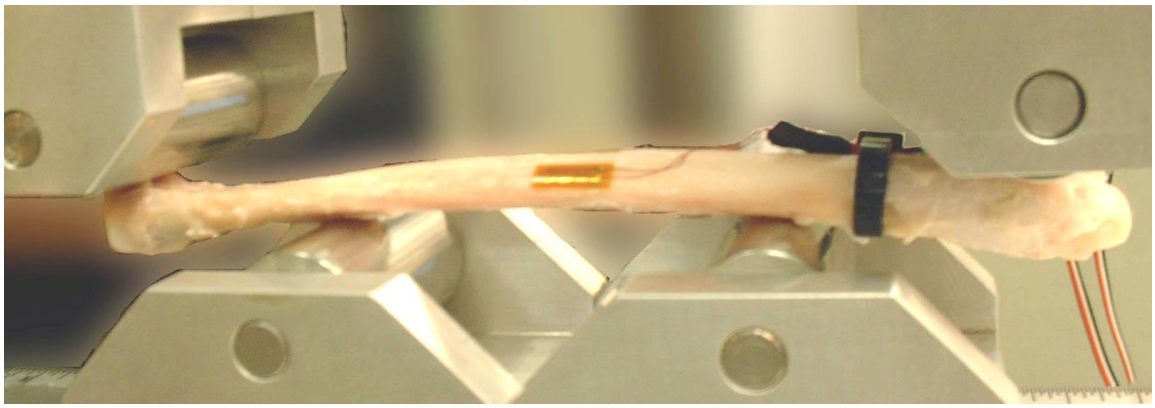

Figure 5.1. Canine radius in loading frame during four-point bending mechanical test.

Strain gages were connected to an SC-2043-SG strain gage conditioning board (National Instruments Corp., Austin, TX) configured in quarter bridge circuit and used in conjunction with a Lab-PC-1200 data acquisition board (National Instruments Corp., Austin, TX). An in-house program written in LabVIEW (National Instruments Corp.) processed and recorded signals from the strain gages on three channels at 10 Hz with 38 με resolution on one workstation computer.

Mechanical loading was conducted using an in-house four point bending apparatus and an 858 Mini Bionix II machine (MTS, Eden Prairie, MN). Center supports were set 76.2 mm apart and contacted the medio-caudal surface of the radius. Load was applied from above with supports 158.75 mm apart and contacting the cranio-lateral surface of the bone (Fig. 5.1).

The crosshead and upper loading frame were manually brought into contact with the bone. The quasistatic loading regimen applied to the bone was a sequence of ten 0.25 mm displacements separated by 5 second holds. The testing machine recorded displacement and force at 10 Hz on a second workstation computer. Resulting force was recorded with a 2500 N load cell. Elastic modulus was calculated based on force-displacement data and an average moment of inertia across the CT slices (Fig. 5.2) corresponding to strain gage locations. Moment of inertia was calculated by a custom Matlab program (The MathWorks Inc., Natick, MA). This program calculated centroid and moment of inertia across 13 CT slices representing bone contacting strain gages.

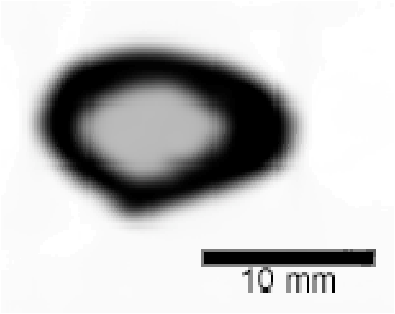

Figure 5.2. Computed tomography image of canine radius at mid-diaphysis.

5.2.3 Geometry-based model

A geometry-based CT segmentation method was used for comparison with the new voxel-based methodology. In order to conduct such a comparison, a full geometry-based model was created. The Mimics (Materialise, Ann Arbor, MI) software package was used to convert the CT data into a series of contours to simulate outer bone and intramedullary surfaces. These contours were converted into 20-point non-uniform rational B-spline (NURBS) surfaces by lofting the curves using the Rhinoceros NURBS modeling package (Robert McNeel & Associates, Seattle, WA). TrueGrid (XYZ Scientific Applications Inc., Livermore, CA) was then used to generate the finite element mesh based on NURBS surfaces. The outer edges and internal edges bordering the intramedullary space on an idealized hexahedral block model were projected onto NURBS surfaces for the outer diaphysis and intramedullary canal, respectively. Several surface nodes were adjusted to correct element warping and shape errors resulting from the projection. The mesh was incrementally built using TrueGrid in an iterative process while correcting any shape errors reported by the ANSYS finite element solver (Ansys Inc., Canonsburg, PA). Uniform material properties were assigned: 20.4 GPa (Gies and Carter 1982) elastic modulus and 0.39 Poisson's ratio. The model was constrained in all dimensions at a point representing the lower proximal support and from displacement in the vertical direction at a point representing the lower distal support. A negative vertical force was symmetrically divided and applied to the cranial side on points representing each of the upper loading posts of the four-point

bending fixture. This force was distributed among nodes corresponding to points of contact with the loading posts during mechanical testing. The estimated user time required to create this model was 80 hours. The model consisted of 263,999 hexahedron elements and 287952 nodes. This model was solved with a small displacement static condition in ANSYS in 2 hours 36 minutes.

5.2.4 Voxel-based models

To create voxel-based models, custom code was written in Matlab with Image Processing Toolbox to threshold voxels into elements. The first voxel-based model was created with nonuniform material properties. Separate equations were developed to represent cortical and trabecular bone material properties, based on data in the literature (Gies and Carter 1982, Hu et al 2002, Kang et al 1998). Elastic modulus (E, MPa) was calculated using CT Hounsfield Units (HU):

$$E = \begin{Bmatrix} 26.8657(\mathrm{HU}) - 8865.67 & 330 \le \mathrm{HU} < 1000 \\ 10(\mathrm{HU}) + 8000 & 1000 \le \mathrm{HU} < 2000 \\ 28000 & \mathrm{HU} \ge 2000 \end{Bmatrix}$$

In-plane voxel resolution was decreased in the interest of computational time, yielding effective voxel and element dimensions of 1 x 0.32 x 0.32 mm (slice thickness, width, height). Elastic moduli ranging from 0.001 to 28,000 MPa, as determined by data in the literature (Gies and Carter 1982, Hu et al 2002, Kang et al 1998), were assigned to each element based on the Hounsfeld Units for each group of 4 voxels. The volume representing the intramedullary canal was automatically

created and represented by low moduli elements and empty space. This model consisted of 275,395 nodes and 251,995 hexahedron elements with 168 different values for the elastic modulus. The model was constrained to match the mechanical testing procedure of the radius. A 492.3 N load was symmetrically divided and placed on the distal and proximal loading points. These loads were distributed over nodes corresponding to the points of contact with the loading posts in the mechanical testing apparatus. The model was supported by two constraints from below, corresponding to the supports in the mechanical testing machine (Fig. 5.3). One constraint allowed for sliding motion orthogonal to loading direction, and the other constrained all displacements. Computational meshes are shown in figure 5.3. This model was solved in 2 hours 38 minutes.

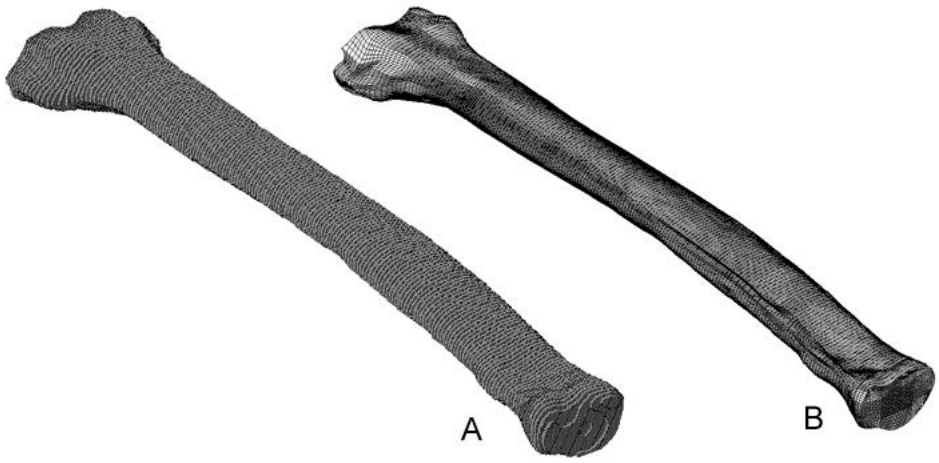

Figure 5.3. Finite element models of canine radius. A. Nonuniform voxel-based model. B. Geometry-based model. The uniform voxel-based mesh (not shown) appears nearly identical to the nonuniform voxel-based mesh.

A second uniform-modulus voxel-based model was also created for additional comparison to the geometry-based model. The program to create this model was altered to neglect voxels corresponding to bone marrow, since marrow does not significantly contribute to the structural properties of bone. The same 20.4 GPa uniform elastic modulus and 0.39 Poisson's ratio was assigned to this model as the geometry-based model. Loading and boundary conditions matched the above nonuniform voxel-based model. This model consisted of 236,213 nodes and 209,112 hexahedron elements. The computational time required was 42 minutes.

5.2.5 Overview of the voxel-based model creation program

The program used to create the voxel-based models consisted of several steps, resulting in an output script file readable by ANSYS. The source data set of computed tomography dicom images was loaded and combined into a three dimensional image tensor. This image tensor may be multiplied by a fractional scaling factor to reduce the final mesh size as desired. Each value within the image tensor represents a discrete volume in space.

The program then sequentially examined each intensity value within the scaled image tensor. When an intensity value was found which exceeded the threshold for bone marrow, new nodes were created around the volume represented by that value. The nodes were stored into a second 3D tensor called *nodes*. Node definition lines were written to the output file as new nodes were created.

As intensity values were found to exceed the marrow threshold within the image tensor, material property bin numbers were assigned to cells within a third 3D tensor called *matls*. After all values within the image tensor were examined, the values within the *matls* tensor were examined. As nonzero bin numbers were found, commands were written to the output file to specify material property bins and define elements based on the surrounding eight nodes of each brick element.

5.3 Results

Mechanical testing data was recorded by workstation PCs (Fig. 5.4). The three computational models were solved and nodal strains were averaged for areas corresponding to each of the three strain gages (Fig. 5.5). These averaged strains were compared to strain gage readings from mechanical testing of the canine radius in four-point bending. Standard deviation values were greater for computational models than mechanical testing results (Fig. 5.6). This is due to the nodal strain averaging in computational models, versus electrical noise from strain gage measurements. A correction factor multiple of 2.66 was empirically derived and applied to account for computational model overestimation of bone stiffness. The nonuniform voxel-based model was run ten times with different loads, equivalent to mechanical testing. The uniform voxel-based model and the geometry-based models were each run once, applying the highest load.

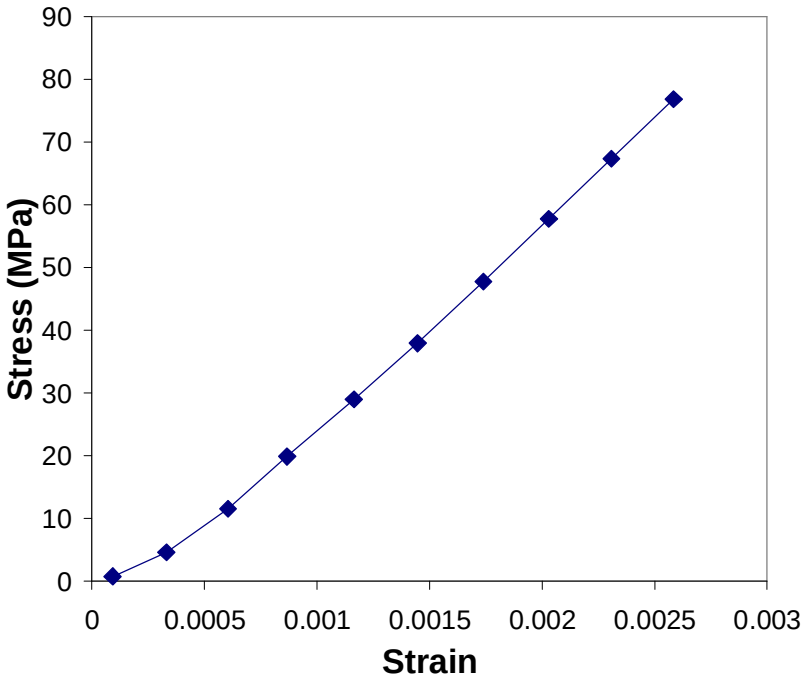

Figure 5.4. Stress-strain response of canine radius during mechanical testing. Note toe region during lowest strains, followed by highly linear elastic region.

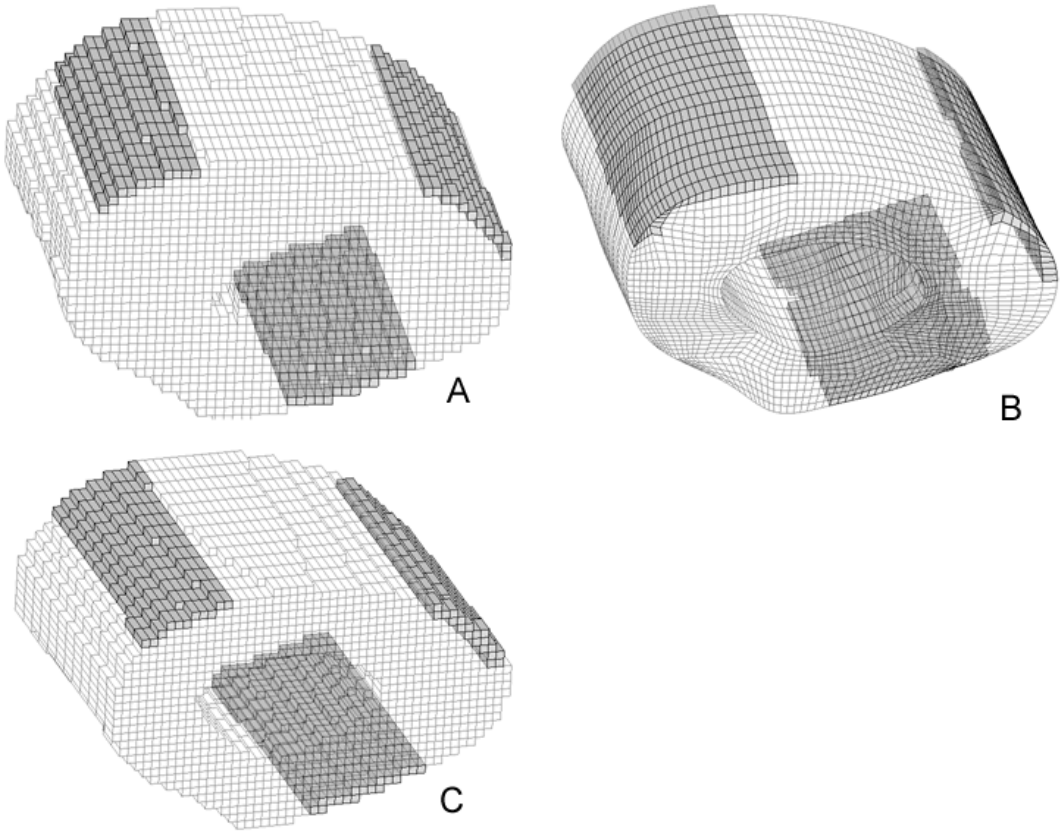

Figure 5.5. Midshaft slices of computational models with gage location elements highlighted. A. Nonuniform voxel-based model. B. Geometry-based model. C. Uniform voxel-based model. Note intramedullary canal appears larger in image C than A, since voxels representing low modulus tissue such as marrow are not included in the model.

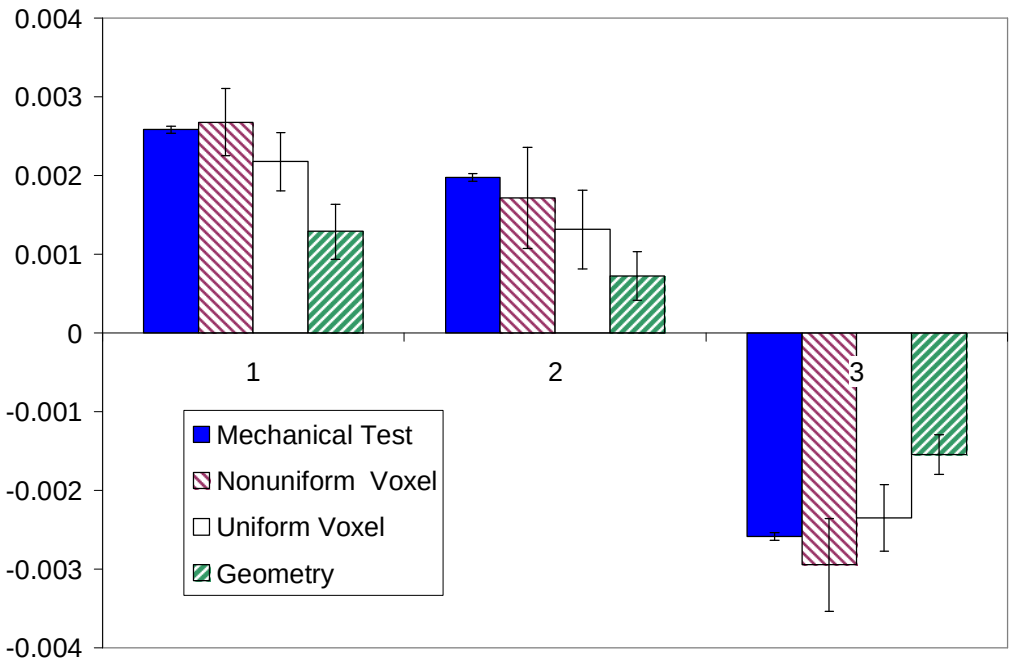

Figure 5.6. Comparison of strains measured by mechanical testing and predicted by computational models, with correction factor applied. Error bars indicate standard deviation. Note the closest results to mechanical test were found using the nonuniform voxel-based model.

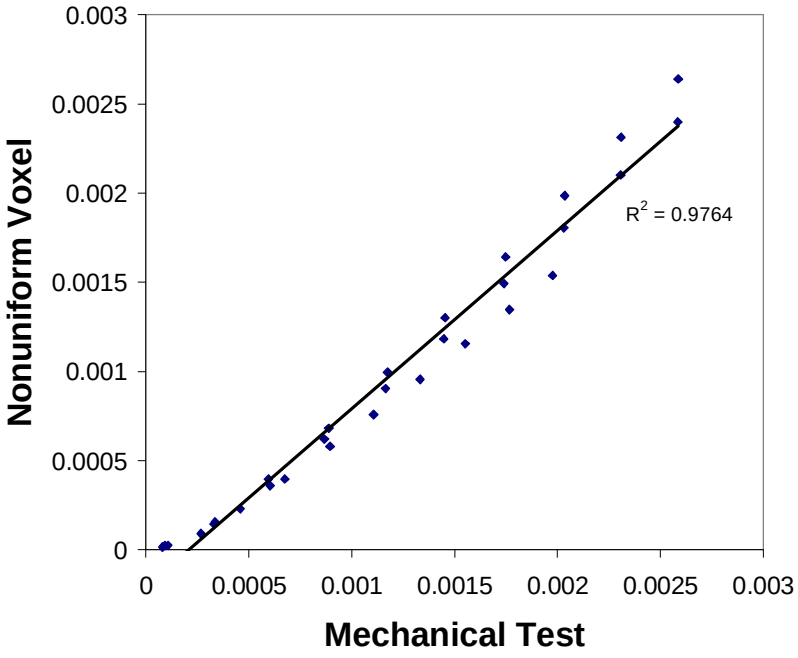

Figure 5.7. Strains found by mechanical testing correlate strongly with strains predicted by the corrected nonuniform voxel-based model.

A strong correlation (R^2 = 0.9764) was found between the strains during mechanical testing and corrected nonuniform voxel model strains (Figure 5.7). The nonuniform voxel-based model predicted strains with the best correlation (R^2 = 0.9972) to mechanical testing results at the maximum loading condition.

The average moment of inertia was 762 mm^4 $\pm$ 40. From this, the modulus of elasticity due to bending was determined to be 11.5 GPa, based on geometrical data from the bone and mechanical testing data. The following four-point bending equation was used to determine the modulus of elasticity:

$$E = \frac{F(L-a)^2(L+2a)}{48 \cdot d \cdot I},$$

where elastic modulus (E) was calculated from applied force (F), outer loading post span (L), inner loading post span (a), vertical deflection (d), and moment of inertia (I). The elastic modulus found in this study compares closely to recent findings on mechanical properties of canine trabecular bone, which found an elastic modulus of 11.2 GPa along the principal trajectory (Viceconti et al 1998). Geometry-based and uniform voxel-based models were additionally tested using the 11.5 GPa elastic modulus with little improvement over original modulus (Fig. 5.8).

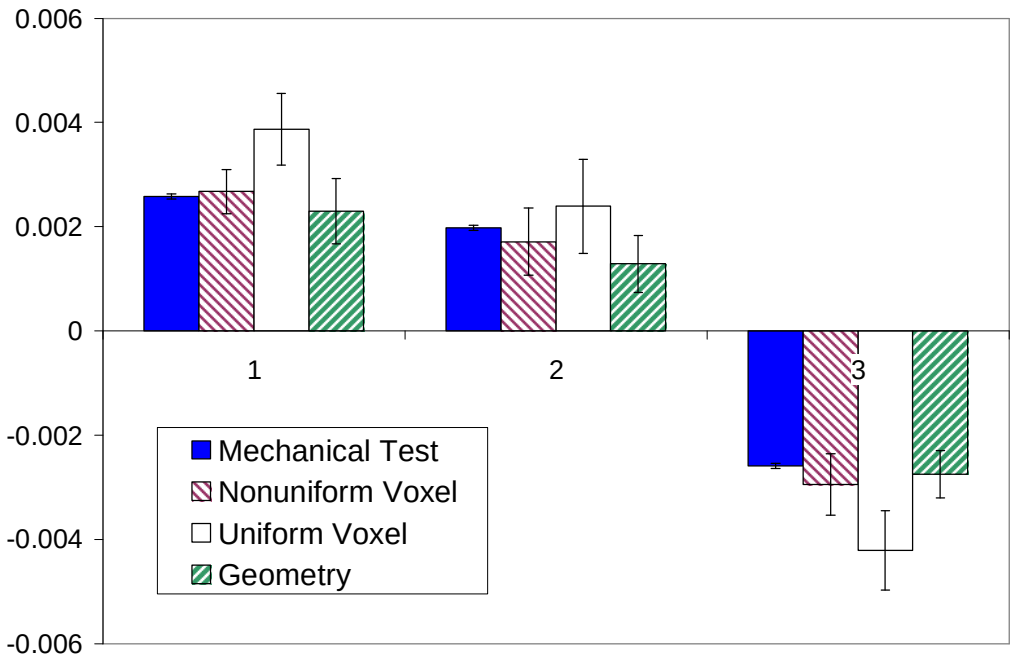

Figure 5.8. Comparison of strains when setting elastic moduli of uniform voxel and geometry models to 11.5 GPa, as found through mechanical testing. Error bars indicate standard deviation.

5.4 Discussion

The potential for improving an injured patient's life through orthopaedic surgery can be great. However, increasingly complex procedures require great physiological detail about the patient to be successful. A rapidly produced image-based computational model of bone could provide such detail for presurgical planning. In the present study, a method to quickly create a physiologically accurate finite element mesh from CT imaging data was developed. Although the speed at which such a finite element mesh can be created and analyzed (approximately 4 hours post CT-image data acquisition) would allow for use in patient-specific presurgical planning, this might not be fast enough to be implemented for emergency surgery situations. This method was compared to mechanical testing results and traditional geometry based finite element meshing techniques.

All computational methods included a correction factor to produce strains comparable to strains recorded with mechanical testing. This correction factor may vary with the conditions under which the bone is imaged that would typically affect CT imaging (e.g. beam hardening). Once corrected, the nonuniform voxel-based model results produced strains closest to mechanical testing strains. Our findings are consistent with previous studies that have also found accurate results with voxel based mesh generation methods (Crawford et al 2003, Lengsfeld et al 1998, Cattaneo et al 2000, Rho et al 1995, Viceconti et al 1998). The elastic modulus calculated from mechanical testing data is equivalent to results found in a recent study on canine trabecular bone (Pressel et al 2005) and to other investigators'

findings of the elastic modulus of selected canine radii (Gies and Carter 1982). Although the canine radius is a long bone with a cortical shell, the composite material properties of the bone examined in this study approximate that of trabecular bone.

In order to limit user interaction required and to speed model creation, no smoothing routines were required or used in the creation of the voxel based models. Only eight-node hexahedral elements were used in the voxel based mesh creation. This element formulation is generally considered to produce more accurate results than tetrahedral element meshes.

A current limitation to this study is that the material properties can only be used to describe bone. The nonuniform voxel-based method would need to be adapted to accurately describe other tissues or to employ other imaging modalities. Also, only physiological strains were examined in this study. Our approach could be adapted to simulate super-physiological and failure strains. If simulation of contact problems was desired, our approach would likely require modification to include smoothing. The geometry-based model was constructed of elements consisting of only one elastic modulus in order to speed model creation. This model could be expanded to encompass multiple bone types, but would require much more effort as compared to the voxel-based model.

The mesh generation method developed in this study met the goal of rapidly creating a finite element model by converting CT image data of a long bone into a physiologically accurate mesh. This mesh responded proportionally to mechanical

tests performed on the same bone imaged. When a correction factor multiple was applied to the strains found through solution of the computational model, the results compared closely with mechanical testing. In future work, the method described in this study could be adapted for use on additional tissue types to expand its functionality. The non-uniform voxel-based method described in this study is readily adaptable for use in new tissue types, given proper physiological data.

This is the first study to compare a non-uniform elastic modulus voxel-based finite element meshing method to traditional geometry based and uniform modulus voxel-based methods created from CT data of a canine radius. Furthermore, this study has also validated the results of these different methods against mechanical testing results. The speed at which a non-uniform voxel-based model can be created and the ability to fine-tune equations to specify material properties based on imaging data make it the method of choice to rapidly create patient-specific finite element models.

Creation of the geometry-based finite element mesh proved to take much more time than anticipated. This was due in large part to the mesh density requirements in order to match the voxel-based models. While geometry-based models are certainly required in many circumstances, their mesh densities should be optimized as low as possible to limit the required user interaction. Voxel-based models hold great potential for providing fast and accurate finite element simulation of bone, and are preferred when numerous unique models are required in a short amount of time.

5.5 Summary

The objective of this study was to develop and test a semi-automated finite element mesh generation method using computed tomography (CT) image data of a canine radius. This study employed a direct conversion from CT Hounsfield units to elastic moduli. Our method attempted to minimize user interaction and eliminate the need for mesh smoothing to produce a model suitable for finite element analysis in a clinically-relevant time period. Validation of the computational model was conducted by loading the CT-imaged canine radius in four-point bending and using strain gages to record resultant strains that were then compared to strains calculated with the computational model. Geometry-based and uniform modulus voxel-based models were also constructed from the same imaging data set and compared. The nonuniform voxel based model most accurately predicted the axial strain response of the sample bone ($R^2 = 0.9764$).

6. Conclusions and Recommendations for Future Research

6.1 Conclusions

The studies comprising this dissertation examine mechanical stimuli applied to human stem cells using both experimental and computational approaches. Human adipose derived adult stem cells and bone marrow derived mesenchymal stem cells were exposed to multiple forms of mechanical stimuli while maintained in either two or three-dimensional culture. Viability, proliferation, calcium accretion, actin cytoskeletal alignment, and BMP2 and RUNX2 mRNA expression were measured in order to determine the effects of the diverse mechanical stimuli for inducing osteogenesis in human adipose and bone marrow derived adult stem cells. Finite element analyses were also conducted to simulate the loading regimes applied to these adult stem cells in order to predict and elucidate local strains most effective for inducing osteogenic differentiation. In addition, three different finite element mesh generation methods were evaluated in an effort to automate the time-intensive process of creating accurate models of bone.

Chapter two described a novel three-dimensional porous scaffold for human stem cell culture and the response of human adipose derived adult stem cells to three magnitudes of pulsatile fluid shear stress. These investigations found the scaffold material to be a viable substrate for human stem cells for at least three days in culture. Initial investigations also found a significant increase in hASC mRNA

expression of RUNX2 following one hour of pulsatile fluid shear stimulation at a shear stress of 3 dynes/cm^2.

The third chapter examined hASC calcium accretion in 2D culture in response to 14 days of uniaxial cyclic tensile strain on a Bioflex plate in the Flexcell system. A strain of 10% was applied to the center portion of each well membrane and finite element analysis was conducted to calculate global strain induced local strains throughout the strained well diameter. Results indicated that greatest calcium accretion occurred after 14 days in regions of the membrane that experienced between 7.7% and 20.4% local cyclic tensile strain.

Chapter four described investigations into the local strains experienced by hMSCs as a result of 10% and 12% global cyclic tensile strain application within three-dimensional Type I collagen gels. Finite element analyses were conducted using geometry and material property data of the hMSC-seeded collagen gels at 7 and 14 days. Results indicated that local cyclic tensile strains of 16.8% were effective in promotion of osteogenesis. Further analysis of the actin cytoskeleton within cell-seeded collagen gels found greater axial alignment in the 10% globally strained specimens (16.8% local), and suggested global strains of 12% (21.8% local) may induce cytoskeletal damage.

The final study examined different methods of semi-automated mesh generation for finite element models of bone. Computed tomography image data of a canine radius was used to create one geometry-based and two voxel-based finite element models. Mechanical testing of the canine radius in four-point bending was

then used to validate the effectiveness of each finite element model for predicting physiological strains. The nonuniform voxel based model was found to most closely predict both compressive and tensile strains experienced during mechanical testing.

Combined, this dissertation addresses the problem of creating engineered bone tissue replacements. This is the first work to show the influence of fluid shear on adipose derived human adult stem cells in three dimensional culture. It is also the first publication to determine global induced local strains effective for inducing osteogenesis of adult stem cells in two dimensional and three dimensional culture. By determining mechanical stimuli appropriate for osteogenesis, this work significantly advances the field of functional bone tissue engineering.

6.2 Recommendations for future research

This body of work describes several new findings resulting from original research, but as is always the case in science, there are several questions that may be answered by additional future research by other investigators. One limitation of Chapter 2, the study in which pulsatile fluid shear stress was applied to hASCs, was that only a single time point was investigated for mRNA expression of osteogenic markers. The one hour fluid shear excitation applied to hASCs may not have been long enough to induce a detectable change in BMP2 mRNA expression. Further investigations could examine combinations of additional stimulation times and longer incubation periods following application of pulsatile fluid shear in order to allow hASCs additional time to respond to the fluid shear stimulus.

A limitation of the study in Chapter 3 was the size of each rectangle used to quantify calcium accretion. While only 3.5 mm wide, a large range of strains existed within some segments of the strained well diameter. This prevented more precise correlations between regions of greatest calcium accretion and the local strains. Future studies could employ techniques that allow for a higher spatial resolution in the measurement of calcium accretion, such as Raman or Fourier transform infrared spectroscopy (FTIR).

Two potential limitations were evident in the study described in Chapter 4. The first is that the geometry and mechanical property data of the hMSC-seeded collagen gels used in the finite element models was taken from only one donor cell line. We expect some donor-to-donor variability; however the extent to which this is a factor cannot be fully understood until replicate experiments are performed with additional cell lines. A second potential limitation is that the finite element model assumed linear elastic material property behavior as is appropriate for physiologic loading of 1 Hz and in accordance with our experimental protocol. If one wanted to investigate hMSC response to strains applied at a slower loading rate, a different constitutive model which includes viscoelastic effects should be incorporated. Future studies should take this into consideration and potentially add time-dependent effects to the finite element model.

A limitation to the study presented in Chapter 5 is that the semi-automated mesh generation methods can only build models consisting of bone from computed tomography data sets. Additionally, the rectangular shape of each element created

in that study can prevent accurate simulation of contact between two objects. In order to address these limitations, future studies may benefit by including additional imaging modalities, such as magnetic resonance, and assign material properties for a broader range of tissues, such as muscle or ligament.

While this dissertation suggests future studies that may be performed by other investigators, it has also answered many questions about the mechanical stimuli effective for the induction of osteogenesis by human bone marrow and adipose derived adult stem cells. This research presents the first evidence that pulsatile fluid shear stress of 3 dynes/cm^2 can induce osteogenesis of hASCs in three-dimensional culture even in the absence of soluble osteogenic inductive factors. A novel three dimensional scaffold material was validated for cell culture and the application of fluid shear stress. The range of local cyclic tensile strains effective for maximum calcium accretion by hASCs in two-dimensional culture were also determined. The local strain most effective for BMP2 mRNA expression in three-dimensional hMSC collagen gel culture was calculated as 16.8%. Experimental evidence suggested an actin damage threshold limit for the application of cyclic tensile strain in hMSC-seeded collagen gels significantly above this strain level. And finally, a semi-automated mesh generation method was created and validated for three dimensional finite element models of bone. The findings presented in this body of work lead to a more complete understanding of the *in vitro* mechanobiology of bone marrow and adipose derived adult stem cells for tissue engineering and regenerative medicine.

References

Ajubi NE, Klein-Nulend J, Nijweide PJ, Vrijheid-Lammers T, Alblas MJ, Burger EH. 1996. Pulsating fluid flow increases prostaglandin production by cultured chicken osteocytes--a cytoskeleton-dependent process. Biochem Biophys Res Commun. 225(1):62-8.

Altman GH, Horan RL, Martin I, Farhadi J, Stark PR, Volloch V, Richmond JC, Vunjak-Novakovic G, Kaplan DL, 2002. Cell differentiation by mechanical stress. FASEB J. 16(2), 270-272.

Beck LR, Cowsar DR, Lewis DH, Gibson JW, Flowers CE Jr. 1979. New long-acting injectable microcapsule contraceptive system. Am J Obstet Gynecol. 135(3):419-26.

Bernacki SH, Wall ME, Loboa EG. 2008. Isolation of human mesenchymal stem cells from bone and adipose tissue. Methods Cell Biol. 86:257-7.

Birnbaum BA, Hindman N, Lee J, Babb JS. 2007. Multi-detector row CT attenuation measurements: assessment of intra- and interscanner variability with an anthropomorphic body CT phantom. Radiology. 242(1):109-19.

Bonewald LF. 2006. Mechanosensation and Transduction in Osteocytes. Bonekey Osteovision. 3(10):7-15.

Bruder SP, Fink DJ, Caplan AI. 1994. Mesenchymal stem cells in bone development, bone repair, and skeletal regeneration therapy. J Cell Biochem. 56(3):283-94.

Bunnell BA, Estes BT, Guilak F, Gimble JM. 2008. Differentiation of adipose stem cells. Methods Mol Biol. 456:155-71.

Burger EH, Klein-Nulend J, van der Plas A, Nijweide PJ. 1995. Function of osteocytes in bone--their role in mechanotransduction. J Nutr. 125(7 Suppl):2020S-2023S

Burr DB, Milgrom C, Fyhrie D, Forwood M, Nyska M, Finestone A, Hoshaw S, Saiag E, Simkin A, 1996. In vivo measurement of human tibial strains during vigorous activity. Bone. 18, 405-10.

Camacho DL, Hopper RH, Lin GM, Myers BS. 1997. An improved method for finite element mesh generation of geometrically complex structures with application to the skullbase. J Biomech. 30(10):1067-70.

Campbell JJ, Lee DA, Bader DL, 2006. Dynamic compressive strain influences chondrogenic gene expression in human mesenchymal stem cells. Biorheology 43, 455-70.

Caplan AI, Bruder SP. 2001. Mesenchymal stem cells: building blocks for molecular medicine in the 21st century. Trends Mol Med. 7(6):259-64.

Carter DR, Beaupre GS, Giori NJ, Helms JA, 1998. Mechanobiology of skeletal regeneration. Clin Orthop Relat Res 355 Suppl, S41-55.

Carter DR, Caler WE, Harris WH. 1981. Resultant loads and elastic modulus calibration of long bone cross sections. J Biomech. 14(11):739-45.

Cattaneo PM, Dalstra M, Frich LH. 2001. A three-dimensional finite element model from computed tomography data: a semi-automated method. Proc Inst Mech Eng H. 215(2):203-13.

Chandran PL, Barocas VH. 2007. Deterministic material-based averaging theory model of collagen gel micromechanics. J Biomech Eng. 129(2):137-47

Chawla AS, Chang TM. 1985. In-vivo degradation of poly(lactic acid) of different molecular weights. Biomater Med Devices Artif Organs. 13(3-4):153-62.

Choquet D, Felsenfeld DP, Sheetz MP, 1997. Extracellular matrix rigidity causes strengthening of integrin-cytoskeleton linkages. Cell. 88(1):39-48.

Crawford RP, Cann CE, Keaveny TM. 2003. Finite element models predict in vitro vertebral body compressive strength better than quantitative computed tomography. Bone. 33(4):744-50.

Cudkowicz G, Bennett M, Shearer GM. 1964. Pluripotent Stem Cell Function of the Mouse Marrow "Lymphocyte". Science. 144:866-8.

Cullinane DM, Salisbury KT, Alkhiary Y, Eisenberg S, Gerstenfeld L, Einhorn TA. 2003. Effects of the local mechanical environment on vertebrate tissue differentiation during repair: does repair recapitulate development? J Exp Biol. 206(Pt 14):2459-71.

Cutright DE, Hunsuck EE. 1971. Tissue reaction to the biodegradable polylactic acid suture. Oral Surg Oral Med Oral Pathol. 31(1):134-9.

Danchakoff V. 1916. The Differentiation of Cells as a Criterion for Cell Identification, Considered in Relation to the Small Cortical Cells of the Thymus. J Exp Med. 24(1):87-105.

Darling EM, Topel M, Zauscher S, Vail TP, Guilak F. 2008. Viscoelastic properties of human mesenchymally-derived stem cells and primary osteoblasts, chondrocytes, and adipocytes. J Biomech. 41(2):454-64.

De Ugarte DA, Morizono K, Elbarbary A, Alfonso Z, Zuk PA, Zhu M, Dragoo JL, Ashjian P, Thomas B, Benhaim P, Chen I, Fraser J, Hedrick MH. 2003. Comparison of multi-lineage cells from human adipose tissue and bone marrow. Cells Tissues Organs. 174(3):101-9.

Deguchi S, Ohashi T, Sato M. 2006. Tensile properties of single stress fibers isolated from cultured vascular smooth muscle cells. J Biomech. 39(14):2603-10.

Dejong ES, DeBerardino TM, Brooks DE, Judson K. 2004. In vivo comparison of a metal versus a biodegradable suture anchor. Arthroscopy. 20(5):511-6.

Dhawan, A. 2003. Medical Image Analysis. Hoboken, New Jersey: John Wiley & Sons.

Engelmayr GC Jr, Sacks MS. 2008. Prediction of extracellular matrix stiffness in engineered heart valve tissues based on nonwoven scaffolds. Biomech Model Mechanobiol.7(4):309-21.

Estes BT, Wu AW, Guilak F. 2006. Potent induction of chondrocytic differentiation of human adipose-derived adult stem cells by bone morphogenetic protein 6. Arthritis Rheum. 54(4):1222-32.

Frank O, Heim M, Jakob M, Barbero A, Schäfer D, Bendik I, Dick W, Heberer M, Martin I. 2002. Real-time quantitative RT-PCR analysis of human bone marrow stromal cells during osteogenic differentiation in vitro. J Cell Biochem. 85(4):737-46.

Garvin J, Qi J, Maloney M, Banes AJ, 2003. Novel system for engineering bioartificial tendons and application of mechanical load. Tissue Eng. 9, 967-79.

Gies AA, Carter DR. 1982. Experimental determination of whole long bone sectional properties. J Biomech. 15(4):297-303.

Golde DW, Hocking WG, Quan SG, Sparkes RS, Gale RP. 1980. Origin of human bone marrow fibroblasts. Br J Haematol. 44(2):183-7.

Gronthos S, Franklin DM, Leddy HA, Robey PG, Storms RW, Gimble JM. 2001. Surface protein characterization of human adipose tissue-derived stromal cells. J Cell Physiol. 189(1):54-63.

Grosland NM, Brown TD. 2002. A voxel-based formulation for contact finite element analysis. Comput Methods Biomech Biomed Engin. 5(1):21-32.

Halvorsen YD, Franklin D, Bond AL, Hitt DC, Auchter C, Boskey AL, Paschalis EP, Wilkison WO, Gimble JM. 2001. Extracellular matrix mineralization and osteoblast gene expression by human adipose tissue-derived stromal cells. Tissue Eng. 7(6):729-41.

Hanson AD, Marvel SW, Bernacki SH, Banes AJ, van Aalst J, Loboa EG. 2009. Osteogenic effects of rest inserted and continuous cyclic tensile strain on hASC lines with disparate osteodifferentiation capabilities. Ann Biomed Eng. 37(5):955-65.

Harris AK, 1987. Cell motility and the problem of anatomical homeostasis. J Cell Sci Suppl. 8:121-40.

Hillam R, Jackson M, Goodship A, Skerry T, 1996. Comparison of physiological strains in the human skull and tibia. Bone 19, 686-686.

Hopper KD, Gouldy CA, Kasales CJ, TenHave TR, Fisher AL. 1997. The effect of helical CT on X-ray attenuation. J Comput Assist Tomogr. 21(1):152-5.

Hu JH, Ding M, Søballe K, Bechtold JE, Danielsen CC, Day JS, Hvid I. 2002. Effects of short-term alendronate treatment on the three-dimensional microstructural, physical, and mechanical properties of dog trabecular bone. Bone. 31(5):591-7.

Huda W and Slone R. 2003. Review of Radiologic Physics, (Second Edition). Philadelphia: Lippincott Williams & Wilkins.

Ignatius A, Blessing H, Liedert A, Kaspar D, Kreja L, Friemert B, Claes L, 2004. [Effects of mechanical strain on human osteoblastic precursor cells in type I collagen matrices] [Article in German] Orthopade. 33, 1386-93.

Jackson S and Thomas R. 2004. Cross-Sectional Imaging Made Easy. Edinburgh: Churchill Livingstone.

Jaiswal RK, Jaiswal N, Bruder SP, Mbalaviele G, Marshak DR, Pittenger MF. 2001. Adult human mesenchymal stem cell differentiation to the osteogenic or adipogenic lineage is regulated by mitogen-activated protein kinase. J Biol Chem. 275(13):9645-52.

Kang Q, An YH, Friedman RF. 1998. Mechanical properties and bone densities of canine trabecular bone. J Mater Sci Mater Med. 9(5):263-7.

Karamichos D, Brown RA, Mudera V, 2006. Complex dependence of substrate stiffness and serum concentration on cell-force generation. J Biomed Mater Res A. 78, 407-15.

Kelly DJ, Prendergast PJ, 2005. Mechano-regulation of stem cell differentiation and tissue regeneration in osteochondral defects. J Biomech 38, 1413-1422.

Keyak JH, Meagher JM, Skinner HB, Mote CD Jr. 1990. Automated three-dimensional finite element modelling of bone: a new method. J Biomed Eng. 12(5):389-97.

Klein-Nulend J, Semeins CM, Ajubi NE, Nijweide PJ, Burger EH. 1995. Pulsating fluid flow increases nitric oxide (NO) synthesis by osteocytes but not periosteal fibroblasts--correlation with prostaglandin upregulation. Biochem Biophys Res Commun. 217(2):640-8.

Knippenberg M, Helder MN, Doulabi BZ, Semeins CM, Wuisman PI, Klein-Nulend J. 2005. Adipose tissue-derived mesenchymal stem cells acquire bone cell-like responsiveness to fluid shear stress on osteogenic stimulation. Tissue Eng. 11(11-12):1780-8.

Kulkarni RK, Moore EG, Hegyeli AF, Leonard F. 1971. Biodegradable poly(lactic acid) polymers. J Biomed Mater Res. 5(3):169-81.

Lee KS, Kim HJ, Li QL, Chi XZ, Ueta C, Komori T, Wozney JM, Kim EG, Choi JY, Ryoo HM, Bae SC. 2000. Runx2 is a common target of transforming growth factor beta1 and bone morphogenetic protein 2, and cooperation between Runx2 and Smad5 induces osteoblast-specific gene expression in the pluripotent mesenchymal precursor cell line C2C12. Mol Cell Biol. 20(23):8783-92.

Lengsfeld M, Schmitt J, Alter P, Kaminsky J, Leppek R. 1998. Comparison of geometry-based and CT voxel-based finite element modelling and experimental validation. Med Eng Phys. 20(7):515-22.

Les CM, Keyak JH, Stover SM, Taylor KT. 1997. Development and validation of a series of three-dimensional finite element models of the equine metacarpus. J Biomech. 30(7):737-42.

Levi C, Gray JE, McCullough EC, Hattery RR. 1982. The unreliability of CT numbers as absolute values. AJR Am J Roentgenol. 139(3):443-7.

Liedert A, Kaspar D, Blakytny R, Claes L, Ignatius A. 2006. Signal transduction pathways involved in mechanotransduction in bone cells. Biochem Biophys Res Commun. 349(1):1-5.

Loboa EG, Fang TD, Warren SM, Lindsey DP, Fong KD, Longaker MT, and Carter DR, 2004. Mechanobiology of mandibular distraction osteogenesis: experimental analyses with a rat model. Bone 34, 336-343.

Marom SA, Linden MJ. 1990. Computer aided stress analysis of long bones utilizing computed tomography. J Biomech. 23(5):399-404.

McCarthy TL, Ji C, Chen Y, Kim KK, Imagawa M, Ito Y, Centrella M. 2000. Runt domain factor (Runx)-dependent effects on CCAAT/ enhancer-binding protein delta expression and activity in osteoblasts. J Biol Chem. 275(28):21746-53.

McCullen SD, Stevens DR, Roberts WA, Clarke LI, Bernacki SH, Gorga RE, Loboa EG. Characterization of electrospun nanocomposite fibers and biocompatibility with adipose-derived human mesenchymal stem cells. Int J Nanomedicine 2(2):1-11 (2007).

McCullough EC, Morin RL. 1983. CT-number variability in thoracic geometry. AJR Am J Roentgenol. 141(1):135-40.

Mikić B, Carter DR, 1995. Bone strain gage data and theoretical models of functional adaptation. J Biomech. 28(4):465-9.

Nirmalanandhan VS, Dressler MR, Shearn JT, Juncosa-Melvin N, Rao M, Gooch C, Bradica G, Butler DL. 2007. Mechanical stimulation of tissue engineered tendon constructs: effect of scaffold materials. J Biomech Eng. 129:919-23.

Ohsumi TK, Flaherty JE, Evans MC, Barocas VH. 2008. Three-dimensional simulation of anisotropic cell-driven collagen gel compaction. Biomech Model Mechanobiol. 7(1):53-62.

Oreffo RO, Kusec V, Romberg S, Triffitt JT. 1999. Human bone marrow osteoprogenitors express estrogen receptor-alpha and bone morphogenetic proteins 2 and 4 mRNA during osteoblastic differentiation. J Cell Biochem. 75(3):382-92.

Park JS, Chu JS, Cheng C, Chen F, Chen D, Li S, 2004. Differential effects of equiaxial and uniaxial strain on mesenchymal stem cells. Biotechnol Bioeng. 88, 359-68.

Parker AM, Katz AJ. 2006. Adipose-derived stem cells for the regeneration of damaged tissues. Expert Opin Biol Ther. 6(6):567-78.

Patt HM, Maloney MA. 1975. Bone marrow regeneration after local injury: a review. Exp Hematol. 3(2):135-48.

Pfeiler TW, Sumanasinghe RD, Loboa EG. 2008. Finite element modeling of 3D human mesenchymal stem cell-seeded collagen matrices exposed to tensile strain. J Biomech. 41(10):2289-96.

Pistner H, Bendix DR, Mühling J, Reuther JF. 1993. Poly(L-lactide): a long-term degradation study in vivo. Part III. Analytical characterization. Biomaterials. 14(4):291-8.

Pressel T, Bouguecha A, Vogt U, Meyer-Lindenberg A, Behrens BA, Nolte I, Windhagen H. 2005. Mechanical properties of femoral trabecular bone in dogs. Biomed Eng Online. 4(1):17.

Qi J, Chi L, Faber J, Koller B, Banes AJ, 2006. ATP reduces gel compaction in osteoblast-populated collagen gels. J Appl Physiol., 102, 1152-60.

Qi MC, Hu J, Zou SJ, Han LC, Luo E. 2005. [The changes of cytoskeleton F-actin in rat bone marrow mesenchymal stem cells and calvarial osteoblasts under mechanical strain]. West China Journal of Stomatology 23, 110-2.

Rawlinson SC, Pitsillides AA, Lanyon LE. 1996. Involvement of different ion channels in osteoblasts' and osteocytes' early responses to mechanical strain. Bone. 19(6):609-14.

Remmler D, Olson L, Ekstrom R, Duke D, Matamoros A, Matthews D, Ullrich CG. 1998. Pre-surgical CT/FEA for craniofacial distraction: I. Methodology, development, and validation of the cranial finite element model. Med Eng Phys. 20(8):607-1

Rho JY, Hobatho MC, Ashman RB. 1995. Relations of mechanical properties to density and CT numbers in human bone. Med Eng Phys. 17(5):347-55.

Riddle RC, Donahue HJ. 2009. From streaming-potentials to shear stress: 25 years of bone cell mechanotransduction. J Orthop Res. 27(2):143-9.

Roeder BA, Kokini K, Sturgis JE, Robinson JP, Voytik-Harbin SL, 2002. Tensile mechanical properties of three-dimensional type I collagen extracellular matrices with varied microstructure. J Biomech Eng. 124, 214-22.

Roy P, Petroll WM, Chuong CJ, Cavanagh HD, Jester JV. 1999. Effect of cell migration on the maintenance of tension on a collagen matrix. Ann Biomed Eng. 27(6):721-30.

Rubin J, Rubin C, Jacobs CR. 2006. Molecular pathways mediating mechanical signaling in bone. Gene. 367:1-16.

Sabin Fr, Miller Fr, Smithburn KC, Thomas RM, Hummel Le. 1936. Changes in The Bone Marrow And Blood Cells Of Developing Rabbits. J Exp Med. 64(1):97-120.

Shearn JT, Juncosa-Melvin N, Boivin GP, Galloway MT, Goodwin W, Gooch C, Dunn MG, Butler DL. 2007. Mechanical stimulation of tendon tissue engineered constructs: effects on construct stiffness, repair biomechanics, and their correlation. J Biomech Eng. 129:848-54.

Simha NK, Fedewa M, Leo PH, Lewis JL, Oegema T. 1999. A composites theory predicts the dependence of stiffness of cartilage culture tissues on collagen volume fraction. J Biomech. 32:503-509.

Sumanasinghe RD, Bernacki SH, Loboa EG. 2006. Osteogenic differentiation of human mesenchymal stem cells in collagen matrices: effect of uniaxial cyclic tensile strain on bone morphogenetic protein (BMP-2) mRNA expression. Tissue Eng. 12(12):3459-65.

Sumanasinghe RD, Osborne JA, Loboa EG. 2009 A. Mesenchymal stem cell-seeded collagen matrices for bone repair: effects of cyclic tensile strain, cell density, and media conditions on matrix contraction in vitro. J Biomed Mater Res A. 88(3):778-86.

Sumanasinghe RD, Pfeiler TW, Monteiro-Riviere NA, Loboa EG. 2009 B. Expression of proinflammatory cytokines by human mesenchymal stem cells in response to cyclic tensile strain. J Cell Physiol. 219(1):77-83.

Sumanasinghe RD, Pfeiler TW, Loboa EG. 2009 C. Cyclic Tensile Strain Increases Alkaline Phosphatase mRNA Expression, Calcium Deposition, and Stiffness of 3D hMSC-Seeded Collagen Matrices. (In preparation)

Tapp H, Hanley EN Jr, Patt JC, Gruber HE. 2009. Adipose-derived stem cells: characterization and current application in orthopaedic tissue repair. Exp Biol Med (Maywood). 234(1):1-9.

Tholpady SS, Llull R, Ogle RC, Rubin JP, Futrell JW, Katz AJ. 2006. Adipose tissue: stem cells and beyond. Clin Plast Surg. 33(1):55-62.

Thompson MS, Bleckwehl FH, Ott CE, Epari DR, Duda GN, 2007. Mechanical Characterisation of the BioFlex System. Tissue Eng. 13(6): 1367-1392.

Tranquillo RT, Durrani MA, Moon AG, 1992. Tissue engineering science: consequences of cell traction force. Cytotechnology. 10(3):225-50.

Turner CH, Burr DB. 1993. Basic biomechanical measurements of bone: a tutorial. Bone. 14(4):595-608.

Van Epps-Fung C, Williams JP, Cornwell TL, Lincoln TM, McDonald JM, Radding W, Blair HC. 1994. Regulation of osteoclastic acid secretion by cGMP-dependent protein kinase. Biochem Biophys Res Commun. 204(2):565-71.
van't Hof RJ, Ralston SH. 2001. Nitric oxide and bone. Immunology. 103(3):255-61.

Viceconti M, Bellingeri L, Cristofolini L, Toni A. 1998. A comparative study on different methods of automatic mesh generation of human femurs. Med Eng Phys. 20(1):1-10.

Vishay Measurements Group, Inc. 1992. Student manual for strain gage technology, bulletin 309E.

Wall ME, Bernacki SH, Loboa EG. Effects of serial passaging on adipogenic and osteogenic differentiation potential of adipose-derived human mesenchymal stem cells. Tissue Engineering 13(6):1291-8 (2007).

Wells RG, Discher DE. 2008. Matrix elasticity, cytoskeletal tension, and TGF-beta: the insoluble and soluble meet. Sci Signal. 1(10):pe13.

Wickham MQ, Erickson GR, Gimble JM, Vail TP, Guilak F. 2003. Multipotent stromal cells derived from the infrapatellar fat pad of the knee. Clin Orthop Relat Res. (412):196-212.

Wimalawansa SJ. 2007. Rationale for using nitric oxide donor therapy for prevention of bone loss and treatment of osteoporosis in humans. Ann N Y Acad Sci. 1117:283-97.

Wipff PJ, Rifkin DB, Meister JJ, Hinz B. 2007. Myofibroblast contraction activates latent TGF-1 from the extracellular matrix. J. Cell Biol. 179:1311–1323.

Wirtz DC, Schiffers N, Pandorf T, Radermacher K, Weichert D, Forst R. 2000. Critical evaluation of known bone material properties to realize anisotropic FE-simulation of the proximal femur. J Biomech. 33(10):1325-30.

Zhang J, Jin GC, Meng LB, Jian LH, Wang AY, Lu SB. 2005. Strain and mechanical behavior measurements of soft tissues with digital speckle method. J Biomed Opt. May-Jun;10(3):4854-57.

Zuk PA, Zhu M, Ashjian P, De Ugarte DA, Huang JI, Mizuno H, Alfonso ZC, Fraser JK, Benhaim P, Hedrick MH. 2002. Human adipose tissue is a source of multipotent stem cells. Mol Biol Cell. 13(12):4279-95.

Zuk PA, Zhu M, Mizuno H, Huang J, Futrell JW, Katz AJ, Benhaim P, Lorenz HP, Hedrick MH. 2001. Multilineage cells from human adipose tissue: implications for cell-based therapies. Tissue Eng. 7(2):211-28.

Appendices

Appendix A. Finite Element Mesh Generation MATLAB Code

```
%
% Voxel to FEA
% Ansys version
% Wayne Pfeiler
%

clear all;
close all;
clc;
tic;

% number of images
imnum=188; % max of 188
% image scaling factor
imscale=.5;
a=zeros(512*imscale,512*imscale,imnum);

% image filename
imnamebase='radius';
imfmt='dcm';

% Image-containing box dimensions
ymin=round(150*imscale);
ymax=round(380*imscale);
xmin=round(275*imscale);
xmax=round(412*imscale); % was 425

xrange=xmax-xmin+1;
yrange=ymax-ymin+1;

% multiplier for 1 voxel = x units
s1=0.16/imscale;
s2=0.16/imscale;
s3=0.98;

% load all these images into a huge 3d tensor
w=waitbar(0,['Loading ',num2str(imnum),' images, please be patient']);
for ii = 1:imnum
    waitbar(ii/imnum);
    imcurrent=[imnamebase,num2str(ii,'%03.0f'),'.',imfmt];
    a(:,:,ii)=imresize(dicomread(['images\',imcurrent]),imscale);
end
close(w);
fprintf('Images loaded.\n');

% create 3d tensor for materials
```

```
matls=zeros(xrange, yrange, imnum);
nodes=zeros(xrange+1, yrange+1, imnum+1);
ecount=0;
ncount=0;

% ------------------------------------------------------------------------
% open a file for writing in text mode:
fid=fopen('c:\Docume~1\twpfeile\MyDocu~1\sbcfinal\ansys\dcm2ansy.txt','wt'
);

% Ansys header info
fprintf(fid,'\n');
fprintf(fid,'/Prep7\n');
fprintf(fid,'/Title, Canine Radius. Wayne Pfeiler\n');
fprintf(fid,'CSYS, 0\n');
fprintf(fid,'ET, 1, Solid45\n');
fprintf(fid,'\n');

% Materials:
% -43 to 350: low mod [1]
% 350 to 2000: bone [2 to 167]
% >2000: super high mod [168]
fprintf(fid,'! ------------------------------------------------------
\n');
fprintf(fid,'! Defining Materials:\n');
for ii=1:168
    if ii == 1
        E(ii)=0.001;
    elseif (ii+33)*10 < 1000
        E(ii)=26.8657*(ii+33)*10-8865.67;
    elseif (ii+33)*10 < 2000
        E(ii)=10*(ii+33)*10+8000;
    else
        E(ii)=28000;
    end
    fprintf(fid,'MP, EX,   %1.0f, %1.5E \n',ii, E(ii));
    fprintf(fid,'MP, NUXY, %1.0f, 0.39 \n',ii);
end % of for loop
% ------------------------------------------------------------------------
% Define Nodes:
w=waitbar(0,['Segmenting ',num2str(imnum),' images and writing node
code.']);
fprintf(fid,'! ------------------------------------------------------
\n');
fprintf(fid,'! Define Nodes:\n');

for zz=1:imnum
    waitbar(zz/imnum);
    for jj=1:yrange
        for ii=1:xrange
            if a(ii+xmin-1,jj+ymin-1,zz)>2000 % high modulus ceiling limit
                matls(ii,jj,zz)=168;
```

```
            elseif a(ii+xmin-1,jj+ymin-1,zz) >=350 % bone
                qq=double(a(ii+xmin-1,jj+ymin-1,zz));
                matls(ii,jj,zz)=round(qq*.10)-33;
            % remark out next two lines to remove marrow from model
            elseif a(ii+xmin-1,jj+ymin-1,zz)>=-43 % marrow, low modulus
floor limit
               matls(ii,jj,zz)=1;
            end

            % see if we made a new block
            if matls(ii,jj,zz)~=0
                % check and create each of 8 nodes surrounding the new
                % element, increment node # as we go.
                % (0 0 0) (0 0 1) .. (1 1 1)
                for n3=0:1 % *** n3=0:1 ***
                    for n1=0:1
                        for n2=0:1
                            if nodes(ii+n1,jj+n2,zz+n3)==0 % no node here
yet
                                ncount=ncount+1; % up the node count
                                % record the new node # in node tensor
                                nodes(ii+n1,jj+n2,zz+n3)=ncount;
                                % add another line to the file
                                fprintf(fid,'N, %6.0f, %6.2f, %6.2f,
%6.2f\n',ncount,(jj+n2)*s2,(ii+n1)*-s1,(zz+n3)*s3);
                            end
                        end
                    end
                end

            end % of matls~=0
        end % of ii loop
    end % of jj loop
end % of zz loop
close(w);
fprintf('Images segmented.\n');

% ------------------------------------------------------------------------
% Define Elements
fprintf(fid,'! ------------------------------------------------------------
\n');
fprintf(fid,'! Defining Elements:\n');
w=waitbar(0,['Writing element code.']);
q2=0;
    for zz=1:imnum
        waitbar(zz/imnum);
        for jj=1:yrange
            for ii=1:xrange
                if matls(ii,jj,zz) ~= 0 % we have an element here, make
code for it
                    ecount=ecount+1; % up the element #
```

```
                    q=matls(ii,jj,zz); % the intensity of this
voxel/element
                    % set the material properties:
                    if q2~=q;
                        q2=q;
                        fprintf(fid,'Mat, %1.0f\n',q);
                    end
                    a=nodes(ii,jj,zz);
                    b=nodes(ii+1,jj,zz);
                    c=nodes(ii+1,jj+1,zz);
                    d=nodes(ii,jj+1,zz);
                    e=nodes(ii,jj,zz+1);
                    f=nodes(ii+1,jj,zz+1);
                    g=nodes(ii+1,jj+1,zz+1);
                    h=nodes(ii,jj+1,zz+1);
                    fprintf(fid,'E, %6.0f, %6.0f, %6.0f, %6.0f, %6.0f,
%6.0f, %6.0f, %6.0f\n',a,b,c,d,e,f,g,h);
                end
            end
        end
    end
close(w);

% save and close the newly written file
fclose(fid);

fprintf('Done!\n');
fprintf('Model contains %1.0f nodes and %1.0f elements.\n',ncount,ecount)
t=toc;
fprintf('Operation took %1.1f seconds.\n\n',t);
```

Appendix B. TrueGrid Finite Element Mesh Projection Code.

```
ansys
ansymats 1 stif3 ex 24500;nuxy 0.39;;

iges outerradius20pt.igs 1 1;
iges innerradius20pt.igs 2 2;
merge

c following moves IM canal into bone:
TRSD 2 MX -54.5;
TRSD 2 MY -39;
TRSD 2 MZ 15;

c interrupt
Block 1 6 11 16 21 26 31 36 41 46 51; 1 6 11 16 21 26 31 36;
c z:
1 6 11 16 21 26 31 36 41 46 51 56 61 66 71
76 81 86 91 96 101 106 111 116 121 126 131 136 141 146
151 156 161 166 171 176 181 186 191;

-7.5 -6 -4.5 -3 -1.5 0 1.5 3 4.5 6 7.5; -4.5 -3.21 -1.93 -0.64 0.64 1.93
3.21 4.5;
c z:
0 4.45 8.89 13.34 17.79 22.24 26.68 31.13 35.58 40.03 44.47 48.92 53.37
57.82
62.26 66.71 71.16 75.61 80.05 84.5 88.95 93.39 97.84 102.29 106.74 111.18
115.63 120.08 124.53 128.97 133.42 137.87 142.32 146.76 151.21 155.66
160.11
164.55 169;

c move both surfaces into place with the blocks:
TRSD 1 MX -192 MY -97 MZ -13.5;
TRSD 2 MX -192 MY -97 MZ -13.5;

c for section 1:
DEI  1 2 0 10 11; 1 2 0 7 8; 1 2;
mbi ;; -1 0 -2; xyz 0.188681E-01 5.51701 0.431387E-01
mbi ;; -1 0 -2; xyz -2.13546 -0.491764 -0.116472
mbi ;; -1 0 -2; xyz 0.611023 0.261637 0.374427E-01
mbi 2 10; -8; 1 2; xyz -0.262936 1.06058 0.484884E-01
mbi 2 10; -1; 1 2; xyz 0.562246E-01 -1.01931 -0.425422E-01
mbi -1; 2 7; 1 2; xyz -1.95063 -0.176749 0.331361E-01
mbi -11; 2 7; 1 2; xyz 1.20073 -0.892062E-01 -0.284355E-01
mbi -11; 2 4;; xyz 1.01764 -0.128533 0.328948E-01
mbi -11; 5 6;; xyz 0.599817 0.211916E-01 0.204902E-01
mbi -2; -7; 1 2; xyz -1.57051 0.964852 -0.156226E-01
mbi -2; -2; 1 2; xyz -1.78733 -1.83870 -0.406899E-01
mbi -10; -2; 1 2; xyz 1.53795 -1.70166 0.939131E-02
mbi -10; -7; 1 2; xyz 0.781099 1.32410 -0.420103E-01
```

```
mbi 4 8; -8; 1 2; xyz 0.349056E-01 1.10098 -0.830188E-01
mbi -9; -2; 1 2; xyz 0.335620 -0.661880 -0.522091E-01
mbi -10; -3; 1 2; xyz 0.755537 -0.455783 -0.437722E-01
mbi -9; -7; 1 2; xyz 0.238011 0.929194 0.627208E-01
mbi -10; -6; 1 2; xyz 0.660720 0.410943 0.194557E-01
mbi -3; -7; 1 2; xyz -0.759539 0.747886 0.646639E-01
mbi -2; -6; 1 2; xyz -1.41312 0.353575 0.462883E-01
mbi -2; -3; 1 2; xyz -1.07158 -0.652198 -0.305359E-01
mbi -3; -2; 1 2; xyz -0.657624 -0.949365 -0.579028E-01
mbi -1; 4 5; 1 2; xyz -0.922631 -0.936728E-01 0.713944E-01
mbi -1; -3; 1 2; xyz -0.616146 -0.319273 0.351384E-01
mbi -1; -6; 1 2; xyz -0.570785 0.156870E-01 0.477605E-01
mbi -10; -2; 1 2; xyz 0.343014 -0.458005 -0.247226E-01
mbi -9; -3; 1 2; xyz 0.372150 -0.544792 0.425806E-01
mbi 3 4; -1; 1 2; xyz -0.123284 0.382302 0.130198E-01
mbi 7 8; -1; 1 2; xyz -0.466844E-01 -0.895973 -0.749021E-01
mbi -9; -1; 1 2; xyz 0.341494 -0.923404 -0.256727E-01
mbi -10; -1; 1 2; xyz 0.322237 -0.799219 -0.186923E-01
mbi 6 7; -8; 1 2; xyz 0.186082 0.611619 0.235081E-03
mbi -3; -7; -1 0 -2; xyz 0.882442 -0.569180 0.366976E-01
mbi -2; -2; 1 2; xyz -1.32259 0.899813 0.147290
mbi -2; -1; 1 2; xyz -1.21033 -0.129766 0.164548
mbi -3; -2; 1 2; xyz 0.689845E-01 0.695131 0.301051E-01
mbi -2; -3; -1 0 -2; xyz -0.528111 0.368576 0.424428E-01
mbi -10; -6; -1 0 -2; xyz 0.709891E-01 -0.424888 0.452900E-02
mbi -1; -2; 1 2; xyz 0.134151 -0.806113 0.198574E-01
mbi -10; 1 2; 1 2; xy 0.910664 0.551665
mbi -10; -1; 1 2; xyz -0.517530E-01 -0.254033 0.229869E-01
mbi 10 11; -7; 1 2; xyz 0.557183 -0.487963 0.471940E-01
mbi -11; -7; 1 2; xyz -0.217072 0.583660 -0.702271E-01
mbi -10; -6; -1 0 -2; xyz 0.665912 -0.218364 0.835109E-02
mbi -10; -5; -1 0 -2; xyz 1.06278 -0.224133 -0.305200E-02
mbi -10; -4; -1 0 -2; xyz 0.890315 -0.253033 0.604081E-02
mbi -10; -8; 1 2; xyz 0.440281 -0.293797 -0.122952E-01
mbi 9 10; -8; 1 2; xyz 0.263289 -0.130959E-01 -0.215197E-01
mbi -2; -2; -1 0 -2; xyz 0.658431 -1.37422 0.162265E-01
mbi -2; -1; -1 0 -2; xyz 0.554689 -0.428374 -0.104961E-01
mbi -3; -2; -1 0 -2; xyz 0.103070 -0.529034 0.129409E-01
mbi -2; -4 0 -5; -1 0 -2; xyz -1.40105 -0.151886 0.673923E-01
pb 1 2 2 1 2 2 xyz -10.4190 1.30584 3.85498
pb 1 2 2 1 2 2 xyz -10.6478 1.45840 3.94304
mbi 1 2; -2; 1 2; xyz 0.499365 -0.532398 -0.723504E-01
mbi 1 2; -7; -2; xyz 0.522381 0.690080 0.425882E-01
mbi 1 2; -7; -2; xyz -0.614535 -0.564735 -0.625315E-01
pb 1 2 2 1 2 2 xyz -10.3704 1.08214 4.00539
pb 1 2 1 1 2 1 xyz -10.0184 0.581747 0.100036
pb 1 2 2 1 2 2 xyz -10.5061 1.38286 4.05561
pb 1 3 2 1 3 2 xyz -10.8295 3.35256 4.30933
pb 2 2 2 2 2 2 xyz -9.51125 0.291992 3.90771
pb 2 1 1 2 1 1 xyz -7.70100 0.153901 0.680739
mbi -3; -2; -1 0 -2; xyz -0.924331 -0.158664 -0.257473E-01
pb 10 8 2 10 8 2 xyz 4.43831 10.7142 4.38142
pb 10 8 1 10 8 1 xyz 5.00998 10.1560 -0.364238E-01
```

```
mbi -2; -7; 1 2; xyz -1.32331 -0.836390 0.142264E-02
mbi -2; -8; 1 2; xyz -1.78430 -0.689371 0.558152E-01
mbi -1; -7; 1 2; xyz -0.411531 -0.230771 0.414227E-01
mbi 1 2; -6; -1 0 -2; xyz -0.225611 -0.335163 0.687194E-02
mbi -9; -7; -1 0 -2; xyz -0.449596 -0.990344 0.795786E-01
c -----------------------
c section 2:
DEI  1 2 0 10 11; 1 2 0 7 8; 2 3;

mbi ;; -3; xyz 0.939786E-02 5.21743 -0.271730E-01
mbi ;; -3; xyz -1.28184 0.496740E-01 0.789270E-01
mbi 2 10; -8; -3; xyz -0.200884E-01 0.687461 -0.199308E-01
mbi 2 10; -1; -3; xyz -0.289440E-01 -0.700785 0.644779E-02
mbi -1; 4 5; -3; xyz -0.243424 -0.126826 0.590897E-02
pb 1 7 3 1 7 3 xyz -8.00828 8.03064 9.20373
pb 2 7 3 2 7 3 xyz -7.31671 8.53976 8.91613
pb 2 8 3 2 8 3 xyz -6.39135 9.45202 9.36662
pb 3 8 3 3 8 3 xyz -5.18342 9.69352 9.24629
pb 7 8 3 7 8 3 xyz 0.210024 9.98964 9.00614
pb 8 8 3 8 8 3 xyz 1.56048 9.40711 9.14424
pb 9 8 3 9 8 3 xyz 2.68302 8.87266 9.32217
pb 10 8 3 10 8 3 xyz 3.63038 8.38343 9.52919
pb 10 7 3 10 7 3 xyz 4.31680 7.81922 9.14936
pb 11 7 3 11 7 3 xyz 5.18761 7.08782 9.41687
pb 11 6 3 11 6 3 xyz 5.94725 6.12458 9.34938
pb 11 5 3 11 5 3 xyz 6.49724 5.53773 9.10391
pb 11 3 3 11 3 3 xyz 7.52642 3.30579 8.95063
pb 11 4 3 11 4 3 xyz 7.47894 4.51609 8.92575
pb 10 2 3 10 2 3 xyz 5.81727 1.06068 8.25715
pb 10 2 3 10 2 3 xyz 6.21300 0.674624 7.99655
pb 8 1 3 8 1 3 xyz 1.76705 0.458722E-01 8.92604
pb 7 1 3 7 1 3 xyz 0.276415 0.442645 9.12080
pb 5 1 3 5 1 3 xyz -2.93441 1.28033 9.00673
pb 6 1 3 6 1 3 xyz -1.36175 1.03289 9.16388
pb 4 1 3 4 1 3 xyz -4.45303 1.36102 8.97432
pb 3 1 3 3 1 3 xyz -5.96668 1.25798 8.87675
pb 2 1 3 2 1 3 xyz -7.41373 1.17700 9.03649
pb 2 2 3 2 2 3 xyz -7.28157 1.63010 8.71341
pb 1 2 3 1 2 3 xyz -8.73213 2.06789 9.09624
pb 10 2 3 10 2 3 xyz 6.16028 0.825625 8.81747
pb 2 8 3 2 8 3 xyz -6.39209 9.45117 9.26345
pb 2 8 3 2 8 3 xyz -6.39272 9.44266 9.10388
pb 1 7 3 1 7 3 xyz -8.03246 8.05858 9.04282
pb 10 8 3 10 8 3 xyz 3.66493 8.39464 9.27391
pb 10 7 3 10 7 3 xyz 4.33897 7.82296 9.06539
pb 11 7 3 11 7 3 xyz 5.15879 7.10587 9.00400
pb 9 7 3 9 7 3 xyz 2.83527 8.01135 8.94588
pb 10 6 3 10 6 3 xyz 4.47315 6.83883 8.93395
pb 3 2 3 3 2 3 xyz -6.02356 1.89470 8.91743
pb 8 7 3 8 7 3 xyz 1.65312 8.25722 8.93920
pb 9 6 3 9 6 3 xyz 3.17402 7.02130 8.94297
pb 10 5 3 10 5 3 xyz 4.49770 5.75201 8.94344
pb 9 2 3 9 2 3 xyz 3.56563 1.63182 8.93626
```

```
pb 10 3 3 10 3 3 xyz 5.21322 3.07293 8.93549
pb 9 3 3 9 3 3 xyz 3.53847 3.06014 8.93724
pb 2 2 3 2 2 3 xyz -7.56111 1.44783 8.71544
pb 2 1 3 2 1 3 xyz -7.18473 1.16569 9.03404
pb 2 2 3 2 2 3 xyz -7.69886 1.32924 8.71629

c -----------------------
c section 3
DEI  1 2 0 10 11; 1 2 0 7 8; 3 4;
mbi ;; -4; xyz 0.224357 3.96264 -0.203791E-01
mbi ;; -4; xyz -1.57297 -0.176229 0.792885E-02
mbi ;; -4; xyz 0.857335E-02 0.373002 -0.366964E-01
pb 2 8 4 2 8 4 xyz -6.42889 7.55880 13.3811
pb 1 7 4 1 7 4 xyz -7.97451 6.27349 13.4011
pb 2 7 4 2 7 4 xyz -7.12406 7.15335 13.3198
pb 1 6 4 1 6 4 xyz -8.31434 5.66289 13.3705
pb 3 8 4 3 8 4 xyz -5.55366 8.21644 13.3120
pb 1 2 4 1 2 4 xyz -7.75171 1.96921 13.8175
pb 1 3 4 1 3 4 xyz -8.27327 2.56462 13.5099
pb 2 2 4 2 2 4 xyz -6.88212 1.68617 13.5991
pb 2 1 4 2 1 4 xyz -6.61977 0.422150 13.6641
pb 3 2 4 3 2 4 xyz -4.94556 2.25344 13.8549
pb 3 1 4 3 1 4 xyz -5.26996 1.54143 13.9463
pb 2 1 4 2 1 4 xyz -6.18539 1.56970 14.0829
pb 4 1 4 4 1 4 xyz -4.08242 1.22824 14.2030
pb 5 1 4 5 1 4 xyz -2.70373 0.922104 14.0056
pb 5 1 4 5 1 4 xyz -2.60546 1.17953 14.1706
pb 6 1 4 6 1 4 xyz -1.05241 0.841924 14.0039
pb 7 1 4 7 1 4 xyz 0.377882 0.424928 13.7611
pb 8 1 4 8 1 4 xyz 1.65867 0.185941 13.5730
pb 9 1 4 9 1 4 xyz 3.19292 -0.445525E-02 13.4802
pb 10 1 4 10 1 4 xyz 4.34124 0.864151E-01 13.4330
pb 10 2 4 10 2 4 xyz 5.35755 0.510850 13.0621
pb 10 2 4 10 2 4 xyz 5.55597 0.364226 12.9881
pb 11 2 4 11 2 4 xyz 6.72901 1.17431 13.5000
pb 2 1 4 2 1 4 xyz -6.23380 1.54652 13.6178
mbi 4 7; -1; -4; xyz -0.122149 0.887156E-03 -0.270736
mbi 3 5; -1; -4; xyz -0.802855E-01 -0.527167E-02 -0.272853
pb 3 2 4 3 2 4 xyz -4.97427 2.19613 13.4838
pb 11 6 4 11 6 4 xyz 6.19399 5.41619 13.4804
pb 11 7 4 11 7 4 xyz 5.16750 6.08340 13.5235
pb 10 7 4 10 7 4 xyz 4.21188 6.70003 13.3912
pb 10 8 4 10 8 4 xyz 3.43710 6.89600 13.5681
pb 9 8 4 9 8 4 xyz 2.39396 7.26174 13.4491
pb 8 8 4 8 8 4 xyz 1.05906 7.56858 13.4153
pb 7 8 4 7 8 4 xyz -0.164249 8.08082 13.3585
pb 6 8 4 6 8 4 xyz -1.40578 8.32947 13.2933
pb 9 7 4 9 7 4 xyz 3.02583 6.73818 13.4033
pb 8 7 4 8 7 4 xyz 1.53477 6.84618 13.3394
pb 9 7 4 9 7 4 xyz 2.96495 6.42489 13.4297
pb 9 6 4 9 6 4 xyz 2.80497 5.78017 13.3731
pb 10 6 4 10 6 4 xyz 4.33992 5.56494 13.3766
pb 10 2 4 10 2 4 xyz 5.41613 0.593239 13.0083
```

```
pb 10 3 4 10 3 4 xyz 5.06496 2.15453 13.2277
pb 3 7 4 3 7 4 xyz -5.55005 7.01823 13.3428
pb 2 6 4 2 6 4 xyz -6.88196 5.89659 13.4186
pb 3 6 4 3 6 4 xyz -5.60621 6.03255 13.3613
pb 2 3 4 2 3 4 xyz -7.01886 2.70206 13.4571
pb 3 2 4 3 2 4 xyz -4.72987 2.74752 13.6345
pb 3 2 4 3 2 4 xyz -4.89468 2.30525 13.6234
pb 3 3 4 3 3 4 xyz -5.28362 2.69631 13.3089
pb 4 3 4 4 3 4 xyz -4.20678 2.53752 13.2989
pb 4 2 4 4 2 4 xyz -4.08869 1.66132 13.3086
pb 5 2 4 5 2 4 xyz -2.65106 1.57010 13.3731
pb 6 2 4 6 2 4 xyz -1.26290 1.37167 13.3460
pb 7 2 4 7 2 4 xyz 0.199291 1.19278 13.3225
pb 3 2 4 3 2 4 xyz -5.05870 2.22666 13.5983
pb 1 2 4 1 2 4 xyz -7.76689 1.96634 13.4706
mbi 4 8; 4 6; -4; xyz 0.797586E-01 -0.114380 -1.78969
pb 4 4 4 4 4 4 xyz -3.84713 4.01417 11.6533


pb 8 6 4 8 6 4 xyz 1.06814 5.08481 11.5283
pb 7 6 4 7 6 4 xyz -0.106618 4.91397 11.6265
pb 8 5 4 8 5 4 xyz 1.15848 4.48330 11.6935
pb 8 4 4 8 4 4 xyz 1.10567 3.80767 11.7557
pb 7 4 4 7 4 4 xyz 0.246372 3.56984 11.5312
pb 6 4 4 6 4 4 xyz -1.23775 3.94768 11.6205
pb 5 4 4 5 4 4 xyz -2.69538 4.30071 11.7190
pb 4 4 4 4 4 4 xyz -3.57421 4.47687 11.8363
pb 4 5 4 4 5 4 xyz -3.52641 4.98955 11.9695
pb 4 6 4 4 6 4 xyz -3.47618 5.62787 12.0492
pb 5 6 4 5 6 4 xyz -2.65773 5.77693 11.5749
pb 6 6 4 6 6 4 xyz -1.40747 5.63495 11.4830
mbi 3 9; -2; -4; xyz 0.419414E-02 0.497155 0.263668
mbi 3 4; -1; -4; xyz 0.859838E-01 0.231371 0.182722
mbi 5 6; -1; -4; xyz -0.227873E-01 0.282405 0.174342
mbi 7 8; -1; -4; xyz 0.227898E-01 0.286391 0.194291
pb 8 1 4 8 1 4 xyz 1.85227 0.242919 13.6837
pb 3 2 4 3 2 4 xyz -5.10788 2.42336 13.8571
pb 3 3 4 3 3 4 xyz -5.07612 2.81966 13.3248
mbi 4 8; -3; -4; xyz 0.583193E-01 0.451928 -0.993347E-02
pb 3 4 4 3 4 4 xyz -5.55530 3.64757 13.3080
mbi 6 7; -7; -4; xyz -0.190924E-01 -0.437060 -0.921631E-02
pb 9 7 4 9 7 4 xyz 2.65088 6.29415 13.4110
pb 8 7 4 8 7 4 xyz 1.42752 6.56968 13.3287

c -----------------------
c section 4:
DEI  1 2 0 10 11; 1 2 0 7 8; 4 5;
DEI  4 8; 4 6; 4 5;

mbi ;; -5; xyz 0.468688E-01 3.88623 0.343170E-01
mbi ;; -5; xyz -1.25591 -0.242727E-01 0.346527E-01
pb 9 7 5 9 7 5 xyz 2.64206 5.93317 18.1595
pb 10 6 5 10 6 5 xyz 4.41300 5.41173 17.9822
```

```
pb 10 7 5 10 7 5 xyz 4.42261 6.23059 18.0652
pb 9 8 5 9 8 5 xyz 2.94029 6.75875 18.2794
pb 10 8 5 10 8 5 xyz 3.89100 6.51059 18.4863
pb 11 7 5 11 7 5 xyz 5.50914 5.84085 18.3287
pb 11 6 5 11 6 5 xyz 6.44964 5.00119 18.1679
pb 11 3 5 11 3 5 xyz 7.06599 1.85269 17.9739
pb 10 2 5 10 2 5 xyz 5.56956 0.302333 17.5398
pb 10 2 5 10 2 5 xyz 5.67986 0.205364 17.4807
pb 10 2 5 10 2 5 xyz 5.62121 0.150578 17.7695
pb 11 2 5 11 2 5 xyz 6.66703 0.904000 18.0712
pb 10 1 5 10 1 5 xyz 4.73079 -0.199951 17.9368
mbi 3 6; -2; -5; xyz -0.156512 1.07300 0.484020
pb 7 2 5 7 2 5 xyz 0.357634 1.12627 18.1083
pb 3 3 5 3 3 5 xyz -5.64649 2.32149 18.0985
pb 2 2 5 2 2 5 xyz -6.71003 1.28260 18.4310
pb 2 3 5 2 3 5 xyz -6.95087 2.49556 18.2832
pb 1 2 5 1 2 5 xyz -8.21554 1.54455 18.5701
pb 2 1 5 2 1 5 xyz -5.90652 0.828900 19.2553
mbi 3 4; -1; -5; xyz 0.598707E-01 1.78007 0.989946
mbi 5 6; -1; -5; xyz -0.672367E-01 1.59799 0.832640
pb 6 1 5 6 1 5 xyz -1.17336 0.680551 18.5883
mbi 7 8; -1; -5; xyz 0.159204 0.853036 0.534855
pb 8 1 5 8 1 5 xyz 1.92532 0.602500E-01 18.2987
pb 9 1 5 9 1 5 xyz 3.21643 -0.277780 18.0192
pb 1 7 5 1 7 5 xyz -8.08025 6.41246 17.8715
pb 2 8 5 2 8 5 xyz -6.25162 7.47704 17.8960
pb 2 7 5 2 7 5 xyz -7.25764 7.02636 17.8434
pb 3 8 5 3 8 5 xyz -5.50371 8.01007 17.8425
mbi -1; 4 5; -5; xyz -0.278419 -0.143513 -0.119267
mbi 7 8; -8; -5; xyz 0.355188E-01 -1.30334 -0.191969
pb 6 8 5 6 8 5 xyz -1.26789 7.71808 17.8299
mbi 7 8; -7; -5; xyz -0.448948E-01 -0.536503 0.792065E-01
pb 2 1 5 2 1 5 xyz -5.90386 1.02155 18.2968
pb 2 2 5 2 2 5 xyz -6.71919 1.20745 18.2310
pb 1 2 5 1 2 5 xyz -8.22185 1.55472 18.0630
pb 3 1 5 3 1 5 xyz -5.65442 1.02989 18.4879
pb 4 1 5 4 1 5 xyz -4.15593 0.996697 18.4422
pb 5 1 5 5 1 5 xyz -2.78133 0.851780 18.3539
pb 6 1 5 6 1 5 xyz -1.17516 0.644037 18.3229
pb 3 2 5 3 2 5 xyz -5.87213 1.74859 18.1613
pb 2 3 5 2 3 5 xyz -6.96588 2.41627 18.0480
pb 4 2 5 4 2 5 xyz -4.37377 1.66543 18.0842
pb 5 2 5 5 2 5 xyz -2.89909 1.64065 18.0444
pb 6 2 5 6 2 5 xyz -1.39898 1.61985 18.0777
pb 9 8 5 9 8 5 xyz 2.93881 6.79036 17.9827
pb 10 8 5 10 8 5 xyz 3.88523 6.50391 18.1052
pb 11 7 5 11 7 5 xyz 5.49990 5.77738 18.0338
mbi 4 6; -3; -5; xyz -0.783229E-02 0.461388 0.112936
pb 8 2 5 8 2 5 xyz 1.72283 0.922373 17.9106
pb 8 6 5 8 6 5 xyz 1.53731 5.18356 17.9643
pb 8 5 5 8 5 5 xyz 2.08675 3.85199 17.7655
pb 8 4 5 8 4 5 xyz 2.05541 2.92706 17.7755
pb 7 6 5 7 6 5 xyz 0.783257E-01 5.19751 17.8786
```

```
pb 6 6 5 6 6 5 xyz -1.19835 5.38824 17.8570
pb 4 6 5 4 6 5 xyz -3.93564 5.19171 17.8605
pb 4 5 5 4 5 5 xyz -4.40686 4.42735 17.8044
pb 4 4 5 4 4 5 xyz -3.98605 3.59924 17.9462
pb 6 4 5 6 4 5 xyz -1.31878 2.90380 17.7519
pb 7 4 5 7 4 5 xyz 0.293726 2.80751 17.6628
pb 8 4 5 8 4 5 xyz 2.06652 2.88852 17.7628
pb 8 6 5 8 6 5 xyz 1.18488 4.58888 17.9777
pb 5 6 5 5 6 5 xyz -2.65496 5.36852 17.8411
c 22 neg jacs this layer at the moment...

mbi -2; -8; 4 5; xyz -0.915523E-01 0.143318 -0.423717E-02
pb 9 6 5 9 6 5 xyz 3.04163 5.26557 17.7717
pb 9 7 5 9 7 5 xyz 2.96728 5.92217 18.1237
pb 7 6 4 7 6 4 xyz 0.269144 4.98448 11.6782
pb 8 5 5 8 5 5 xyz 1.86377 3.80876 17.7682
pb 8 4 5 8 4 5 xyz 1.72218 3.02348 17.7913
pb 8 6 5 8 6 5 xyz 1.58217 4.53508 17.9672
pb 8 6 5 8 6 5 xyz 1.52646 4.69294 17.9781

DEI  4 8; 3 4; 4 5;
pb 4 4 5 4 4 5 xyz -4.34728 3.96801 17.9828
pb 4 4 4 4 4 4 xyz -4.06837 4.50210 11.8357
pb 4 3 4 4 3 4 xyz -3.90308 3.96480 13.3865
pb 4 3 5 4 3 5 xyz -3.87598 3.56935 18.0892
mbi 5 8; -4; -4; xyz 0.110332 0.259714 0.194416E-01
pb 5 5 4 5 5 4 xyz -2.71752 5.01749 11.5362
pb 5 3 4 5 3 4 xyz -2.50755 3.88736 13.4666
pb 6 3 4 6 3 4 xyz -1.12836 3.62582 13.4267
pb 7 3 4 7 3 4 xyz 0.353165 3.30502 13.3770
pb 8 4 4 8 4 4 xyz 1.49670 3.59704 11.6921
pb 8 3 4 8 3 4 xyz 1.16590 3.24279 13.4015
pb 8 3 5 8 3 5 xyz 1.44794 2.59834 18.0149
pb 7 3 5 7 3 5 xyz 0.354659 2.58791 17.9669
pb 6 3 5 6 3 5 xyz -1.11668 2.82708 18.0367
pb 5 3 5 5 3 5 xyz -2.46789 3.06034 18.0607
mbi 4 8; -2; -5; xyz 0.644677E-01 0.505568 0.814247E-01
sfi -4 -8; -3 -6; 4 5;sd 2
pb 4 3 4 4 3 4 xyz -3.83127 3.97311 13.4430
pb 7 6 4 7 6 4 xyz -0.360998 4.91057 11.5060
pb 8 6 4 8 6 4 xyz 0.148013 4.35945 11.4177
pb 7 5 4 7 5 4 xyz -0.124599 4.09409 11.4401
pb 8 3 4 8 3 4 xyz 1.05773 3.23015 13.4290
pb 8 5 5 8 5 5 xyz 2.29208 3.57843 17.7724
pb 8 4 5 8 4 5 xyz 2.22873 3.07283 17.8330
pb 8 5 4 8 5 4 xyz 0.687871 3.86620 12.4548
pb 4 4 5 4 4 5 xyz -4.34728 3.96801 17.9828
pb 4 4 4 4 4 4 xyz -4.06837 4.50210 11.8357
pb 4 3 4 4 3 4 xyz -3.90308 3.96480 13.3865
pb 4 3 5 4 3 5 xyz -3.87598 3.56935 18.0892
mbi 5 8; -4; -4; xyz 0.110332 0.259714 0.194416E-01
pb 5 5 4 5 5 4 xyz -2.71752 5.01749 11.5362
pb 5 3 4 5 3 4 xyz -2.50755 3.88736 13.4666
```

```
pb 6 3 4 6 3 4 xyz -1.12836 3.62582 13.4267
pb 7 3 4 7 3 4 xyz 0.353165 3.30502 13.3770
pb 8 4 4 8 4 4 xyz 1.49670 3.59704 11.6921
pb 8 3 4 8 3 4 xyz 1.16590 3.24279 13.4015
pb 8 3 5 8 3 5 xyz 1.44794 2.59834 18.0149
pb 7 3 5 7 3 5 xyz 0.354659 2.58791 17.9669
pb 6 3 5 6 3 5 xyz -1.11668 2.82708 18.0367
pb 5 3 5 5 3 5 xyz -2.46789 3.06034 18.0607
mbi 4 8; -2; -5; xyz 0.644677E-01 0.505568 0.814247E-01
pb 7 4 4 7 4 4 xyz -0.996642E-02 3.78136 11.5656
pb 6 4 4 6 4 4 xyz -1.05684 4.06980 11.6392
pb 5 4 4 5 4 4 xyz -2.53372 4.36534 11.7351
pb 5 5 4 5 5 4 xyz -2.49950 4.92527 11.5258
pb 8 3 4 8 3 4 xyz 0.866394 3.35394 13.3991
pb 8 4 4 8 4 4 xyz 0.499444 3.90171 12.5444
pb 8 5 4 8 5 4 xyz 0.285482 4.04077 12.4630

pb 7 4 4 7 4 4 xyz 0.566221E-01 3.70202 11.5548
pb 7 4 4 7 4 4 xyz 0.608006E-02 3.87088 11.5658
pb 7 3 4 7 3 4 xyz 0.280248 3.61871 13.4034
pb 7 3 4 7 3 4 xyz 0.362102 3.44067 12.5358
pb 7 3 4 7 3 4 xyz 0.242831 3.94674 11.5516
mbi 5 6; -3; -4; xyz 0.117527 0.961999 -1.34391
pb 4 3 4 4 3 4 xyz -3.86391 5.15643 12.0564
pb 6 3 4 6 3 4 xyz -1.13961 3.75065 11.9605
pb 7 3 4 7 3 4 xyz 0.336362E-01 3.78073 11.8612
pb 7 3 4 7 3 4 xyz -0.384528E-01 3.79708 11.9321
pb 4 3 4 4 3 4 xyz -3.25399 4.48549 12.2757
pb 7 5 4 7 5 4 xyz -0.160546 4.28614 11.4394
pb 7 3 4 7 3 4 xyz 0.437605E-01 3.62782 11.9510
pb 5 3 4 5 3 4 xyz -2.74830 4.26095 11.8633
pb 5 4 4 5 4 4 xyz -2.50248 4.64207 11.7422
pb 6 4 4 6 4 4 xyz -1.09112 4.36718 11.6487
pb 7 4 4 7 4 4 xyz -0.186027E-01 4.04920 11.5717
pb 8 5 4 8 5 4 xyz -0.817580E-01 4.23406 12.3035
pb 8 5 4 8 5 4 xyz 0.433663 4.05486 12.2484
pb 8 6 4 8 6 4 xyz 0.245433 4.15289 11.6840
pb 7 6 4 7 6 4 xyz 0.259584E-01 4.31967 11.5227
pb 7 4 4 7 4 4 xyz -0.188255 4.07842 11.5403
pb 8 5 4 8 5 4 xyz 0.383705 4.15353 12.3265
pb 7 6 4 7 6 4 xyz 0.609498E-01 4.12907 11.7192
pb 7 5 4 7 5 4 xyz 0.361045E-01 4.02086 11.4818
pb 7 4 4 7 4 4 xyz 0.187484E-01 4.00821 11.6016
pb 7 3 4 7 3 4 xyz -0.105479 3.70564 12.0038
pb 7 4 4 7 4 4 xyz 0.302868E-01 3.84480 11.6123
pb 8 6 4 8 6 4 xyz 0.177262 4.12045 11.9352
pb 8 4 4 8 4 4 xyz 0.818396 3.68610 12.5562
pb 8 5 5 8 5 5 xyz 2.33267 3.35261 17.7816
pb 8 5 5 8 5 5 xyz 2.31481 3.44343 17.7765
pb 8 5 5 8 5 5 xyz 2.30364 3.56818 17.7650
pb 8 4 5 8 4 5 xyz 2.29401 3.22137 17.8547
pb 8 5 5 8 5 5 xyz 2.34694 3.44527 17.7664
pb 8 4 5 8 4 5 xyz 2.32017 3.31115 17.8660
```

```
pb 8 6 5 8 6 5 xyz 1.95901 3.95868 18.1207
pb 8 5 5 8 5 5 xyz 2.31647 3.66049 17.7688
pb 8 5 5 8 5 5 xyz 2.29299 3.59905 17.7722
mbi -4 -8; -3 -6; -5; xyz -0.968349E-01 -0.613606E-01 -1.31862
pb 8 5 4 8 5 4 xyz 0.763430 4.01570 12.5717
mbi -9; -5; 4 5; xyz -0.814910E-01 -0.489161 -0.100975E-01
pb 8 5 4 8 5 4 xyz 1.20098 3.97908 12.7660
pb 8 4 4 8 4 4 xyz 1.10127 3.63450 12.7181
pb 8 6 4 8 6 4 xyz 0.359841 3.98633 12.1567
pb 8 6 4 8 6 4 xyz 0.309680 3.94042 12.2191
pb 7 5 4 7 5 4 xyz 0.437014 3.76945 11.6471
pb 7 5 4 7 5 4 xyz 0.956381E-01 3.89988 11.6844
pb 8 5 4 8 5 4 xyz 1.50616 3.75733 12.8554
pb 8 4 4 8 4 4 xyz 1.26868 3.60565 12.8047
pb 4 4 4 4 4 4 xyz -3.35769 4.58342 12.3051
pb 4 5 4 4 5 4 xyz -3.31270 5.09619 12.1074
pb 4 4 4 4 4 4 xyz -3.35769 4.58342 12.3051
pb 4 5 4 4 5 4 xyz -3.31270 5.09619 12.1074
pb 8 6 4 8 6 4 xyz 0.221655 3.96351 12.2065
pb 8 5 4 8 5 4 xyz 0.768628 3.84966 13.0124
mbi -8; 5 6; -4; xyz -0.563326E-01 0.198825 -0.315490
pb 8 5 4 8 5 4 xyz 0.841089 3.97560 12.6959
pb 8 5 5 8 5 5 xyz 2.27508 3.71478 16.4594
pb 8 5 4 8 5 4 xyz 1.04354 3.84024 12.8059
pb 8 5 4 8 5 4 xyz 0.539589 4.03581 12.6563
pb 8 6 3 8 6 3 xyz 1.57491 7.43279 9.07312
pb 7 6 4 7 6 4 xyz -0.219597E-01 4.25127 11.6026
pb 8 6 4 8 6 4 xyz 0.617984E-01 4.22873 11.8307
pb 9 5 4 9 5 4 xyz 3.03101 4.51169 12.9839
c zero neg jacs!
c -----------------------
c section 5:
DEI  1 2 0 10 11; 1 2 0 7 8; 5 6;
DEI  4 8; 3 6; 5 6;
mbi ;; -6; xyz 0.182451 3.61755 0.119085
mbi ;; -6; xyz -1.10478 -0.124013E-01 0.139524
pb 8 6 6 8 6 6 xyz 2.10822 4.02805 22.5074
pb 8 5 6 8 5 6 xyz 2.11872 3.45088 22.4360
pb 7 3 6 7 3 6 xyz 0.622256 1.87470 22.5256
pb 6 3 6 6 3 6 xyz -0.729808 2.01385 22.5366
pb 5 3 6 5 3 6 xyz -1.81597 2.22040 22.5396
pb 4 3 6 4 3 6 xyz -3.32637 2.93015 22.4880
pb 4 4 6 4 4 6 xyz -3.85763 3.58351 22.4985
pb 4 6 6 4 6 6 xyz -3.58324 5.14922 22.4296
pb 5 6 6 5 6 6 xyz -2.34725 5.17967 22.4395
pb 6 6 6 6 6 6 xyz -0.946760 5.16541 22.4699
pb 7 6 6 7 6 6 xyz 0.401351 4.81818 22.4506
pb 8 6 6 8 6 6 xyz 1.99449 3.92260 22.4964
pb 8 3 6 8 3 6 xyz 1.46937 2.39561 22.4830
pb 7 3 6 7 3 6 xyz 0.441837 2.32621 22.5290
pb 6 3 6 6 3 6 xyz -0.865528 2.23308 22.5581
pb 5 3 6 5 3 6 xyz -1.86816 2.48890 22.5650
mbi 1 11; -7; -6; xyz -0.265884E-01 -0.688191 -0.118885E-01
```

```
mbi 1 11; -2; -6; xyz 0.190159E-01 0.487105 0.144501E-01
mbi -2;; -6; xyz 0.612532 -0.184481E-01 -0.438519E-01
pb 7 1 6 7 1 6 xyz 0.462005 -0.352853 22.6137
pb 6 1 6 6 1 6 xyz -0.787960 0.771273E-01 22.7108
pb 5 1 6 5 1 6 xyz -2.36912 0.450054 22.7900
pb 4 1 6 4 1 6 xyz -3.76989 0.512577 22.8052
pb 3 1 6 3 1 6 xyz -4.91387 0.706048 22.8529
pb 2 1 6 2 1 6 xyz -5.90768 0.908230 22.8549
pb 2 2 6 2 2 6 xyz -7.18020 1.38569 22.5671
pb 1 2 6 1 2 6 xyz -7.94712 1.71488 22.7005
pb 1 3 6 1 3 6 xyz -8.28810 1.93464 22.5491
pb 1 4 6 1 4 6 xyz -8.82151 2.85164 22.3591
pb 1 5 6 1 5 6 xyz -8.87593 4.21425 22.3417
pb 1 6 6 1 6 6 xyz -8.17289 5.36938 22.5820
pb 2 7 6 2 7 6 xyz -6.89312 6.33855 22.2546
pb 1 7 6 1 7 6 xyz -7.84645 5.79109 22.6891
pb 2 8 6 2 8 6 xyz -6.13813 6.68309 22.9240
pb 3 8 6 3 8 6 xyz -4.99179 6.91764 22.9803
pb 4 8 6 4 8 6 xyz -3.68847 7.19389 22.8396
pb 5 8 6 5 8 6 xyz -2.37792 7.00750 22.8389
pb 6 8 6 6 8 6 xyz -0.998746 6.97826 22.8117
pb 7 8 6 7 8 6 xyz 0.513703 6.68161 22.9038
pb 8 8 6 8 8 6 xyz 1.92457 6.44696 22.9472
pb 9 8 6 9 8 6 xyz 3.61225 5.97922 22.4557
pb 10 8 6 10 8 6 xyz 4.84304 5.68295 22.4995
pb 10 7 6 10 7 6 xyz 5.67078 5.46723 22.3628
pb 11 7 6 11 7 6 xyz 6.66016 4.94047 22.4465
pb 11 6 6 11 6 6 xyz 6.94289 4.76472 22.5481
pb 11 5 6 11 5 6 xyz 7.46789 4.26127 22.4744
pb 10 2 6 10 2 6 xyz 6.06822 -0.127581E-01 22.2713
pb 10 2 6 10 2 6 xyz 6.53559 -0.372322 22.1638
pb 11 4 6 11 4 6 xyz 7.91133 2.61137 22.4611
pb 11 3 6 11 3 6 xyz 7.65850 1.28757 22.4907
pb 9 8 6 9 8 6 xyz 3.62651 6.14974 22.4971
pb 10 8 6 10 8 6 xyz 4.79362 5.90827 22.5565
pb 9 7 6 9 7 6 xyz 3.57116 5.83222 22.4137
pb 9 6 6 9 6 6 xyz 3.58393 5.03910 22.3766
pb 10 6 6 10 6 6 xyz 5.09181 4.96248 22.3575
pb 10 6 6 10 6 6 xyz 5.67519 4.90780 22.2676
pb 11 7 6 11 7 6 xyz 6.35257 5.09641 22.5279
pb 10 5 6 10 5 6 xyz 5.50168 4.22296 22.4342
pb 9 2 6 9 2 6 xyz 3.98649 0.536295 22.2702
pb 2 3 6 2 3 6 xyz -6.67797 1.76495 22.4947
pb 1 2 6 1 2 6 xyz -7.66848 1.57254 22.6971
pb 2 2 6 2 2 6 xyz -6.86458 1.27165 22.5544
pb 2 4 6 2 4 6 xyz -6.58566 2.95940 22.4655
pb 8 7 6 8 7 6 xyz 2.16496 5.61105 22.6241
pb 3 2 6 3 2 6 xyz -5.38900 1.17067 22.5354
pb 3 3 6 3 3 6 xyz -5.43719 2.17063 22.5215
pb 2 7 6 2 7 6 xyz -6.87184 6.18472 22.6013
pb 6 2 5 6 2 5 xyz -1.18746 2.15072 18.2205
c zero bad jacs, no changes!
```

```
c -----------------------
c Section 6:
DEI  1 2 0 10 11; 1 2 0 7 8; 6 7;
DEI  4 8; 3 6; 6 7;
mbi ;; -7; xyz 0.186641 2.98538 -0.606003E-01
mbi ;; -7; xyz -0.439003 0.427341E-02 0.252991E-01
pb 8 6 7 8 6 7 xyz 2.58921 3.75664 26.5529
pb 8 5 7 8 5 7 xyz 2.73411 3.20828 26.6090
pb 8 3 7 8 3 7 xyz 2.04499 1.91567 26.7572
pb 7 3 7 7 3 7 xyz 0.786929 1.78201 26.7324
pb 6 3 7 6 3 7 xyz -0.624634 1.64175 26.7154
pb 5 3 7 5 3 7 xyz -1.59971 1.89619 26.7086
pb 4 3 7 4 3 7 xyz -3.00305 2.27397 26.7359
pb 4 4 7 4 4 7 xyz -3.25653 3.12670 26.7101
pb 4 6 7 4 6 7 xyz -2.89274 4.34782 26.5399
pb 5 6 7 5 6 7 xyz -1.72245 4.54775 26.6044
pb 6 6 7 6 6 7 xyz -0.233426 4.49400 26.6005
pb 7 6 7 7 6 7 xyz 1.15298 4.40612 26.6063
pb 10 2 7 10 2 7 xyz 6.23422 -0.572029 26.5203
pb 10 1 7 10 1 7 xyz 5.34233 -1.18251 26.7519
pb 11 2 7 11 2 7 xyz 7.47601 0.167355 26.8737
pb 9 7 7 9 7 7 xyz 4.17655 4.41475 26.8758
pb 9 7 7 9 7 7 xyz 4.14278 5.12713 26.9419
pb 10 8 7 10 8 7 xyz 4.37573 5.30722 26.7185
pb 10 7 7 10 7 7 xyz 5.59576 4.99569 26.6342
pb 11 7 7 11 7 7 xyz 6.36538 4.63241 26.6890
pb 11 6 7 11 6 7 xyz 7.04069 4.33627 26.7218
pb 11 5 7 11 5 7 xyz 7.91155 3.66756 26.6601
pb 8 7 7 8 7 7 xyz 2.59007 5.20347 26.6387
pb 9 8 7 9 8 7 xyz 3.76231 5.39340 26.7267
pb 8 8 7 8 8 7 xyz 2.58133 5.64317 26.6886
pb 7 8 7 7 8 7 xyz 1.13366 5.97465 26.6782
pb 6 8 7 6 8 7 xyz -0.339125 6.15417 26.7336
mbi 4 5; -8; -7; xyz -0.357025E-01 -0.935056 0.624142E-01
pb 3 8 7 3 8 7 xyz -4.43893 6.37543 26.7219
pb 2 7 7 2 7 7 xyz -6.18548 5.60412 26.6851
pb 2 8 7 2 8 7 xyz -5.55977 5.75275 26.7667
pb 1 6 7 1 6 7 xyz -7.48456 4.53026 26.6729
pb 1 7 7 1 7 7 xyz -6.96477 5.09360 26.7251
pb 2 2 7 2 2 7 xyz -6.05743 0.688847 26.9396
pb 1 2 7 1 2 7 xyz -6.89045 0.961693 27.0478
pb 1 3 7 1 3 7 xyz -7.39493 1.56685 26.8173
pb 1 4 7 1 4 7 xyz -7.89405 2.59177 26.7169
pb 2 1 7 2 1 7 xyz -5.22608 0.228376 27.2299
pb 3 2 7 3 2 7 xyz -4.12972 0.534835 26.9046
pb 3 1 7 3 1 7 xyz -4.50443 0.573430E-01 27.1504
mbi 4 5; -1; -7; xyz -0.148816E-01 1.38021 0.437704
mbi 6 7; -1; -7; xyz -0.309679E-01 0.819973 0.259356
mbi 8 9; -1; -7; xyz -0.301254E-01 0.340690 0.107254
pb 5 7 7 5 7 7 xyz -1.70153 5.47881 26.5667
pb 6 7 7 6 7 7 xyz -0.223851 5.45705 26.5617
pb 7 7 7 7 7 7 xyz 1.27568 5.32613 26.5464
pb 8 7 7 8 7 7 xyz 2.58352 4.81252 26.5926
```

```
pb 9 7 7 9 7 7 xyz 4.20497 4.70333 26.8997
pb 9 6 7 9 6 7 xyz 4.24926 4.16184 26.5569
pb 10 6 7 10 6 7 xyz 5.76102 4.21730 26.5647
pb 3 7 7 3 7 7 xyz -4.72295 5.71426 26.5223
pb 4 7 7 4 7 7 xyz -3.16115 5.75253 26.5169
pb 4 2 7 4 2 7 xyz -3.17383 0.721839 26.5859
pb 5 2 7 5 2 7 xyz -1.79408 0.638526 26.6179
pb 6 2 7 6 2 7 xyz -0.373718 0.679690 26.6350
pb 7 2 7 7 2 7 xyz 1.37072 0.225618 26.6821
pb 8 2 7 8 2 7 xyz 2.52607 0.485758 26.7874
pb 2 8 7 2 8 7 xyz -5.49305 5.97143 26.8134
pb 4 5 7 4 5 7 xyz -3.98801 4.04943 26.6993
pb 4 6 7 4 6 7 xyz -3.33659 4.45788 26.5685
pb 3 3 7 3 3 7 xyz -4.40894 1.42936 26.7466
pb 2 3 7 2 3 7 xyz -6.18542 1.54658 26.7452
pb 8 6 7 8 6 7 xyz 1.93680 3.44865 26.5960
pb 8 7 7 8 7 7 xyz 2.39022 4.50358 26.5509
pb 7 7 7 7 7 7 xyz 1.19364 5.07605 26.5011
pb 9 5 7 9 5 7 xyz 4.26288 3.14743 26.5307
pb 9 7 7 9 7 7 xyz 3.94085 4.68992 26.9373
pb 8 2 7 8 2 7 xyz 2.60567 0.202161 26.7042
pb 4 3 7 4 3 7 xyz -2.60719 2.30636 26.6825
c ----------------------
c Section 7:
DEI  1 2 0 10 11; 1 2 0 7 8; 7 8;
DEI  4 8; 3 6; 7 8;
mbi ;; -8; xyz 0.646883E-01 2.12679 0.260086E-01
mbi ;; -8; xyz -0.952515E-01 -0.773072E-02 0.919189E-01
pb 2 8 8 2 8 8 xyz -5.26331 5.72810 31.7299
pb 1 7 8 1 7 8 xyz -7.01734 4.65968 31.5734
pb 3 8 8 3 8 8 xyz -4.35852 6.02838 31.3722
pb 2 3 8 2 3 8 xyz -5.68960 0.756654 31.4959
pb 3 2 8 3 2 8 xyz -4.22732 0.248638 31.5438
pb 3 3 8 3 3 8 xyz -4.27375 0.518086 31.4258
pb 2 2 8 2 2 8 xyz -5.53801 -0.231162E-01 31.6285
pb 1 2 8 1 2 8 xyz -6.59951 0.401143 31.9198
pb 1 3 8 1 3 8 xyz -7.12761 1.12457 31.5649
pb 1 4 8 1 4 8 xyz -7.41071 1.89034 31.3542
pb 1 5 8 1 5 8 xyz -7.65529 2.75664 31.1757
pb 1 5 8 1 5 8 xyz -7.69644 2.82987 31.1585
pb 2 1 8 2 1 8 xyz -4.66248 -0.457081 31.9110
pb 3 1 8 3 1 8 xyz -3.62474 -0.631337 31.7987
pb 4 1 8 4 1 8 xyz -2.30201 -0.866256 31.7162
pb 5 1 8 5 1 8 xyz -1.06232 -1.06122 31.6302
pb 6 1 8 6 1 8 xyz 0.209940 -1.38470 31.5191
pb 7 1 8 7 1 8 xyz 1.61735 -1.53094 31.4704
pb 4 2 8 4 2 8 xyz -2.58421 -0.404989 31.4779
pb 5 2 8 5 2 8 xyz -1.37407 -0.548543 31.3995
pb 8 1 8 8 1 8 xyz 2.99273 -1.60792 31.4331
pb 10 2 8 10 2 8 xyz 6.31427 -1.30181 31.1015
pb 10 1 8 10 1 8 xyz 5.63606 -1.52868 31.5721
pb 9 1 8 9 1 8 xyz 4.31521 -1.68951 31.4816
pb 11 2 8 11 2 8 xyz 7.47469 -0.722891 31.6764
```

```
pb 11 3 8 11 3 8 xyz 8.07206 0.139010 31.4078
pb 9 7 8 9 7 8 xyz 3.63718 4.25132 31.4639
pb 10 6 8 10 6 8 xyz 5.43358 3.23966 31.3867
pb 10 7 8 10 7 8 xyz 5.12619 4.12599 31.4665
pb 11 6 8 11 6 8 xyz 6.76360 3.19700 31.6093
pb 11 7 8 11 7 8 xyz 6.04388 3.61206 31.6182
pb 10 8 8 10 8 8 xyz 4.29573 4.53568 31.6824
pb 9 8 8 9 8 8 xyz 3.68542 4.76636 31.4492
pb 8 8 8 8 8 8 xyz 2.46366 5.09564 31.3769
pb 7 8 8 7 8 8 xyz 1.11353 5.59005 31.3388
pb 6 8 8 6 8 8 xyz -0.249348 6.04397 31.3040
pb 11 5 8 11 5 8 xyz 7.78608 2.36932 31.3418
mbi -4; 4 5; -8; xyz -0.844187 0.428325 -0.791378E-01
pb 4 5 8 4 5 8 xyz -4.07760 3.07955 31.1145
pb 4 6 8 4 6 8 xyz -3.54590 3.90766 31.1372
pb 4 3 8 4 3 8 xyz -2.82011 1.22923 31.4908
pb 6 3 8 6 3 8 xyz -0.387534E-01 0.674151 31.3550
pb 5 3 8 5 3 8 xyz -1.42446 1.29462 31.3378
mbi -8; 4 5; -8; xyz -0.810414 -0.334074E-01 0.459690E-01
mbi -8; 4 5; -8; xyz 0.341923 0.209870 -0.320816E-02
mbi -8; 4 5; -8; xyz 0.265502 -0.282371E-01 -0.182743E-01
pb 8 6 8 8 6 8 xyz 2.23566 3.05303 31.2098
pb 7 6 8 7 6 8 xyz 1.22250 3.56554 31.2229
pb 8 3 8 8 3 8 xyz 2.03487 1.22590 31.3897
pb 7 3 8 7 3 8 xyz 1.15101 0.721906 31.3111
pb 7 7 8 7 7 8 xyz 1.39447 4.70761 31.2198
pb 8 7 8 8 7 8 xyz 2.72907 4.32297 31.2044
pb 9 6 8 9 6 8 xyz 4.08831 3.46510 31.2268
mbi 6 9; -2; -8; xyz -0.182731E-01 0.580187 0.156042
pb 5 2 8 5 2 8 xyz -1.40593 -0.105781 31.5174
pb 3 3 8 3 3 8 xyz -4.37250 0.981918 31.5450
pb 3 4 8 3 4 8 xyz -4.64429 1.98054 31.3763
pb 10 5 8 10 5 8 xyz 5.92815 2.29019 31.2441
pb 2 8 8 2 8 8 xyz -5.21011 5.86960 31.3922
pb 11 2 8 11 2 8 xyz 7.48455 -0.527823 31.4086
pb 1 2 8 1 2 8 xyz -6.44963 0.557819 31.6565
pb 4 2 8 4 2 8 xyz -2.63724 -0.258706E-01 31.5140
pb 9 5 8 9 5 8 xyz 4.43169 2.41362 31.1528
c -----------------------
c Section 8:
DEI  1 2 0 10 11; 1 2 0 7 8; 8 9;
DEI  4 8; 3 6; 8 9;
mbi ;; -9; xyz 0.308210E-02 2.04336 0.637741E-01
pb 2 7 9 2 7 9 xyz -5.61054 4.84034 35.7697
pb 2 8 9 2 8 9 xyz -4.87336 5.40450 36.0052
pb 1 7 9 1 7 9 xyz -6.61516 4.12464 35.9453
pb 3 8 9 3 8 9 xyz -4.06173 5.77385 35.8087
pb 4 8 9 4 8 9 xyz -2.96170 6.08826 35.6869
pb 5 8 9 5 8 9 xyz -1.57743 6.03838 35.6624
pb 1 6 9 1 6 9 xyz -6.98422 3.61612 35.7964
pb 2 2 9 2 2 9 xyz -5.42371 -0.410538 35.8595
pb 1 2 9 1 2 9 xyz -6.41437 0.234516 36.0472
pb 1 3 9 1 3 9 xyz -6.79367 0.869149 35.8830
```

```
pb 1 4 9 1 4 9 xyz -7.14690 1.53320 35.7265
pb 3 1 9 3 1 9 xyz -4.31629 -0.888261 35.9083
pb 3 2 9 3 2 9 xyz -4.34961 -0.611645 35.7525
pb 2 1 9 2 1 9 xyz -5.01577 -0.725001 36.0777
pb 4 1 9 4 1 9 xyz -2.87410 -1.27763 35.9295
pb 5 1 9 5 1 9 xyz -1.38076 -1.56688 35.8604
pb 6 1 9 6 1 9 xyz 0.982016E-01 -1.82945 35.7971
pb 7 1 9 7 1 9 xyz 1.56342 -1.91894 35.7399
pb 8 1 9 8 1 9 xyz 3.03339 -2.00648 35.7246
pb 9 1 9 9 1 9 xyz 4.48391 -1.98394 35.7293
pb 10 2 9 10 2 9 xyz 6.66068 -1.45017 35.5081
pb 10 1 9 10 1 9 xyz 5.82282 -1.81299 35.7582
pb 11 2 9 11 2 9 xyz 7.79982 -0.967261 35.8278
pb 9 7 9 9 7 9 xyz 3.34451 3.77533 35.7410
pb 9 6 9 9 6 9 xyz 3.97919 3.15561 35.6864
pb 10 6 9 10 6 9 xyz 5.44653 2.64845 35.6849
pb 10 7 9 10 7 9 xyz 4.95992 3.57464 35.7281
pb 11 7 9 11 7 9 xyz 6.08286 2.94457 35.7584
pb 11 6 9 11 6 9 xyz 6.64698 2.60155 35.7907
pb 11 5 9 11 5 9 xyz 7.47880 1.95476 35.7171
pb 11 4 9 11 4 9 xyz 8.29970 1.10921 35.6963
pb 8 7 9 8 7 9 xyz 2.59295 4.27778 35.6741
pb 8 8 9 8 8 9 xyz 2.67284 4.73633 35.6589
pb 9 8 9 9 8 9 xyz 3.52046 4.26855 35.7169
pb 10 8 9 10 8 9 xyz 4.34511 3.91289 35.7782
pb 6 8 9 6 8 9 xyz -0.102621 5.54136 35.6447
pb 7 8 9 7 8 9 xyz 1.30908 5.11187 35.6493
pb 8 3 8 8 3 8 xyz 2.25489 1.10063 31.3686
pb 8 3 9 8 3 9 xyz 2.43787 0.597939 35.7135
mbi -8; -6; 8 9; xyz 0.220244E-01 0.272641E-01 0.167084E-02
pb 8 6 9 8 6 9 xyz 2.46402 2.92995 35.5672
pb 4 6 9 4 6 9 xyz -2.65908 3.17792 35.5540
pb 4 3 9 4 3 9 xyz -2.66399 0.662576 35.6820
pb 4 5 9 4 5 9 xyz -3.69545 2.75475 35.6631
pb 4 3 9 4 3 9 xyz -2.47701 1.20417 35.7527
pb 5 3 9 5 3 9 xyz -1.38533 0.791835 35.7340
pb 6 3 9 6 3 9 xyz 0.908137E-01 0.661171 35.7167
pb 7 3 9 7 3 9 xyz 1.47726 0.800850 35.7371
pb 8 3 9 8 3 9 xyz 2.24888 0.897509 35.7639
pb 7 6 9 7 6 9 xyz 1.30710 3.54223 35.6589
pb 4 6 9 4 6 9 xyz -3.14883 3.44675 35.5658
pb 4 6 9 4 6 9 xyz -2.88657 3.53079 35.5704
pb 7 7 9 7 7 9 xyz 1.36868 4.61927 35.6129
pb 6 7 9 6 7 9 xyz -0.505229E-02 4.78022 35.6154
pb 10 6 9 10 6 9 xyz 5.46670 2.94117 35.7357
pb 10 5 9 10 5 9 xyz 5.83578 1.95659 35.5109
pb 9 5 9 9 5 9 xyz 4.49508 2.39590 35.5947
pb 9 6 9 9 6 9 xyz 4.19390 2.95207 35.6646
pb 10 3 9 10 3 9 xyz 6.53749 -0.719178E-01 35.6440
pb 4 2 9 4 2 9 xyz -2.86065 -0.495668 35.7655
pb 3 2 9 3 2 9 xyz -4.35571 -0.408175 35.7866
pb 3 3 9 3 3 9 xyz -4.24882 0.618420 35.7440
pb 2 3 9 2 3 9 xyz -5.58270 0.733983 35.7733
```

```
pb 3 7 9 3 7 9 xyz -4.09040 5.06380 35.6357
pb 3 6 9 3 6 9 xyz -4.47956 3.85226 35.6243
pb 2 6 9 2 6 9 xyz -5.65406 3.87974 35.6482
pb 9 7 9 9 7 9 xyz 3.66262 3.64593 35.7379
pb 8 7 9 8 7 9 xyz 2.55820 3.77524 35.5870
pb 7 7 9 7 7 9 xyz 1.31398 4.35171 35.5644
pb 5 2 9 5 2 9 xyz -1.42372 -0.630749 35.7389
mbi 3 9; -2; -9; xyz 0.968993E-02 0.340244 0.582199E-01
mbi -3; 3 4; -9; xyz -0.401077E-01 0.278059 0.447311E-01
c -----------------------
c section 9
DEI  1 2 0 10 11; 1 2 0 7 8; 9 10;
DEI  4 8; 3 6; 9 10;
mbi ;; -10; xyz 0.308442E-01 1.54748 0.835800E-02
mbi 3 10; -2; -10; xyz 0.492492E-01 0.773482 0.391464E-01
pb 9 7 10 9 7 10 xyz 4.07236 3.25189 39.7908
pb 8 7 10 8 7 10 xyz 2.82581 3.55774 39.7840
pb 7 7 10 7 7 10 xyz 1.41188 3.78467 39.8361
pb 6 7 10 6 7 10 xyz -0.205818E-01 4.28028 39.9397
pb 9 6 10 9 6 10 xyz 4.52511 2.60880 39.9777
pb 10 6 10 10 6 10 xyz 6.01885 2.58761 39.9764
mbi 8 11; -5; -10; xyz 0.216533 -0.386540 -0.322304E-01
mbi 8 11; -3; -10; xyz 0.157212 0.386358 0.232735E-01
pb 2 3 10 2 3 10 xyz -5.79709 -0.630446E-02 40.0105
pb 10 2 10 10 2 10 xyz 7.04750 -1.90933 39.9552
pb 10 6 10 10 6 10 xyz 5.96145 2.29557 39.9373
pb 10 5 10 10 5 10 xyz 6.01957 1.78136 40.0093
c -----------------------
c section 10
DEI  1 2 0 10 11; 1 2 0 7 8; 10 11;
DEI  4 8; 3 6; 10 11;
mbi ;; -11; xyz -0.268140E-01 0.788229 0.144005E-01
mbi ;; -11; xyz 0.318107 -0.111426E-01 -0.297356E-01
pb 8 7 11 8 7 11 xyz 2.95043 3.12782 44.3391
pb 9 7 11 9 7 11 xyz 4.41770 2.53707 44.2537
pb 10 6 11 10 6 11 xyz 6.06614 1.83436 44.3683
pb 9 6 11 9 6 11 xyz 4.62347 1.90010 44.3739
pb 7 7 11 7 7 11 xyz 1.76281 3.53152 44.4114
pb 3 2 11 3 2 11 xyz -3.96023 -1.88056 44.5128
mbi 4 8; -2; -11; xyz 0.180090E-01 0.873414 0.820313E-01
pb 10 2 11 10 2 11 xyz 7.02184 -2.32255 44.4898
pb 9 2 11 9 2 11 xyz 4.85421 -2.15292 44.4814
mbi 9 10; -5; -11; xyz 0.835805E-01 -0.399316 -0.316048E-01
pb 2 3 11 2 3 11 xyz -5.45232 -0.599479 44.5025
pb 3 2 11 3 2 11 xyz -3.89652 -1.64081 44.5341
pb 3 3 11 3 3 11 xyz -4.02790 -0.804080 44.4846
pb 3 4 11 3 4 11 xyz -4.21824 0.511187 44.4893
pb 10 7 11 10 7 11 xyz 5.86740 2.59245 44.3264
pb 9 3 11 9 3 11 xyz 4.87322 -0.844210 44.5203
pb 8 2 11 8 2 11 xyz 3.06282 -1.53011 44.5782
c -----------------------
c section 11
DEI  1 2 0 10 11; 1 2 0 7 8; 11 12;
```

```
DEI  4 8; 3 6; 11 12;
pb 3 2 12 3 2 12 xyz -3.92933 -1.96280 48.9200
pb 3 3 12 3 3 12 xyz -4.46699 -1.06670 48.9200
mbi 4 9; -2; -12; xy 0.401026E-01 0.809113
pb 2 3 12 2 3 12 xyz -5.46265 -1.20609 48.9200
pb 2 3 12 2 3 12 xyz -5.46265 -1.20609 48.9200
pb 9 7 12 9 7 12 xyz 4.11160 2.79349 48.8652
pb 9 3 12 9 3 12 xyz 4.53641 -1.35186 49.0032
mbi 1 3; -4; -12; xyz -0.962696E-01 0.507018 0.304298E-01
c -----------------------
c section 12
DEI  1 2 0 10 11; 1 2 0 7 8; 12 13;
DEI  4 8; 3 6; 12 13;
mbi 3 9; -7; -13; xyz 0.418931E-01 -0.388920 -0.381470E-05
pb 3 2 13 3 2 13 xyz -4.10857 -2.57693 53.3700
pb 10 2 13 10 2 13 xyz 6.44842 -3.05728 53.3383
pb 9 7 13 9 7 13 xyz 4.23559 2.49846 53.3025
pb 10 6 13 10 6 13 xyz 5.94994 1.49316 53.2827
pb 9 6 13 9 6 13 xyz 4.53019 1.65438 53.3156
pb 8 4 13 8 4 13 xyz 3.44192 -0.455063 53.4209
pb 2 3 13 2 3 13 xyz -5.86197 -1.62930 53.3846
c -----------------------
c section 13
DEI  1 2 0 10 11; 1 2 0 7 8; 13 14;
DEI  4 8; 3 6; 13 14;
mbi 3 9; -7; -14; xyz -0.352197E-01 -0.777717 0.381470E-05
c -----------------------
c section 14
DEI  1 2 0 10 11; 1 2 0 7 8; 14 15;
DEI  4 8; 3 6; 14 15;
mbi 3 9; -7; -15; xy 0.433225e-01 -0.833940
mbi 9 10; -6; -15; xy 0.300508e-01 -0.412763
mbi 2 3; -6; -15; xy -0.624657e-02 -0.538444
c -----------------------
c section 15
DEI  1 2 0 10 11; 1 2 0 7 8; 15 16;
DEI  4 8; 3 6; 15 16;
mbi 3 9; -7; -16; xy 0.600028E-01 -0.936692
pb 2 6 16 2 6 16 xyz -5.57769 1.26581 66.7100
pb 10 6 16 10 6 16 xyz 5.96336 1.55937 66.7100
pb 9 6 16 9 6 16 xyz 4.58293 1.50948 66.7100
pb 3 6 16 3 6 16 xyz -4.46233 1.34628 66.7100
pb 2 8 16 2 8 16 xyz -4.78485 2.54556 66.5899
pb 3 7 16 3 7 16 xyz -4.01532 2.02573 66.7100
pb 9 7 16 9 7 16 xyz 4.16061 1.96862 66.7100
mbi 9 10; -6; -16; xy 0.165186E-01 -0.318501
pb 10 2 16 10 2 16 xyz 6.88477 -3.76626 66.7035
c -----------------------
c section 16
DEI  1 2 0 10 11; 1 2 0 7 8; 16 17;
DEI  4 8; 3 6; 16 17;
mbi 3 9; -7; -17; xy 0.412924E-01 -0.980248
mbi 2 3; -6; -17; xy -0.374355E-01 -0.790725
```

```
mbi 9 10; -6; -17; xy -0.237637E-01 -0.790725
pb 2 6 17 2 6 17 xyz -5.54919 0.942961 71.1600
pb 2 5 17 2 5 17 xyz -5.81094 0.484897 71.1600
pb 10 2 17 10 2 17 xyz 7.08077 -3.70328 71.1352
c -----------------------
c section 17
DEI  1 2 0 10 11; 1 2 0 7 8; 17 18;
DEI  4 8; 3 6; 17 18;
mbi 2 3; -6; -18; xy 0.124973 -1.15419
mbi 9 10; -6; -18; xy 0.112419E-01 -1.05335
mbi 8 11; -5; -18; xy 0.463417 -0.577660
mbi 1 4; -5; -18; xyz -0.258101 -0.583609 0.762939E-05
mbi 3 9; -7; -18; xy 0.580237E-01 -1.48632
mbi 5 7; -7; -18; xy 0.201674E-01 0.746201
pb 8 4 18 8 4 18 xyz 3.88974 -0.555270 75.6219
mbi -2; 5 6; -18; xy 0.296176 0.168610E-01
mbi 5 7; -2; -18; xy 0.211859E-01 -0.610437
c -----------------------
c section 18
DEI  1 2 0 10 11; 1 2 0 7 8; 18 19;
DEI  4 8; 3 6; 18 19;
mbi 3 9; -7; -19; xyz 0.957448E-01 -1.55034 0.762939E-05
mbi 5 7; -7; -19; xy -0.754113E-01 0.728975
mbi 5 7; -2; -19; xyz -0.480269E-02 -0.836424 0.762939E-05
mbi 2 3; -6; -19; xyz 0.343492 -1.07472 0.762939E-05
mbi 9 10; -6; -19; xyz -0.117970E-02 -0.898760 0.762939E-05
mbi 2 3; -5; -19; xyz -0.586996E-01 -0.513691 0.762939E-05
mbi 9 10; -5; -19; xyz 0.239577E-01 -0.463416 0.762939E-05
c -----------------------
c section 19
DEI  1 2 0 10 11; 1 2 0 7 8; 19 20;
DEI  4 8; 3 6; 19 20;
mbi ;; -20; xyz -0.320083E-02 -0.867453 -0.508881E-02
mbi ;; -20; xyz 0.419614E-01 0.262260E-05 -0.565338E-02
mbi -2; 3 6; -20; xyz 0.453544 -0.351262 -0.762939E-05
mbi 3 4; -7; -20; xyz 0.163249 -0.596579 -0.762939E-05
pb 8 6 20 8 6 20 xyz 2.00462 0.615269 84.4758
mbi -3; 6 7; -20; xyz 0.203514 -0.160779 -0.762939E-05
c -----------------------
c section 20
DEI  1 2 0 10 11; 1 2 0 7 8; 20 21;
DEI  4 8; 3 6; 20 21;
mbi ;; -21; xyz -0.915438E-02 -0.759802 0.200806E-01
mbi -9; 2 7; -21; xyz 0.335407E-02 -0.428734 -0.762939E-05
mbi -3; 6 7; -21; xyz -0.315189E-03 -0.517609 -0.762939E-05
mbi 3 4; -7; -21; xyz 0.172005E-01 -0.566282 -0.762939E-05
mbi -2; 4 6; -21; xyz 0.323068 -0.792369 -0.762939E-05
pb 2 4 21 2 4 21 xyz -5.76282 -1.77684 88.9701
mbi 8 9; -7; -21; xyz -0.245889 -0.354934 -0.762939E-05
pb 8 6 21 8 6 21 xyz 2.34542 0.602110 88.9905
pb 9 2 21 9 2 21 xyz 4.51978 -4.10450 88.9701
c -----------------------
c section 21
```

```
DEI  1 2 0 10 11; 1 2 0 7 8; 21 22;
DEI  4 8; 3 6; 21 22;
mbi ;; -22; xyz -0.115413E-01 -0.735673 -0.109329E-01
pb 2 6 22 2 6 22 xyz -5.47809 0.820795 93.3791
pb 3 7 22 3 7 22 xyz -4.47419 1.77450 93.3791
mbi 5 7; -7; -22; xy -0.705827E-01 0.404466
mbi 8 9; -7; -22; xy -0.308540E-01 -0.423753
mbi -3; 4 6; -22; xy -0.288920 -0.343409
c ----------------------
c section 22
DEI  1 2 0 10 11; 1 2 0 7 8; 22 23;
DEI  4 8; 3 6; 22 23;
mbi ;; -23; xyz 0.321215E-02 -0.962668 0.211563E-01
pb 2 6 23 2 6 23 xyz -5.67732 0.550706 97.8612
pb 3 7 23 3 7 23 xyz -4.49816 1.65461 97.8612
mbi 5 7; -7; -23; xy -0.104990E-01 0.486087
pb 9 7 23 9 7 23 xyz 4.50867 1.93058 97.8612
c ----------------------
c section 23
DEI  1 2 0 10 11; 1 2 0 7 8; 23 24;
DEI  4 8; 3 6; 23 24;
mbi ;; -24; xyz -0.651795E-02 -0.704755 0.283737E-01
pb 2 6 24 2 6 24 xyz -5.85096 0.877970 102.318
pb 3 7 24 3 7 24 xyz -4.44661 1.98139 102.318
mbi 5 7; -7; -24; xyz 0.488214E-01 0.404020 0.762939E-05

c ----------------------
c section 24
DEI  1 2 0 10 11; 1 2 0 7 8; 24 25;
DEI  4 8; 3 6; 24 25;
mbi ;; -25; xyz -0.181228E-02 -0.712400 0.375061E-01
pb 3 7 25 3 7 25 xyz -4.46658 2.03323 106.778
pb 2 6 25 2 6 25 xyz -5.57546 1.12149 106.778
mbi 5 7; -7; -25; xyz -0.538812E-01 0.545938 -0.381470E-04
pb 2 3 25 2 3 25 xyz -5.92044 -2.35300 106.778
pb 9 7 25 9 7 25 xyz 4.55239 2.13178 106.778
mbi -3; 4 5; -25; xyz -0.432965 0.596749E-01 -0.289917E-03
pb 8 6 25 8 6 25 xyz 2.33451 0.801164 106.786
c ----------------------
c section 25
DEI  1 2 0 10 11; 1 2 0 7 8; 25 26;
DEI  4 8; 3 6; 25 26;
pb 2 6 26 2 6 26 xyz -5.62816 1.30301 111.184
pb 3 7 26 3 7 26 xyz -4.35015 2.48076 111.183
pb 9 7 26 9 7 26 xyz 4.52172 2.68105 111.182
mbi -3; 4 5; -26; xyz -0.251119 -0.196622E-03 -0.149536E-02
pb 8 7 26 8 7 26 xyz 2.99282 2.73120 111.181
pb 3 6 26 3 6 26 xyz -4.55063 1.57860 111.181
mbi 5 7; -2; -26; xyz -0.647268E-01 -0.574814 0.113678E-02
c ----------------------
c section 26
DEI  1 2 0 10 11; 1 2 0 7 8; 26 27;
DEI  4 8; 3 6; 26 27;
```

```
pb 2 6 27 2 6 27 xyz -5.44617 1.63184 115.630
pb 3 7 27 3 7 27 xyz -4.31864 2.78442 115.630
pb 9 7 27 9 7 27 xyz 4.35084 2.83454 115.630
pb 2 3 27 2 3 27 xyz -5.84707 -1.65054 115.630
mbi 5 6; -7; -27; xy -0.106446E-01 0.451393
mbi -3; 4 5; -27; xy -0.294706 -0.469362E-01
pb 8 7 27 8 7 27 xyz 2.97274 2.80948 115.630
c -----------------------
c section 27
DEI  1 2 0 10 11; 1 2 0 7 8; 27 28;
DEI  4 8; 3 6; 27 28;
pb 2 6 28 2 6 28 xyz -5.52031 1.60722 120.080
pb 3 7 28 3 7 28 xyz -4.16760 2.65933 120.080
mbi 5 6; -7; -28; xyz 0.164576 0.426283 0.762939E-05
pb 3 6 28 3 6 28 xyz -4.19265 1.83267 120.080
c -----------------------
c section 28
DEI  1 2 0 10 11; 1 2 0 7 8; 28 29;
DEI  4 8; 3 6; 28 29;
pb 2 6 29 2 6 29 xyz -5.41897 1.83311 124.530
pb 3 7 29 3 7 29 xyz -4.36715 2.70963 124.530
pb 6 7 29 6 7 29 xyz 0.404594E-01 3.88666 124.530
pb 2 3 29 2 3 29 xyz -5.56923 -1.94842 124.530
pb 3 2 29 3 2 29 xyz -4.26698 -2.84998 124.530
mbi -5 0 -7; -7; -29; xyz 0.154156E-01 0.476314 0.762939E-05
c -----------------------
c section 29
DEI  1 2 0 10 11; 1 2 0 7 8; 29 30;
DEI  4 8; 3 6; 29 30;
pb 2 3 30 2 3 30 xyz -5.54348 -1.29651 128.970
pb 2 6 30 2 6 30 xyz -5.51844 1.58298 128.970
mbi 5 7; -7; -30; xy 0.151975E-01 0.851854
pb 8 7 30 8 7 30 xyz 3.42052 3.58611 128.970
pb 9 5 30 9 5 30 xyz 4.99798 0.606459 128.970
c -----------------------
c section 30
DEI  1 2 0 10 11; 1 2 0 7 8; 30 31;
DEI  4 8; 3 6; 30 31;
mbi -2; 3 6; -31; xy 0.582429 0.106255
mbi 3 4; -2; -31; xy 0.335208 0.462295
mbi 5 7; -7; -31; xy 0.650370E-01 1.15216
pb 8 7 31 8 7 31 xyz 3.16934 3.91153 133.420
mbi -9; 4 6; -31; xy 0.546948 0.262366
mbi -10; 3 6; -31; xy 0.473928 0.561857E-01
pb 9 7 31 9 7 31 xyz 4.87170 3.83643 133.420
pb 8 3 31 8 3 31 xyz 2.74340 -1.09502 133.472
pb 8 4 31 8 4 31 xyz 3.54505 -0.494727 133.398
c -----------------------
c section 31
DEI  1 2 0 10 11; 1 2 0 7 8; 31 32;
DEI  4 8; 3 6; 31 32;
mbi ;; -32; xyz -0.167788E-01 1.46362 0.286865E-01
mbi 4 8; 3 6; -32; xyz 0.710359 0.307066 -0.214386E-01
```

```
mbi -9; 3 6; -32; xyz 0.853608 0.276390E-01 -0.988770E-02
mbi -10; 3 6; -32; xyz 0.370702 -0.997388E-02 -0.328064E-02
pb 3 7 32 3 7 32 xyz -3.60232 3.45534 137.946
pb 2 6 32 2 6 32 xyz -4.46028 2.48118 137.926
pb 3 6 32 3 6 32 xyz -3.49242 2.44179 137.933
pb 2 5 32 2 5 32 xyz -5.52861 1.84661 137.906
pb 4 7 32 4 7 32 xyz -2.38548 4.06816 137.921
mbi 2 4; -5; -32; xyz 0.362234E-01 -0.266030 0.120239E-01
mbi 2 3; -6; -32; xyz -0.340682 0.173619 -0.465393E-02
mbi -2; 3 4; -32; xyz 0.322656 0.240045E-01 -0.436401E-02
c ----------------------
c section 32
DEI  1 2 0 10 11; 1 2 0 7 8; 32 33;
DEI  4 8; 3 6; 32 33;
mbi ;; -33; xyz 0.125378E-01 1.70801 0.939941E-02
pb 2 6 33 2 6 33 xyz -5.29452 2.65184 142.303
mbi -2; 3 5; -33; xyz 0.676593 -0.104624 -0.156403E-01
mbi 3 4; -7; -33; xyz 1.08519 -0.626670 -0.355988E-01
pb 3 6 33 3 6 33 xyz -3.54002 3.21137 142.282
mbi 5 8; -7; -33; xyz 0.819312 0.707975 0.183105E-03
pb 9 7 33 9 7 33 xyz 5.27380 5.00339 142.297
mbi -3; 3 5; -33; xyz 0.428639 0.295703E-01 -0.770569E-02
pb 9 6 33 9 6 33 xyz 5.38212 3.67115 142.317
mbi -10; 3 6; -33; xyz 0.234956 -0.189357E-01 -0.502014E-02
mbi 4 9; -2; -33; xyz 0.775122 -0.987232E-02 -0.153961E-01
pb 3 2 33 3 2 33 xyz -4.19307 -1.44945 142.294
pb 9 7 33 9 7 33 xyz 5.21083 5.36326 142.294
mbi 4 8; -2; -33; xyz -0.348656E-01 -0.391496 0.868225E-02
pb 3 7 33 3 7 33 xyz -3.45198 3.69439 142.287
pb 2 6 33 2 6 33 xyz -5.06700 2.68485 142.329
pb 9 2 33 9 2 33 xyz 4.94684 -1.84648 142.314
pb 8 4 33 8 4 33 xyz 4.18672 0.546249 142.438
mbi -9; 3 5; -33; xyz 0.962685 -0.166986E-01 0.825500E-02
pb 8 6 33 8 6 33 xyz 3.91989 3.91877 142.312
mbi -9; -3 0 -6; -33; xyz -0.311317 0.165993 -0.292969E-02
mbi 2 3; -5; -33; xyz 0.123189 -0.323589 0.161743E-02
c ----------------------
c section 33
 DEI  1 2 0 10 11; 1 2 0 7 8; 33 34;
 DEI  4 8; 3 6; 33 34;
 mbi ;; -34; xyz -0.523417E-01 2.12778 0.112915E-01
 mbi 4 8; 3 6; -34; xy 0.645333 0.522999
 mbi 4 8; -3; -34; xy 0.246004 -0.628451
 mbi 4 9; -6; -34; xyz 0.520113 -0.221391E-01 -0.534058E-03
 mbi -8; 3 6; -34; xyz 1.37898 -0.496855E-01 -0.190735E-02
pb 3 7 34 3 7 34 xyz -3.01389 4.11167 146.771
pb 2 6 34 2 6 34 xyz -5.04129 2.86019 146.771
pb 3 6 34 3 6 34 xyz -3.46442 2.88522 146.771
pb 4 7 34 4 7 34 xyz -1.86252 4.38700 146.771
mbi 2 4; -5; -34; xyz -0.142952 -0.310226 0.152588E-04
mbi 2 3; -6; -34; xyz -0.137662 0.387963 0.152588E-04
mbi 5 9; -7; -34; xy 0.819707 0.250643
mbi -9; 2 6; -34; xy 1.01374 0.332238
```

```
mbi -10; 3 6; -34; xy 1.00025 -0.935640E-01
pb 8 6 34 8 6 34 xyz 3.84322 4.01144 146.899
pb 4 4 34 4 4 34 xyz -2.53833 1.60871 146.769
pb 9 2 34 9 2 34 xyz 5.47116 -1.44490 146.771
pb 8 2 34 8 2 34 xyz 4.19465 -1.26970 146.771
pb 2 5 34 2 5 34 xyz -5.91732 2.45972 146.771
c ----------------------
c section 34
 DEI  1 2 0 10 11; 1 2 0 7 8; 34 35;
 DEI  4 8; 3 6; 34 35;
mbi ;; -35; xyz 0.382676E-01 2.98017 0.311127E-01
mbi 2 10; -8; -35; xyz 0.615512E-02 0.866286 0.527954E-01
mbi 2 10; -1; -35; xyz -0.107295E-01 -1.54095 -0.338745E-02
mbi 3 10; 2 7; -35; xy 0.931370 -0.424879E-01
mbi 3 9; 2 7; -35; xy 0.575424 -0.249391E-01
mbi -10; 3 6; -35; xy 0.436172 -0.249391E-01
mbi -3; 3 6; -35; xy -0.612566 -0.349150
mbi -9; 3 5; -35; xy 0.413053 0.464559E-01
mbi 4 8; -2; -35; xy -0.423967 -0.904992
pb 3 2 35 3 2 35 xyz -3.71714 -0.753341 151.241
mbi 5 8; -7; -35; xy -0.575424 0.805235
pb 9 2 35 9 2 35 xyz 6.03414 -1.37682 151.241
pb 10 3 35 10 3 35 xyz 7.97941 0.917596 151.241
c ----------------------
c section 35
 DEI  1 2 0 10 11; 1 2 0 7 8; 35 36;
 DEI  4 8; 3 6; 35 36;
mbi ;; -36; xyz 0.275713E-02 3.72572 0.124969E-01
mbi 2 10; -8; -36; xyz 0.135390E-02 1.77808 -0.148163E-01
mbi 2 10; -1; -36; xyz -0.193054E-02 -2.69248 -0.318756E-01
mbi -1; 2 7; -36; xyz -2.95622 0.524139E-02 0.610809E-01
mbi -11; 2 7; -36; xyz 2.44516 -0.413013E-02 -0.357513E-01
mbi 9 10; 2 7; -36; xyz 1.74729 -0.764546E-01 -0.279236E-01
mbi 4 8; 3 6; -36; xyz 1.35887 -0.483471 0.543213E-02
mbi 3 8; -2; -36; xyz 1.69929 -0.604025 0.675964E-02
pb 2 7 36 2 7 36 xyz -6.81613 7.70344 155.378
mbi 3 9; -2; -36; xyz -0.965962 -0.779481 0.431824E-02
mbi -9; 2 3; -36; xyz 0.145151 -0.484993 0.127869E-01
mbi 3 4; 6 7; -36; xyz 0.546590 -0.470299 0.178833E-01
pb 2 6 36 2 6 36 xyz -6.52546 5.67946 155.665
mbi 5 8; -7; -36; xyz 1.04611 0.664592E-01 0.126648E-01
mbi -2; 3 6; -36; xyz -0.596241 -0.560343E-01 -0.682068E-02
mbi -9; 1 2; -36; xyz 0.806367 0.424211E-01 0.997925E-02
pb 10 1 36 10 1 36 xyz 7.96879 -3.17053 155.653
pb 3 2 36 3 2 36 xyz -4.41155 -0.834607 155.674
c ----------------------
c section 36
 DEI  1 2 0 10 11; 1 2 0 7 8; 36 37;
 DEI  4 8; 3 6; 36 37;
mbi ;; -37; xyz 0.327225E-01 3.89481 0.407013
mbi 2 10; -1; -37; xyz -0.447205E-01 -3.09267 -0.793457E-03
mbi 1 11; -8; -37; xyz 0.393692E-01 2.73295 -0.110321E-01
mbi -11; 2 7; -37; xyz 4.89454 -0.163107E-01 0.817566E-01
```

```
mbi -1; 2 7; -37; xyz -6.77761 0.225449E-01 -0.111816
mbi 4 8; 3 6; -37; xy 0.737775 -0.395571
mbi -10; 3 6; -37; xyz 2.55527 -0.615254 0.885010E-02
mbi -9; 3 6; -37; xyz 1.21963 -0.285527 0.419617E-02
mbi 3 9; -2; -37; xyz 0.806783 -1.65865 0.903320E-02
mbi -2; 3 6; -37; xyz -2.06245 0.406934 -0.674438E-02
pb 10 2 37 10 2 37 xyz 9.22896 -3.12964 159.658
pb 1 7 37 1 7 37 xyz -11.6917 7.66491 160.314
pb 1 2 37 1 2 37 xyz -10.1649 1.47176 161.234
pb 1 3 37 1 3 37 xyz -11.5532 2.58933 160.848
mbi -11; 2 3; -37; xyz -0.200857 -1.25758 0.486755E-02
mbi 9 10; -3; -37; xyz 0.659538 -0.707817 0.462341E-02
mbi 3 9; -7; -37; xyz 0.147313 1.05452 -0.413513E-02
mbi 1 3; -6; -37; xyz 0.396621 0.878140 -0.277710E-02
mbi 1 3; -5; -37; xyz -0.253124E-01 0.486649 -0.213623E-02
pb 2 1 37 2 1 37 xyz -7.33753 -3.05098 160.523
mbi -3; 1 3; -37; xyz -0.764084 0.715303E-01 -0.216675E-02
pb 3 2 37 3 2 37 xyz -5.26029 -0.742935 160.521
pb 10 2 37 10 2 37 xyz 11.2098 -2.04019 159.659
pb 10 1 37 10 1 37 xyz 7.99506 -3.51329 160.511
pb 11 6 37 11 6 37 xyz 11.1940 5.09286 160.463
pb 8 4 37 8 4 37 xyz 4.46186 2.86533 160.499
mbi -9; 1 3; -37; xyz 1.06986 -0.125642 0.314331E-02
c ----------------------
c section 36
 DEI  1 2 0 10 11; 1 2 0 7 8; 37 38;
mbi ;; -38; xyz -0.120229E-02 4.41429 -0.392914E-01
mbi ;; -38; xyz 0.492930E-04 -0.296577 -0.299072E-02
mbi 2 10; -8; -38; xyz -0.944198E-03 3.40558 -0.208282E-01
mbi 2 10; -1; -38; xyz 0.103336E-02 -3.77588 -0.378418E-01
mbi -11; 2 7; -38; xyz 4.91974 0.120959E-01 0.352325E-01
mbi -1; 2 7; -38; xyz -7.19036 -0.176177E-01 -0.241730
mbi -2; 2 7; -38; xy -5.04833 -0.167475E-01
mbi -10; 2 7; -38; xy 3.56973 0.167241E-01
mbi 2 10; -7; -38; xy 0.334699E-01 2.93191
mbi 2 11; -2; -38; xyz -1.56566 -3.14955 0.152588E-04
mbi 2 11; -2; -38; xy -0.334668E-01 1.13795
mbi 2 10; -2; -38; xyz 1.29789 -0.165920E-01 0.152588E-04
mbi -3; 2 7; -38; xyz -2.73265 0.334582E-01 0.152588E-04
mbi -9; 2 7; -38; xyz 2.02388 -0.334830E-01 0.152588E-04
mbi -8; 2 7; -38; xyz 1.51563 0.334582E-01 0.152588E-04
mbi -4; 2 7; -38; xyz -1.65539 -0.133514E-04 0.152588E-04
mbi -5; 2 7; -38; xyz -0.645078 -0.133514E-04 0.152588E-04
mbi -7; 2 7; -38; xyz 0.906963 0.334582E-01 0.152588E-04
mbi 2 10; -6; -38; xy 0.669406E-01 2.13671
mbi 2 10; -3; -38; xy -0.100413 -1.60118
mbi 2 10; -4; -38; xy 0.334699E-01 -0.882924
mbi 2 10; -5; -38; xy 0.669406E-01 0.949867
pb 9 7 38 9 7 38 xyz 5.37393 8.28472 164.501
pb 10 6 38 10 6 38 xyz 8.42139 5.87530 164.502
pb 8 7 38 8 7 38 xyz 3.83369 8.78639 164.505
mbi 7 9; 5 7; -38; xyz -0.345592 -0.569480 -0.190735E-02
pb 9 7 38 9 7 38 xyz 5.17308 8.38509 164.498
```

```
pb 8 7 38 8 7 38 xyz 3.69982 8.71941 164.504
pb 10 5 38 10 5 38 xyz 9.15831 4.50295 164.507
pb 9 6 38 9 6 38 xyz 5.87641 7.04632 164.504
pb 2 1 38 2 1 38 xyz -8.04605 -3.23296 164.418
pb 1 3 38 1 3 38 xyz -12.7672 2.25426 164.151
pb 2 6 38 2 6 38 xyz -10.8258 6.60721 164.515
pb 2 5 38 2 5 38 xyz -10.9258 4.86700 164.511
mbi -3; 2 3; -38; xyz 0.458566 0.516194 0.341797E-02
pb 10 3 38 10 3 38 xyz 10.0634 0.385469 164.515
pb 8 6 38 8 6 38 xyz 3.66680 7.17968 164.501
pb 11 3 38 11 3 38 xyz 13.2191 0.445662 164.563
pb 2 3 38 2 3 38 xyz -10.1848 2.00369 164.508
pb 1 3 38 1 3 38 xyz -12.3118 2.55059 164.133
mbi 2 3; 3 4; -38; xyz 0.471454 0.703026 0.152588E-04
pb 1 2 38 1 2 38 xyz -10.4978 1.21576 164.133
mbi 2 3; -4; -38; xy -0.429316E-01 0.579007

pb 11 5 38 11 5 38 xyz 11.2342 3.85113 164.237
pb 11 5 38 11 5 38 xyz 10.8968 4.12241 164.459
pb 10 5 38 10 5 38 xyz 9.20766 4.05929 164.477

pb 2 2 38 2 2 38 xyz 4.83424 3.26938 164.315
mbi 1 2; 2 3; -38; xyz -1.14154 0.808844 0.152588E-04
pb 2 2 38 2 2 38 xyz -10.8695 2.20889 164.474
mbi -3; 3 4; -38; xy -0.210146 1.04464
pb 3 2 38 3 2 38 xyz -7.48231 1.79845 164.511
mbi -1; 6 7; -38; xy 1.17872 1.56991
pb 2 6 38 2 6 38 xyz -10.8347 7.44286 164.515
mbi 1 3; -5; -38; xy 0.298179 1.28047
mbi 1 2; -4; -38; xyz -0.498476E-01 0.630906 0.152588E-04
pb 1 2 38 1 2 38 xyz -12.3118 2.61904 164.133
mbi -4; 2 4; -38; xy 0.250045 1.67706
pb 3 2 38 3 2 38 xyz -7.03760 1.25111 164.511
c ----------------------
c section 36
 DEI  1 2 0 10 11; 1 2 0 7 8; 38 39;
mbi ;; -39; xyz -0.322349E-01 4.74998 0.172424E-02
mbi 2 11; -1; -39; xyz 0.213844E-01 -3.10411 0.621185E-01
mbi 2 11; -8; -39; xyz -0.183714E-01 2.71290 0.978088E-02
mbi -11; 2 7; -39; xyz 3.36063 0.749254E-02 0.110199
mbi -1; 2 7; -39; xyz -5.93991 -0.126076E-01 -0.756531E-01
pb 2 7 39 2 7 39 xyz -8.06774 9.46986 169.955
pb 2 2 39 2 2 39 xyz -8.23898 -0.305834E-01 171.331
pb 10 2 39 10 2 39 xyz 9.02022 -1.50519 171.380
mbi 3 9; -2; -39; xyz 0.905329E-01 -1.75413 -0.696564E-01
mbi -2; 3 6; -39; xyz -1.94987 0.178804 -0.930786E-03
mbi 3 9; -7; -39; xyz -0.632045E-01 1.33634 0.531006E-01
mbi 1 11; -3; -39; xyz 0.447540 -1.28176 -0.493164E-01
pb 1 2 39 1 2 39 xyz -10.5643 1.28692 168.670
mbi -10; 3 6; -39; xyz 1.25292 -0.421381E-02 0.502014E-02
pb 11 2 39 11 2 39 xyz 10.9561 0.375574 169.060
pb 10 2 39 10 2 39 xyz 8.69224 -1.75371 171.303
```

```
pb 2 2 39 2 2 39 xyz -10.4191 1.41950 171.047
pb 1 2 39 1 2 39 xyz -11.6203 2.25554 168.547
pb 2 3 39 2 3 39 xyz -9.38692 3.31784 168.881

c -----------------------

c project:
 sfi 2 10; -1 0 -8; 1 39;sd 1
 sfi -1 0 -11; 2 7; 1 39;sd 1
 sfi 1 -2 0 -10 11; 1 -2 0 -7 8; 1 39;sd 1
 sfi -4 -8; -3 -6; 4 37;sd 2
c -----------------------

c relax 1 1 1 11 8 2 1000 .01 1
c relax 1 1 7 11 8 39 1000 .01 1

c mea 1 1 1 11 8 39 jacobian
c elm -1000 0
c ------------------------------------------------------------------------
--------------------
c ------------------------------------------------------------------------
--------------------
c delete strips in phases, to work with pns
c DEI 10 11;;;
c DEI 10 11; 6 8;;
c DEI 8 9; 5 6; 4 37;
c kill first half to see the damn bad part
c DEI 1 8;;;

c ------------------------------------------------------------------------
--------------------
c ------------------------------------------------------------------------
--------------------
merge
c -----------------------
c these are the pns:
c strip 1:
pn 1300 -6.41387081E+00 3.17624599E-01 3.51684265E+01
pn 1301 -6.40050888E+00 2.40694776E-01 3.60498962E+01
pn 1479 -6.30111599E+00 -1.21950015E-01 3.86235924E+01
pn 1509 -6.15110064E+00 -2.62624145E-01 3.85825920E+01
pn 1479 -6.31094837E+00 -1.24998391E-01 3.86215286E+01
pn 1484 -6.39495039E+00 -9.71484277E-03 3.85856094E+01
pn 1484 -6.39223289E+00 -6.80862088E-03 3.85865097E+01
pn 3641 -6.56098270E+00 -3.32406974E+00 9.33485718E+01
pn 3817 -6.52649736E+00 -3.33010483E+00 9.42452621E+01
pn 3640 -6.56690407E+00 -3.35064030E+00 9.24686050E+01
pn 3818 -6.49506569E+00 -3.33766842E+00 9.51418991E+01
pn 3819 -6.46369123E+00 -3.34955001E+00 9.60381927E+01
pn 3820 -6.43688107E+00 -3.36010861E+00 9.69344635E+01
pn 3821 -6.40933466E+00 -3.36839175E+00 9.78306503E+01
pn 6161 -9.35567951E+00 1.24249196E+00 1.55899139E+02
pn 6161 -9.38209820E+00 1.21829855E+00 1.55887955E+02
```

```
pn 6337 -9.61585617E+00 1.25247002E+00 1.56937088E+02
pn 6338 -9.81728840E+00 1.26431417E+00 1.58002243E+02
pn 6339 -1.00046329E+01 1.27755511E+00 1.59070099E+02
pn 6340 -1.01227417E+01 1.34846210E+00 1.60145874E+02
pn 6341 -1.02575979E+01 1.41687906E+00 1.61214523E+02
pn 6517 -1.05707273E+01 1.72505367E+00 1.61837357E+02
pn 6518 -1.09222689E+01 2.13069558E+00 1.62393295E+02
pn 6159 -8.69859886E+00 5.95196426E-01 1.54013657E+02
pn 6160 -9.05328083E+00 9.12232220E-01 1.54950012E+02
pn 6161 -9.40281677E+00 1.20150757E+00 1.55876999E+02
pn 6340 -1.01436911E+01 1.33813608E+00 1.60137131E+02
pn 6339 -1.00241585E+01 1.27206039E+00 1.59061066E+02
pn 6341 -1.02890539E+01 1.40953612E+00 1.61198990E+02
pn 6520 -1.17218533E+01 2.65970850E+00 1.63566132E+02
pn 6521 -1.22520552E+01 2.74489260E+00 1.64118271E+02
pn 6520 -1.17297087E+01 2.64327717E+00 1.63555618E+02
pn 6697 -1.20483532E+01 2.76460290E+00 1.64984329E+02
pn 6698 -1.19204998E+01 2.64463496E+00 1.65862366E+02
pn 6698 -1.19243174E+01 2.63699341E+00 1.65858566E+02
pn 6699 -1.18195372E+01 2.48078513E+00 1.66735214E+02
pn 6700 -1.15809259E+01 2.54519176E+00 1.67594955E+02
pn 6701 -1.13641281E+01 2.59207582E+00 1.68463379E+02
pn 6791 -1.04718094E+01 2.10254598E+00 1.69857468E+02
pn 6791 -1.04837885E+01 2.06587768E+00 1.69849564E+02
pn 6518 -1.09574881E+01 2.10924435E+00 1.62363907E+02
pn 6519 -1.12921343E+01 2.42840028E+00 1.62985367E+02
c strip 2:
pn 5436 -5.42003107E+00 -1.79900098E+00 1.33417023E+02
pn 5436 -5.39443207E+00 -1.79634786E+00 1.33413681E+02
c strip 3:
pn 5612 -5.45276117E+00 -1.55173004E+00 1.34314026E+02
pn 5613 -5.49914360E+00 -1.27288914E+00 1.35207489E+02
pn 5435 -5.42503119E+00 -1.71742451E+00 1.32526596E+02
c strip 4:
c (no changes)
c strip 5:
pn 5431 -5.33601093E+00 -1.93044865E+00 1.33401566E+02
pn 5426 -5.26493120E+00 -2.04909182E+00 1.33387619E+02
pn 5607 -5.41108847E+00 -1.68077540E+00 1.34302200E+02
pn 5602 -5.34503460E+00 -1.82304966E+00 1.34288757E+02
pn 5597 -5.29665661E+00 -1.96044326E+00 1.34280991E+02
pn 24267 -9.97960091E+00 7.86413002E+00 4.92479324E+00
pn 24268 -9.52852726E+00 7.94284582E+00 5.96965313E+00
pn 25170 -6.68909931E+00 4.20497227E+00 3.50552330E+01
pn 25320 -6.50093937E+00 3.94448876E+00 3.89675407E+01
pn 25321 -6.46169186E+00 3.88883066E+00 3.97258301E+01
pn 25467 -6.39249563E+00 3.71815419E+00 4.06554756E+01
pn 25468 -6.43755341E+00 3.66333771E+00 4.16011696E+01
pn 25469 -6.48286152E+00 3.58930755E+00 4.25469627E+01
pn 27868 -6.18803120E+00 1.84301305E+00 1.13011398E+02
pn 27869 -6.19056177E+00 1.87731183E+00 1.13893570E+02
pn 27870 -6.20212650E+00 1.92743003E+00 1.14776535E+02
pn 27871 -6.20409060E+00 1.96187806E+00 1.15659805E+02
```

```
pn 28017 -6.20050287E+00 1.99127197E+00 1.16558105E+02
pn 28018 -6.20481777E+00 2.02005291E+00 1.17456680E+02
pn 28019 -6.22408962E+00 2.06715178E+00 1.18354393E+02
pn 28020 -6.25193691E+00 2.11526918E+00 1.19251602E+02
pn 29067 -6.18399096E+00 3.63660169E+00 1.47950180E+02
pn 29068 -6.28413868E+00 3.92876840E+00 1.48970245E+02
pn 29069 -6.42809057E+00 4.27585268E+00 1.49969208E+02
pn 29070 -6.59506989E+00 4.66718054E+00 1.50951920E+02
pn 29071 -6.80888557E+00 5.12041569E+00 1.51893982E+02
pn 23463 -5.47299528E+00 3.90549803E+00 1.48559921E+02
pn 23464 -5.61529207E+00 4.23516178E+00 1.49453445E+02
pn 29174 -5.57628822E+00 4.32761145E+00 1.49515869E+02
pn 29175 -5.73123121E+00 4.68034935E+00 1.50411194E+02
pn 29176 -5.87917709E+00 5.01341009E+00 1.51313187E+02
pn 29180 -5.67292404E+00 4.78408527E+00 1.50476501E+02
pn 29179 -5.52666378E+00 4.41803837E+00 1.49577927E+02
pn 23466 -5.93769550E+00 4.90094948E+00 1.51242126E+02
pn 29217 -7.42010593E+00 5.31315517E+00 1.52825180E+02
pn 29218 -8.08401680E+00 5.54593086E+00 1.53727005E+02
pn 29219 -8.78676319E+00 5.87032223E+00 1.54562759E+02
pn 29220 -9.55778790E+00 6.29129076E+00 1.55286011E+02
pn 29371 -1.17016020E+01 7.62189960E+00 1.60290634E+02
pn 29370 -1.16741819E+01 7.86899853E+00 1.59317932E+02
pn 29371 -1.17495193E+01 7.63726711E+00 1.60276291E+02
pn 29366 -1.20871201E+01 7.39263391E+00 1.60302185E+02
pn 29365 -1.20104752E+01 7.57926226E+00 1.59328445E+02
pn 29512 -1.21189747E+01 7.28289175E+00 1.61130646E+02
pn 29513 -1.21352119E+01 7.24501276E+00 1.61958832E+02
pn 29518 -1.18570728E+01 7.45889235E+00 1.61955643E+02
pn 29508 -1.24130526E+01 7.03983355E+00 1.61942459E+02
pn 29520 -1.21767130E+01 7.51190615E+00 1.63600433E+02
pn 29515 -1.23478289E+01 7.35885477E+00 1.63576828E+02
pn 29510 -1.25069990E+01 7.20461559E+00 1.63556396E+02
pn 29505 -1.26882200E+01 7.05314875E+00 1.63532776E+02
pn 29500 -1.28668337E+01 6.89595890E+00 1.63511978E+02
pn 23790 -1.30075140E+01 6.76703453E+00 1.63483444E+02
pn 23785 -1.32565384E+01 6.55881166E+00 1.63483719E+02
pn 29515 -1.23616171E+01 7.36822414E+00 1.63570892E+02
pn 29510 -1.25289602E+01 7.20717621E+00 1.63552719E+02
pn 29667 -1.25411072E+01 7.65525293E+00 1.65277740E+02
pn 29662 -1.26629963E+01 7.51392889E+00 1.65255646E+02
pn 29657 -1.27607746E+01 7.36167002E+00 1.65246613E+02
pn 29652 -1.28726692E+01 7.21114779E+00 1.65233582E+02
pn 29668 -1.27987938E+01 7.75682878E+00 1.66120712E+02
pn 29663 -1.29088802E+01 7.60733557E+00 1.66124237E+02
pn 29663 -1.29222383E+01 7.60686684E+00 1.66120071E+02
pn 29658 -1.30288057E+01 7.46586466E+00 1.66120361E+02
pn 29671 -1.30617714E+01 7.71391821E+00 1.68697983E+02
pn 29670 -1.31480255E+01 7.84129429E+00 1.67826065E+02
pn 23465 -5.78372574E+00 4.56228495E+00 1.50333191E+02
pn 23466 -5.93871355E+00 4.89913368E+00 1.51269806E+02
pn 23465 -5.78529596E+00 4.55994892E+00 1.50364807E+02
pn 23464 -5.62521744E+00 4.22868872E+00 1.49491638E+02
```

```
pn 23463 -5.47835112E+00 3.90137506E+00 1.48593185E+02
pn 23462 -5.34337378E+00 3.57608795E+00 1.47687378E+02
pn 23612 -6.19328928E+00 5.05208158E+00 1.52145996E+02
pn 23612 -6.18399715E+00 5.05444956E+00 1.52141174E+02
pn 29471 -7.79519367E+00 9.08164597E+00 1.59230133E+02
pn 29446 -8.86736202E+00 8.89937305E+00 1.59392349E+02
pn 29421 -9.89869881E+00 8.59383583E+00 1.59606812E+02
pn 29396 -1.08111820E+01 8.16630650E+00 1.59947678E+02
pn 29371 -1.17006054E+01 7.66637468E+00 1.60238174E+02
pn 29517 -1.17563992E+01 7.56199837E+00 1.61087677E+02
pn 29542 -1.10088339E+01 8.15898323E+00 1.60852188E+02
pn 29543 -1.11731310E+01 8.00581551E+00 1.61780273E+02
pn 29518 -1.18499174E+01 7.47897243E+00 1.61956223E+02
pn 29513 -1.21313801E+01 7.26780701E+00 1.61956390E+02
pn 29519 -1.20015574E+01 7.53884792E+00 1.62783142E+02
pn 29518 -1.18470840E+01 7.50182486E+00 1.61953064E+02
pn 29515 -1.23558245E+01 7.39303541E+00 1.63569336E+02
pn 29520 -1.21738663E+01 7.54031754E+00 1.63595901E+02
pn 29510 -1.25350933E+01 7.23085499E+00 1.63542664E+02
pn 29505 -1.26924601E+01 7.07370567E+00 1.63524673E+02
pn 29515 -1.23497677E+01 7.40884924E+00 1.63568054E+02
pn 29520 -1.21644421E+01 7.56106043E+00 1.63594833E+02
pn 29546 -1.19400024E+01 8.06756496E+00 1.64517242E+02
pn 29546 -1.19281254E+01 8.08764553E+00 1.64517670E+02
pn 29545 -1.16291914E+01 7.96656322E+00 1.63626755E+02
pn 29667 -1.25363674E+01 7.70671129E+00 1.65272812E+02
pn 29668 -1.27839260E+01 7.80944538E+00 1.66140823E+02
pn 29517 -1.17663708E+01 7.57875633E+00 1.61068008E+02
pn 29512 -1.21238899E+01 7.29834747E+00 1.61130692E+02
pn 29507 -1.24217682E+01 7.09532261E+00 1.61135010E+02
pn 29502 -1.27836199E+01 6.90808773E+00 1.61151764E+02
pn 29366 -1.20879021E+01 7.40582705E+00 1.60316757E+02
pn 29361 -1.24527683E+01 7.15764046E+00 1.60355927E+02
pn 29356 -1.28533897E+01 6.92430592E+00 1.60376480E+02
pn 29351 -1.32559767E+01 6.70270634E+00 1.60397903E+02
pn 29520 -1.21753330E+01 7.59366989E+00 1.63598770E+02
pn 29521 -1.23773956E+01 7.64220142E+00 1.64406204E+02
pn 29667 -1.25431814E+01 7.73497486E+00 1.65307953E+02
pn 29662 -1.26676292E+01 7.52793312E+00 1.65258347E+02
c strip 6:
c no changes
c proactive j fix:
pn 5436 -5.34316444E+00 -1.74977517E+00 1.33408798E+02
pn 5435 -5.36987495E+00 -1.68945241E+00 1.32507187E+02
pn 5436 -5.32522154E+00 -1.73789525E+00 1.33404358E+02
pn 5431 -5.29311943E+00 -1.88731945E+00 1.33400177E+02
pn 5426 -5.22399282E+00 -2.02547097E+00 1.33375076E+02
pn 5421 -5.17710352E+00 -2.14286804E+00 1.33382416E+02
pn 5416 -5.10382128E+00 -2.28257942E+00 1.33353195E+02
pn 5592 -5.21819210E+00 -2.08998752E+00 1.34254700E+02
pn 5597 -5.27355242E+00 -1.93844020E+00 1.34279495E+02
pn 5602 -5.31183434E+00 -1.79937112E+00 1.34281494E+02
pn 5607 -5.37063217E+00 -1.65024996E+00 1.34294403E+02
```

```
pn 5607 -5.33832169E+00 -1.60603487E+00 1.34300873E+02
pn 5607 -5.35727739E+00 -1.62064934E+00 1.34309891E+02
pn 5612 -5.42393208E+00 -1.49314523E+00 1.34296661E+02
pn 11386 -5.38875246E+00 -1.51563036E+00 1.33400696E+02
pn 5436 -5.31477118E+00 -1.71579695E+00 1.33398438E+02
pn 5431 -5.28054285E+00 -1.85999668E+00 1.33393158E+02
pn 5421 -5.16999722E+00 -2.14215946E+00 1.33375168E+02
pn 5430 -5.36399126E+00 -1.86024129E+00 1.32502930E+02
pn 11385 -5.43914938E+00 -1.46137261E+00 1.32512238E+02
c strip 7:
pn 30188 -6.80100441E+00 1.85015953E+00 1.07485380E+01
pn 30183 -6.70357990E+00 1.83323073E+00 1.07855568E+01
pn 30193 -6.89831781E+00 1.87245762E+00 1.07073374E+01
pn 30365 -6.11841726E+00 1.50935042E+00 1.74114475E+01
pn 30364 -6.15953541E+00 1.58282208E+00 1.64522228E+01
pn 30360 -5.97026157E+00 1.51968074E+00 1.74339981E+01
pn 30359 -6.01797247E+00 1.57555366E+00 1.64686413E+01
pn 30360 -5.96340609E+00 1.50731528E+00 1.74328442E+01
pn 30361 -5.91703844E+00 1.37128842E+00 1.83789997E+01
pn 30361 -5.91142082E+00 1.36071110E+00 1.83803844E+01
pn 30360 -5.95974684E+00 1.50173914E+00 1.74273491E+01
pn 30533 -5.91144133E+00 1.06623149E+00 2.01393681E+01
pn 30533 -5.91070080E+00 1.06311452E+00 2.01486282E+01
pn 30533 -5.90710449E+00 1.05565894E+00 2.01419067E+01
pn 30532 -5.91491270E+00 1.19802606E+00 1.92469292E+01
pn 31061 -4.99974108E+00 -7.02153683E-01 3.60490303E+01
pn 31060 -4.91039371E+00 -5.96875489E-01 3.52164650E+01
pn 31061 -5.00075817E+00 -7.09705889E-01 3.60590973E+01
pn 31060 -4.91167116E+00 -6.06331885E-01 3.52328835E+01
pn 31233 -5.04262877E+00 -9.19482827E-01 3.77536201E+01
pn 31232 -5.02530479E+00 -8.18806350E-01 3.69027634E+01
pn 31584 -4.82715464E+00 -2.18394542E+00 4.74519844E+01
pn 31585 -4.84859514E+00 -2.30658102E+00 4.83506126E+01
pn 31584 -4.82884693E+00 -2.19852424E+00 4.74467659E+01
pn 35609 -5.30086136E+00 -1.78308070E+00 1.49530151E+02
pn 35610 -5.27598143E+00 -1.86660385E+00 1.50462891E+02
pn 35611 -5.28244972E+00 -1.98281908E+00 1.51381348E+02
pn 35782 -5.33509779E+00 -2.09934592E+00 1.52273758E+02
pn 35608 -5.32553387E+00 -1.73448026E+00 1.48614670E+02
c strip 8:

pn 4895 -5.93174553E+00 -1.84646773E+00 1.19181053E+02
pn 4896 -5.95380211E+00 -1.88916349E+00 1.20068550E+02
pn 5072 -5.88041830E+00 -1.89353633E+00 1.20960953E+02
pn 34906 -4.46650362E+00 -3.17697811E+00 1.28961441E+02
pn 34905 -4.42144680E+00 -3.11796832E+00 1.28074646E+02
pn 35077 -4.39250040E+00 -3.11427641E+00 1.29852249E+02
pn 5434 -5.44640398E+00 -1.60397375E+00 1.31631668E+02
pn 5435 -5.39637661E+00 -1.69018829E+00 1.32511337E+02
pn 5436 -5.37100506E+00 -1.78445101E+00 1.33401886E+02

c *
pn 29094 -6.20422316E+00 4.35103750E+00 1.49939285E+02
```

```
pn 29095 -6.36266851E+00 4.76928234E+00 1.50894562E+02
pn 29065 -6.67271376E+00 4.57320118E+00 1.50881134E+02
pn 29064 -6.52418327E+00 4.20062780E+00 1.49911942E+02
pn 29059 -6.62172413E+00 4.11583853E+00 1.49855453E+02
pn 29060 -6.76811886E+00 4.47196150E+00 1.50806900E+02
pn 6547 -1.02411909E+01 1.42405331E+00 1.61670822E+02
pn 6577 -9.98056126E+00 1.05241215E+00 1.61470871E+02
pn 6548 -1.06543770E+01 1.82264602E+00 1.62286301E+02
pn 6579 -1.07267809E+01 1.95293081E+00 1.62883804E+02
pn 6549 -1.10104551E+01 2.20319700E+00 1.62950912E+02
pn 6523 -1.11475401E+01 2.32464743E+00 1.62405136E+02
pn 6548 -1.06612558E+01 1.80796599E+00 1.62300385E+02
pn 6547 -1.02867241E+01 1.40962636E+00 1.61666275E+02
pn 6528 -1.14076424E+01 2.53802395E+00 1.62333694E+02
pn 6524 -1.15056572E+01 2.63074303E+00 1.62993286E+02
pn 6579 -1.07486448E+01 1.94622803E+00 1.62880096E+02
pn 6609 -1.05064774E+01 1.66758084E+00 1.62804672E+02
pn 6517 -1.06121492E+01 1.73919547E+00 1.61807678E+02
pn 6518 -1.09514313E+01 2.09467268E+00 1.62379227E+02
pn 29093 -6.08212948E+00 4.00846577E+00 1.48941269E+02
pn 29118 -5.89219809E+00 4.08220243E+00 1.48918030E+02
pn 29119 -6.02361965E+00 4.42746496E+00 1.49904953E+02
pn 29094 -6.24352169E+00 4.36879253E+00 1.49926025E+02
pn 29119 -6.02795124E+00 4.43926096E+00 1.49894226E+02
pn 29144 -5.81181288E+00 4.51738596E+00 1.49855331E+02
pn 29143 -5.69010830E+00 4.17787695E+00 1.48873230E+02
pn 29168 -5.50322580E+00 4.28029823E+00 1.48826630E+02
pn 29169 -5.60439539E+00 4.61881351E+00 1.49794693E+02
pn 29120 -6.16239071E+00 4.86083937E+00 1.50834442E+02
pn 29145 -5.94795561E+00 4.94731569E+00 1.50777481E+02
pn 29144 -5.83240271E+00 4.52320671E+00 1.49850418E+02
pn 40156 -5.24985886E+00 -1.81660068E+00 1.33412704E+02
pn 40156 -5.25703335E+00 -1.78803301E+00 1.33403275E+02
pn 40155 -5.26100349E+00 -1.72861516E+00 1.32519073E+02
pn 5436 -5.36021090E+00 -1.74812460E+00 1.33386063E+02
pn 40181 -5.05788279E+00 -1.84033322E+00 1.33410614E+02
pn 5436 -5.34936571E+00 -1.73005092E+00 1.33376297E+02
pn 5435 -5.39293146E+00 -1.67269742E+00 1.32500534E+02
pn 40277 -5.28111696E+00 -1.54303706E+00 1.34302689E+02
pn 5612 -5.41140747E+00 -1.48155546E+00 1.34287109E+02
pn 6371 -9.98431206E+00 1.00621700E+00 1.60948746E+02
pn 6401 -9.70471478E+00 5.92925727E-01 1.60698502E+02
pn 6577 -1.00064116E+01 1.01684391E+00 1.61461884E+02
pn 6547 -1.03268356E+01 1.41031444E+00 1.61646530E+02
pn 6371 -1.00348072E+01 1.05071950E+00 1.60919373E+02
pn 6341 -1.03149357E+01 1.42666650E+00 1.61174759E+02
pn 6346 -1.04773865E+01 1.71283019E+00 1.61122040E+02
pn 29194 -5.37108517E+00 4.67420244E+00 1.49776169E+02
pn 29189 -5.42768097E+00 4.58548307E+00 1.49717697E+02
pn 29184 -5.48000717E+00 4.49649239E+00 1.49652634E+02
pn 29179 -5.52919722E+00 4.40659428E+00 1.49599533E+02
pn 29174 -5.57896519E+00 4.31926012E+00 1.49533844E+02
pn 29194 -5.37327528E+00 4.67367935E+00 1.49783585E+02
```

```
pn 23464 -5.62305164E+00 4.21822500E+00 1.49516510E+02
pn 23465 -5.77675962E+00 4.54178762E+00 1.50394058E+02
pn 29175 -5.72216415E+00 4.66735458E+00 1.50427841E+02
pn 29180 -5.66777563E+00 4.77749395E+00 1.50486771E+02
pn 29174 -5.57567310E+00 4.31026459E+00 1.49553177E+02
pn 29179 -5.52698183E+00 4.40138245E+00 1.49612595E+02
pn 29184 -5.47585964E+00 4.48776340E+00 1.49669662E+02
pn 29189 -5.42550373E+00 4.58070374E+00 1.49729874E+02
pn 29185 -5.62171698E+00 4.89222050E+00 1.50543549E+02
pn 29175 -5.72229052E+00 4.66578007E+00 1.50437546E+02
pn 29174 -5.57787132E+00 4.30546761E+00 1.49574203E+02
pn 23464 -5.61733961E+00 4.20978689E+00 1.49529709E+02
pn 29179 -5.52307844E+00 4.39684868E+00 1.49620743E+02
pn 29069 -6.42005348E+00 4.28472948E+00 1.49938629E+02
pn 29070 -6.57381058E+00 4.66952753E+00 1.50911880E+02
pn 29095 -6.36823750E+00 4.76751566E+00 1.50915802E+02
pn 29064 -6.51630116E+00 4.20230484E+00 1.49899048E+02
pn 29066 -6.87600183E+00 5.00988436E+00 1.51811935E+02
pn 29065 -6.66989326E+00 4.58651161E+00 1.50858292E+02
pn 29095 -6.36651850E+00 4.78068304E+00 1.50885391E+02
pn 29069 -6.41491175E+00 4.28797865E+00 1.49925262E+02
pn 29094 -6.24552774E+00 4.37426805E+00 1.49924042E+02
pn 29070 -6.57575607E+00 4.67862463E+00 1.50900513E+02
pn 29064 -6.51463938E+00 4.20894098E+00 1.49885422E+02
pn 29069 -6.41199493E+00 4.29387856E+00 1.49910843E+02
pn 29063 -6.39631796E+00 3.86291146E+00 1.48931381E+02
pn 29068 -6.28236246E+00 3.92676806E+00 1.48943817E+02
pn 29069 -6.41517591E+00 4.29745913E+00 1.49918976E+02
pn 29069 -6.41906691E+00 4.30181932E+00 1.49920120E+02
pn 29068 -6.29151726E+00 3.93698287E+00 1.48938080E+02
pn 29068 -6.29334974E+00 3.93931460E+00 1.48951004E+02
pn 29059 -6.621724 4.115839 149.8555
pn 29064 -6.514639 4.238941 149.8854
pn 29060 -6.768119 4.471961 150.8069
pn 29065 -6.669893 4.616512 150.8583
pn 29084 -6.384763 4.186315 149.8196
pn 29109 -6.159154 4.265448 149.7763
pn 29114 -6.072182 4.383181 149.8415
pn 29089 -6.287531 4.301838 149.8849
pn 29085 -6.531889 4.55261 150.7588
pn 29110 -6.306738 4.639801 150.7041
pn 29115 -6.22634 4.780647 150.7762
pn 29090 -6.44418 4.691423 150.8334
pn 29070 -6.59138298E+00 4.68338490E+00 1.50877548E+02
pn 29069 -6.44390535E+00 4.31033897E+00 1.49889679E+02
pn 29095 -6.38750029E+00 4.80567312E+00 1.50873810E+02
pn 29094 -6.26535892E+00 4.39646053E+00 1.49902313E+02
pn 29120 -6.18376684E+00 4.88771963E+00 1.50833237E+02
pn 29119 -6.05710125E+00 4.47362852E+00 1.49877457E+02
pn 29070 -6.60454798E+00 4.69606113E+00 1.50866714E+02
pn 29071 -6.81305742E+00 5.12109900E+00 1.51866913E+02
pn 29096 -6.57121944E+00 5.22291374E+00 1.51811279E+02
pn 29095 -6.39410114E+00 4.81190109E+00 1.50850464E+02
```

```
pn 29120 -6.19269943E+00 4.89707661E+00 1.50810837E+02
pn 29121 -6.35119247E+00 5.31640100E+00 1.51745651E+02
c strip 9:
c no changes
c strip 10:
c no changes
c strip 11:
c no changes, 47500 elems
c strip 12:
c 52250 elems
c strip 13: 57000 elems
pn 65807 -5.85603809E+00 1.06840076E+01 1.61535843E+02
pn 65654 -5.82985735E+00 9.47321415E+00 1.58744278E+02
pn 65504 -5.41370058E+00 7.26993275E+00 1.54683502E+02
pn 65505 -5.49308109E+00 7.80605125E+00 1.55494873E+02
pn 65502 -5.31946468E+00 6.39130592E+00 1.53005127E+02
pn 65356 -5.28699255E+00 5.98074675E+00 1.52151352E+02
pn 65361 -5.19163275E+00 6.05981493E+00 1.52281494E+02
pn 65507 -5.20160818E+00 6.49839783E+00 1.53127014E+02
pn 65532 -4.82414436E+00 6.66836882E+00 1.53148361E+02
pn 65386 -4.81967831E+00 6.21798229E+00 1.52296036E+02
pn 65510 -5.23830128E+00 8.03252697E+00 1.55635239E+02
pn 65509 -5.19945908E+00 7.47931337E+00 1.54843140E+02
pn 65659 -5.61195993E+00 9.69786644E+00 1.59015900E+02
pn 65660 -5.73949051E+00 1.01018457E+01 1.59847778E+02
pn 65807 -5.88138199E+00 1.07361393E+01 1.61526016E+02
pn 65808 -5.93577528E+00 1.11868668E+01 1.62158325E+02
pn 65803 -6.41836739E+00 1.09266043E+01 1.62112442E+02
pn 65386 -4.83635521E+00 6.17726040E+00 1.52273743E+02
pn 65361 -5.18358517E+00 6.09424973E+00 1.52296158E+02
pn 65532 -4.84181643E+00 6.61881161E+00 1.53123291E+02
pn 60861 -6.34454679E+00 7.64282846E+00 1.78953857E+01
pn 61007 -6.33439016E+00 7.51591301E+00 1.89161568E+01
pn 61032 -6.16719770E+00 7.62176943E+00 1.89190865E+01
pn 60886 -6.18307734E+00 7.72951365E+00 1.78872051E+01
pn 61008 -6.32929850E+00 7.36942005E+00 1.99452820E+01
pn 61003 -6.50320053E+00 7.26467991E+00 1.99116993E+01
pn 61007 -6.36112833E+00 7.52633524E+00 1.89348774E+01
pn 60861 -6.35300350E+00 7.64777470E+00 1.79014606E+01
pn 61161 -5.50337315E+00 5.98951387E+00 2.68227615E+01
pn 61307 -5.44632673E+00 5.97942019E+00 2.77360954E+01
pn 61308 -5.39926672E+00 5.98413086E+00 2.86528282E+01
pn 61309 -5.33988047E+00 5.95100355E+00 2.95682793E+01
pn 62358 -5.27847385E+00 2.56093740E+00 5.94463882E+01
pn 62359 -5.19167137E+00 2.49173164E+00 6.03976936E+01
pn 62360 -5.10490513E+00 2.43150258E+00 6.13476944E+01
pn 62361 -5.05806065E+00 2.45244479E+00 6.23068390E+01
pn 63411 -4.92371559E+00 2.20487857E+00 9.34042664E+01
pn 63557 -4.93732548E+00 2.20116973E+00 9.43171158E+01
pn 63558 -4.94652128E+00 2.19478273E+00 9.52305603E+01
pn 63559 -4.95385790E+00 2.19157410E+00 9.61404190E+01
pn 63861 -5.02937078E+00 2.75999522E+00 1.06796303E+02
pn 64007 -4.94500160E+00 2.83390212E+00 1.07689499E+02
```

```
pn 64008 -4.87127590E+00 2.94160151E+00 1.08583710E+02
pn 64911 -4.50457573E+00 4.07915115E+00 1.37950790E+02
pn 65057 -4.48837852E+00 4.11435032E+00 1.38860336E+02
pn 65058 -4.46825600E+00 4.11550379E+00 1.39772675E+02
pn 65059 -4.42257023E+00 4.12578726E+00 1.40675430E+02
pn 65060 -4.40238237E+00 4.14375305E+00 1.41586899E+02
pn 65061 -4.40061522E+00 4.19166899E+00 1.42493073E+02
pn 65207 -4.48591709E+00 4.24372435E+00 1.43381699E+02
pn 65208 -4.59034204E+00 4.30463839E+00 1.44269699E+02
pn 65211 -4.82551908E+00 4.39304924E+00 1.46935226E+02
pn 65357 -4.77320910E+00 4.50379038E+00 1.48053070E+02
pn 65358 -4.81840944E+00 4.75521183E+00 1.49158783E+02
pn 61160 -5.58460760E+00 6.01990223E+00 2.59969044E+01
pn 61161 -5.50387907E+00 6.00920296E+00 2.67918835E+01
pn 61160 -5.58576870E+00 6.03383493E+00 2.59903450E+01
pn 61307 -5.44652700E+00 5.99501753E+00 2.77074871E+01
pn 61308 -5.39924860E+00 6.00323677E+00 2.86128845E+01
pn 61309 -5.33943224E+00 5.96762800E+00 2.95249557E+01
pn 61310 -5.24934769E+00 5.87589121E+00 3.04599285E+01
pn 61311 -5.15815163E+00 5.78445387E+00 3.13648968E+01
pn 61457 -5.09743309E+00 5.70630264E+00 3.23042030E+01
pn 61458 -5.05347109E+00 5.65302563E+00 3.32396469E+01
pn 61459 -5.00471306E+00 5.61832142E+00 3.41401596E+01
pn 61460 -4.94464445E+00 5.52705717E+00 3.50791855E+01
pn 61461 -4.88649750E+00 5.46095181E+00 3.59890862E+01
pn 61607 -4.96239614E+00 5.38270950E+00 3.67993240E+01
pn 61608 -5.04299545E+00 5.33486366E+00 3.76038284E+01
pn 61609 -5.08896542E+00 5.19778872E+00 3.84506874E+01
pn 61609 -5.08807182E+00 5.20801687E+00 3.84110870E+01
pn 65358 -4.82006788E+00 4.78379488E+00 1.49122177E+02
pn 65353 -4.91624498E+00 4.68655920E+00 1.49082535E+02
pn 65349 -5.11536932E+00 5.00132942E+00 1.50021362E+02
pn 65361 -5.14943981E+00 6.10204458E+00 1.52250351E+02
pn 65507 -5.18946695E+00 6.52033329E+00 1.53105743E+02
pn 65356 -5.29490423E+00 6.00045824E+00 1.52155991E+02
pn 65386 -4.83175278E+00 6.21918344E+00 1.52257309E+02
pn 65532 -4.85549164E+00 6.66844797E+00 1.53128189E+02
pn 65411 -4.41436434E+00 6.34453344E+00 1.52317322E+02
pn 65436 -4.05669737E+00 6.51530504E+00 1.52334595E+02
pn 65411 -4.42573690E+00 6.36284351E+00 1.52326660E+02
pn 65582 -4.12591124E+00 6.94553137E+00 1.53149078E+02
pn 65557 -4.46237421E+00 6.80578470E+00 1.53145035E+02
pn 65507 -5.18909979E+00 6.54850054E+00 1.53069061E+02
pn 65508 -5.16616964E+00 6.99408245E+00 1.53961929E+02
pn 65508 -5.16430235E+00 6.98571444E+00 1.53948456E+02
pn 65509 -5.18881750E+00 7.44989204E+00 1.54770096E+02
pn 65510 -5.22565794E+00 7.98883629E+00 1.55558182E+02
pn 65534 -4.85993242E+00 7.57899141E+00 1.54764740E+02
pn 65535 -4.92237234E+00 8.11949825E+00 1.55553406E+02
pn 65533 -4.83336401E+00 7.10941219E+00 1.53942520E+02
pn 65532 -4.85588455E+00 6.67914248E+00 1.53092285E+02
pn 65361 -5.15043402E+00 6.11562729E+00 1.52214493E+02
pn 65360 -5.07214499E+00 5.66811180E+00 1.51203842E+02
```

```
pn 65359 -4.94179440E+00 5.20630407E+00 1.50148804E+02
pn 65655 -5.93767405E+00 9.90287876E+00 1.59521255E+02
pn 65660 -5.70687389E+00 1.00957136E+01 1.59771957E+02
pn 65659 -5.58829069E+00 9.69411469E+00 1.58960541E+02
pn 65654 -5.83702755E+00 9.48898506E+00 1.58758514E+02
pn 65659 -5.56830359E+00 9.67698669E+00 1.58914444E+02
pn 65660 -5.68870544E+00 1.00620995E+01 1.59738815E+02
pn 65660 -5.68074179E+00 1.00593119E+01 1.59717819E+02
pn 65655 -5.94883537E+00 9.90351963E+00 1.59549683E+02
pn 65646 -6.37708426E+00 9.85445976E+00 1.59677078E+02
pn 65645 -6.27146673E+00 9.41976547E+00 1.59010834E+02
pn 65650 -6.09513760E+00 9.67478085E+00 1.59294235E+02
pn 65655 -5.92396593E+00 9.89532375E+00 1.59523224E+02
pn 65651 -6.17964983E+00 1.00327063E+01 1.60050430E+02
pn 65646 -6.40414476E+00 9.84488964E+00 1.59704956E+02
pn 65641 -6.50726128E+00 9.58237076E+00 1.59419189E+02
pn 65646 -6.40231943E+00 9.83456326E+00 1.59708221E+02
pn 65645 -6.29071808E+00 9.44229507E+00 1.59010574E+02
pn 65640 -6.49186659E+00 9.17822552E+00 1.58709778E+02
pn 65661 -5.73431444E+00 1.03641796E+01 1.60732315E+02
pn 65661 -5.72967148E+00 1.04033508E+01 1.60722183E+02
pn 65832 -5.49539709E+00 1.07346783E+01 1.61509293E+02
pn 65857 -5.20495749E+00 1.07733841E+01 1.61494781E+02
pn 65953 -6.90895557E+00 1.18332233E+01 1.66370972E+02
pn 65947 -7.87843752E+00 1.15400257E+01 1.65593018E+02
pn 65953 -6.91119957E+00 1.19128294E+01 1.66375732E+02
pn 65958 -6.08036613E+00 1.20918255E+01 1.66150375E+02
pn 65983 -5.78191566E+00 1.21918201E+01 1.66145340E+02
pn 65982 -5.78833961E+00 1.22711897E+01 1.65315445E+02
pn 65957 -6.08314037E+00 1.21808901E+01 1.65324921E+02
pn 65958 -6.08648109E+00 1.21203146E+01 1.66171234E+02
pn 65954 -6.68733025E+00 1.17504005E+01 1.67204391E+02
pn 65949 -7.35731506E+00 1.15289173E+01 1.67434021E+02
pn 65948 -7.75361729E+00 1.17485504E+01 1.66492340E+02
pn 65959 -6.00567007E+00 1.19519787E+01 1.66947159E+02
pn 65960 -5.97847986E+00 1.15410767E+01 1.67730103E+02
pn 65955 -6.54538918E+00 1.13123064E+01 1.68001358E+02
pn 65956 -6.35892582E+00 1.08600721E+01 1.68631104E+02
pn 65961 -5.91634321E+00 1.11613836E+01 1.68391525E+02
pn 65961 -5.95328045E+00 1.12043381E+01 1.68438522E+02
pn 65986 -5.61812210E+00 1.11745977E+01 1.68425781E+02
pn 65956 -6.34473038E+00 1.09258327E+01 1.68655518E+02
pn 65961 -5.85521269E+00 1.12238770E+01 1.68421661E+02
pn 65986 -5.60623026E+00 1.12049103E+01 1.68435654E+02
pn 65961 -5.81665230E+00 1.12346783E+01 1.68412689E+02
pn 65956 -6.33456469E+00 1.09729004E+01 1.68669006E+02
pn 65951 -6.79117060E+00 1.05253267E+01 1.68960464E+02
pn 65981 -5.93778515E+00 1.08713303E+01 1.68660614E+02
pn 65981 -6.02942753E+00 1.08457136E+01 1.68682541E+02
pn 65354 -5.00537825E+00 5.13719893E+00 1.50077744E+02
pn 65353 -4.90079832E+00 4.72576904E+00 1.49052322E+02
pn 65355 -5.15045023E+00 5.57776070E+00 1.51092621E+02
pn 65356 -5.28780222E+00 6.01852942E+00 1.52140091E+02
```

```
pn 65502 -5.31278610E+00 6.40847540E+00 1.52983200E+02
pn 65356 -5.28252697E+00 6.03196192E+00 1.52127777E+02
pn 65502 -5.30769539E+00 6.42194700E+00 1.52951080E+02
pn 65507 -5.17667150E+00 6.58158684E+00 1.52983582E+02
pn 65361 -5.12830591E+00 6.17246723E+00 1.52144928E+02
pn 65360 -5.04097986E+00 5.74671888E+00 1.51163559E+02
pn 65359 -4.92257404E+00 5.25438213E+00 1.50139633E+02
pn 65508 -5.14888382E+00 7.02567911E+00 1.53885590E+02
pn 65509 -5.17154551E+00 7.49428797E+00 1.54714523E+02
pn 65510 -5.21660900E+00 8.01338005E+00 1.55477829E+02
pn 65511 -5.22186327E+00 8.52400875E+00 1.56379013E+02
pn 65657 -5.33670759E+00 8.97737980E+00 1.57255676E+02
pn 65658 -5.45468044E+00 9.36941624E+00 1.58081909E+02
pn 65659 -5.55442810E+00 9.71304798E+00 1.58854019E+02
pn 65961 -5.82941866E+00 1.12042980E+01 1.68449677E+02
c 3 bad
pn 65958 -6.08205986E+00 1.21302881E+01 1.66202591E+02
pn 65959 -6.00165462E+00 1.19357033E+01 1.66985245E+02
pn 65959 -5.99999046E+00 1.19212332E+01 1.67004105E+02
pn 65358 -4.82209539E+00 4.83537722E+00 1.49087097E+02
c 1 deep bad
pn 65406 -4.448005 6.267649 152.1453
pn 65381 -4.857028 6.133226 152.1482
pn 65552 -4.519014 6.667127 152.9772
pn 65527 -4.908184 6.538698 152.9943
c 2 surface bad
pn 65582 -4.14315605E+00 6.97604036E+00 1.53152451E+02
pn 65557 -4.48037958E+00 6.83779812E+00 1.53148895E+02
pn 65532 -4.87967348E+00 6.71875048E+00 1.53091080E+02
pn 65386 -4.85877848E+00 6.26322889E+00 1.52253677E+02
pn 65411 -4.45633936E+00 6.41679335E+00 1.52331863E+02
pn 65436 -4.08101940E+00 6.56173038E+00 1.52346970E+02
pn 65461 -3.69766855E+00 6.68312788E+00 1.52332260E+02
pn 65607 -3.78002906E+00 7.12025213E+00 1.53113632E+02
c strip 14: 61750 elems
c no changes
c strip 15: 66500 elems
c no changes
c strip 16: 71250 elems
pn 80968 -2.01772332E+00 8.40852320E-01 1.52947372E+02
pn 80969 -1.96953225E+00 9.16356862E-01 1.53891342E+02
pn 80970 -1.84808826E+00 1.19594371E+00 1.54781479E+02
pn 80971 -1.63692617E+00 1.71392679E+00 1.55537476E+02
pn 80976 -1.71191633E+00 1.93573868E+00 1.55667969E+02
pn 80975 -2.14466643E+00 1.46668077E+00 1.54885818E+02
pn 80967 -2.02089381E+00 8.39015424E-01 1.52059158E+02
pn 80969 -1.96468997E+00 9.77856994E-01 1.53878937E+02
pn 80968 -2.00977516E+00 8.99416208E-01 1.52987854E+02
pn 80974 -2.41573024E+00 1.16432238E+00 1.53936340E+02
pn 80973 -2.48238993E+00 1.15783525E+00 1.52950699E+02
pn 80970 -1.84960604E+00 1.26845860E+00 1.54717880E+02
pn 80969 -1.96825147E+00 1.02918375E+00 1.53845245E+02
pn 80974 -2.41753650E+00 1.20231557E+00 1.53906708E+02
```

```
pn 80975 -2.13715792E+00 1.51267862E+00 1.54803482E+02
pn 80980 -2.36400056E+00 1.79968858E+00 1.54951767E+02
pn 80976 -1.70247054E+00 1.90579975E+00 1.55701263E+02
pn 80981 -1.77222872E+00 2.08119607E+00 1.55758667E+02
c strip 17: 76000 es
c 3 bad
pn 81873 -4.21166754E+00 4.16094971E+00 1.37794724E+01
pn 83746 -3.61331391E+00 -1.71613503E+00 8.44714050E+01
pn 83745 -3.72713351E+00 -1.59018207E+00 8.35163651E+01
pn 83868 -3.62946963E+00 -1.66509950E+00 8.62563019E+01
pn 83867 -3.54169273E+00 -1.74436545E+00 8.53643036E+01
pn 83746 -3.52649117E+00 -1.76138675E+00 8.44242935E+01
pn 81872 -3.86378241E+00 4.43062973E+00 1.29665432E+01
pn 81867 -3.75296092E+00 4.36752558E+00 1.30121603E+01
c strip 18: 80750 es
c no changes
c strip 19: 85500 es
c no changes
c strip 20: 90250 es
c no changes
c strip 21: 95000
c no changes
c strip 22 & 23: 100375 es
c no changes
c strips 24 & 25: 112965 es
c no changes
c strips 26 & 27: 111125 es
c no changes.
c whole slice: 132000 es
c no changes
c whole slice: 152875 es
c no problems
c whole slice: 173750 es
c 2 bad ones
pn 181421 -9.61748976E-03 4.21857929E+00 1.18651915E+01
c 1 bad (164000)
pn 181420 2.95749158E-01 4.87705564E+00 1.13366747E+01
pn 181421 -1.44324061E-02 4.22713900E+00 1.18759499E+01
c fixed!
c (164630) *** Can't fix in a reasonable time, delem and move on***
c 4 bad: 187575 187580 187600 187605 ;
c of 187999
pn 179296 4.34317350E+00 1.27792490E+00 1.55656204E+02
pn 207624 4.84424925E+00 1.02334392E+00 1.53983978E+02
pn 207625 4.67315149E+00 1.18761003E+00 1.54873383E+02
pn 207626 4.47262955E+00 1.48070693E+00 1.55735596E+02
pn 207629 5.12294960E+00 1.21197248E+00 1.53999451E+02
pn 207630 4.86348248E+00 1.27306914E+00 1.54902649E+02
c next sliver, 192749 es
c 5 bad: 188415 188416 188420 188440 188445 ;
pn 208578 1.56809068 4.11166716 14.1631069
pn 208588 1.30972385 4.53959227 14.1257057
pn 208583 1.41187906 4.30761719 14.1488695
```

```
pn 208588 1.29915547 4.4410677 14.1261587
pn 208579 2.02702737 3.97450113 14.8982191
pn 208589 1.68017745 4.22419548 14.8554754
pn 208589 1.71314192 4.52401829 14.9969511
pn 208584 1.79521024 4.17581558 14.8848696
pn 208589 1.68236625 4.30565119 14.9149389
pn 208577 1.33812284 3.92563272 13.3802462
pn 208587 1.24051249 4.26833916 13.1912441
pn 208582 1.27054167 4.10262299 13.3047628
pn 208578 1.53578222 4.06006193 14.1767073
pn 208579 1.93869245 3.88063717 14.9473143
pn 208583 1.38670051 4.25945425 14.1574621
pn 208584 1.75778663 4.14337254 14.9075432
pn 208587 1.16015863 4.22952175 13.2553511
pn 208588 1.26315618 4.39473009 14.1475983
pn 208582 1.23031497 4.06190968 13.3478279
pn 208583 1.35849154 4.19272709 14.1793938
pn 208603 1.861785 4.315212 14.33913
c fixed it
C yay!
pn 180745 0.826138556 4.40681219 11.8228617
pn 180746 0.601175845 4.02738619 12.5404196
pn 180740 0.932049453 4.32142925 11.8891268
pn 180741 0.72809279 3.98535395 12.6211119
c success!
c 211749 es
c bad: 207979 208329 211654 ;
pn 234467 8.14817619E+00 -1.81885004E+00 1.70585800E+02
pn 234444 5.97896194E+00 -3.67573905E+00 1.66270493E+02
pn 234414 5.69269323E+00 -3.59774780E+00 1.66270706E+02
pn 234384 5.42417479E+00 -3.51299071E+00 1.66262390E+02
pn 229947 5.82623959E+00 -1.83800447E+00 3.57482681E+01
pn 229952 6.00215483E+00 -1.81657791E+00 3.56866837E+01
pn 229957 6.17887163E+00 -1.74100232E+00 3.56384468E+01
pn 229946 5.78389597E+00 -1.77128017E+00 3.49127083E+01
pn 229951 5.96685314E+00 -1.73159695E+00 3.48436661E+01
pn 230395 5.74225044E+00 -3.12216663E+00 4.72507057E+01
pn 230400 5.88821077E+00 -3.06386971E+00 4.72234306E+01
pn 230401 5.78999567E+00 -3.22336006E+00 4.81242065E+01
pn 230396 5.68381405E+00 -3.27994347E+00 4.81446800E+01
pn 230365 5.49976206E+00 -3.17670250E+00 4.72522354E+01
pn 229917 5.55776215E+00 -1.88020384E+00 3.57453308E+01
pn 229947 5.83312559E+00 -1.86368608E+00 3.57376938E+01
c doing well
c 11 bad: 235624 235899 236524 236549 236574 237674 237699 237724 240149
240174 240249 ;
pn 258497 4.46057367E+00 1.07081909E+01 4.43663025E+00
pn 258496 4.72556496E+00 1.07925777E+01 3.53416657E+00
pn 258747 3.44807100E+00 6.92246008E+00 1.35676107E+01
pn 258868 3.53820181E+00 6.84695530E+00 1.44567728E+01
pn 258869 3.64751053E+00 6.82532358E+00 1.53684225E+01
pn 258868 3.54470944E+00 6.85826492E+00 1.44496908E+01
pn 259372 4.36229181E+00 3.94102716E+00 3.57732964E+01
```

```
pn 259493 4.42591143E+00 3.82712078E+00 3.65972137E+01
pn 259493 4.43827438E+00 3.83764315E+00 3.65887527E+01
pn 259494 4.51758814E+00 3.73718238E+00 3.74266205E+01
pn 259495 4.58126783E+00 3.63844824E+00 3.82136536E+01
pn 259619 4.88932848E+00 3.26372981E+00 4.16478424E+01
pn 259618 4.80610609E+00 3.35450912E+00 4.07549553E+01
pn 259620 4.98963737E+00 3.19370341E+00 4.25647354E+01
pn 259621 5.07216978E+00 3.10874581E+00 4.34655762E+01
pn 263118 5.01491308E+00 9.80001259E+00 1.65109573E+02
pn 262997 5.05750656E+00 9.83519363E+00 1.64198105E+02
pn 263119 5.02268505E+00 9.88979435E+00 1.65966553E+02
pn 263116 5.60411072E+00 1.02526970E+01 1.67909851E+02
pn 263117 5.40462351E+00 1.01994181E+01 1.68861023E+02
pn 263116 5.49922228E+00 1.01747875E+01 1.67937988E+02
pn 263116 5.55578852E+00 1.02181301E+01 1.67914078E+02
pn 263117 5.44203424E+00 1.02286911E+01 1.68841141E+02
pn 263116 5.50768423E+00 1.02183313E+01 1.67902328E+02
c 6 bad: 236499 236599 237674 237699 237724 240249 ;
pn 263122 5.23630905E+00 1.05187225E+01 1.68600708E+02
pn 263097 4.96058893E+00 1.05888100E+01 1.68616577E+02
pn 263122 5.19093227E+00 1.05358829E+01 1.68563049E+02
pn 263122 5.17983913E+00 1.05242825E+01 1.68569443E+02
pn 263122 5.18426514E+00 1.05422497E+01 1.68553680E+02
pn 259372 4.40551233E+00 3.97089767E+00 3.57634697E+01
pn 259371 4.39172649E+00 4.07893562E+00 3.49617462E+01
pn 259367 4.50171375E+00 3.87560368E+00 3.57742653E+01
pn 259366 4.50427341E+00 3.99798870E+00 3.49500885E+01
pn 259496 4.66975355E+00 3.54888201E+00 3.90319672E+01
pn 259495 4.60280848E+00 3.64964128E+00 3.82124023E+01
pn 259618 4.82318974E+00 3.38603234E+00 4.07315788E+01
pn 259619 4.92815781E+00 3.28681207E+00 4.16427193E+01
pn 259497 4.72290087E+00 3.44876337E+00 3.98479271E+01
pn 259613 4.92030048E+00 3.28102231E+00 4.07829132E+01
pn 259614 4.99032593E+00 3.20276999E+00 4.16481857E+01
pn 259593 4.57569599E+00 3.47259021E+00 4.07690125E+01
pn 259594 4.66575718E+00 3.37186170E+00 4.16744995E+01
pn 259595 4.76322222E+00 3.31499839E+00 4.25546761E+01
pn 259615 5.11272192E+00 3.10795355E+00 4.25691376E+01
pn 259620 5.01105213E+00 3.22449207E+00 4.25440636E+01
pn 259616 5.20163536E+00 3.03767633E+00 4.34443169E+01
pn 259621 5.11594963E+00 3.13887691E+00 4.34557457E+01
pn 259596 4.86241865E+00 3.21661472E+00 4.34736061E+01 c 5 bad
pn 259371 4.38698959E+00 4.09595346E+00 3.49635353E+01
pn 259370 4.34874105E+00 4.22513533E+00 3.41460991E+01
pn 259371 4.38345861E+00 4.11559057E+00 3.49653244E+01
pn 259372 4.40526676E+00 3.98690820E+00 3.57645493E+01
pn 260618 5.07965755E+00 2.24935603E+00 7.65489883E+01
pn 260619 5.08834791E+00 2.27199697E+00 7.74408646E+01
pn 260620 5.10303640E+00 2.25486612E+00 7.83359146E+01
pn 260620 5.10028934E+00 2.28859329E+00 7.83329010E+01
pn 260621 5.11618948E+00 2.28174543E+00 7.92284851E+01
pn 260621 5.11520386E+00 2.30042148E+00 7.92267303E+01
pn 260622 5.13384390E+00 2.29140997E+00 8.01228561E+01
```

```
pn 263121 5.14629412E+00 1.03743010E+01 1.67693558E+02
pn 263116 5.49763441E+00 1.02008924E+01 1.67909409E+02
pn 263117 5.50066185E+00 1.02936134E+01 1.68811371E+02
pn 263112 5.69028664E+00 9.95528412E+00 1.69104721E+02
pn 263097 4.96392012E+00 1.06225662E+01 1.68605301E+02
c good
c 2444999 es, 12 bad
pn 264781 7.98414278E+00 -2.09182453E+00 4.81113930E+01
pn 264780 8.05134010E+00 -1.99955130E+00 4.72154121E+01
pn 264785 8.14969254E+00 -1.89947915E+00 4.71979599E+01
pn 264786 8.09768867E+00 -2.02746773E+00 4.80829735E+01
pn 264782 7.90751219E+00 -2.20900321E+00 4.89980202E+01
pn 264787 8.00447083E+00 -2.12226605E+00 4.89849281E+01
pn 264786 8.11213875E+00 -2.03413844E+00 4.80941124E+01
pn 264781 8.01710129E+00 -2.10528493E+00 4.81194496E+01
pn 264776 7.86246443E+00 -2.17762375E+00 4.81326447E+01
pn 268376 1.06131639E+01 2.22450137E-01 1.54731155E+02
pn 268381 1.06401396E+01 4.82290089E-01 1.54729645E+02
pn 268376 1.06346912E+01 2.24966526E-01 1.54728653E+02
pn 268346 1.05370388E+01 3.54952961E-02 1.54575089E+02
pn 268377 1.10901594E+01 3.88609290E-01 1.55572067E+02
pn 268382 1.10819721E+01 6.43526375E-01 1.55586502E+02
pn 268376 1.06335421E+01 2.25693539E-01 1.54724365E+02
pn 268381 1.06617632E+01 4.85088170E-01 1.54725754E+02
pn 268386 1.06470146E+01 7.43508995E-01 1.54727097E+02
pn 268528 1.15584812E+01 4.30416524E-01 1.56577576E+02
pn 268523 1.15508871E+01 1.81022987E-01 1.56593826E+02
pn 268377 1.11168299E+01 3.93351465E-01 1.55560654E+02
pn 268382 1.10925455E+01 6.45953476E-01 1.55579163E+02
pn 268524 1.20106564E+01 -3.51013765E-02 1.57564514E+02
pn 268523 1.15852623E+01 1.88258857E-01 1.56573364E+02
pn 268528 1.15720205E+01 4.33331549E-01 1.56569168E+02
pn 268525 1.24494781E+01 -2.44963586E-01 1.58593307E+02
pn 268529 1.20417624E+01 2.03293040E-01 1.57572601E+02
pn 268530 1.24930553E+01 -1.76008791E-02 1.58580734E+02
pn 268524 1.20450220E+01 -3.22092623E-02 1.57566299E+02
pn 268531 1.29163666E+01 -2.37502649E-01 1.59597824E+02
pn 268526 1.29057875E+01 -4.69948411E-01 1.59634827E+02
pn 268530 1.25180874E+01 -1.32259112E-02 1.58570404E+02
pn 268525 1.25172138E+01 -2.37268895E-01 1.58586624E+02
pn 268676 1.26822872E+01 -1.58910584E+00 1.64168793E+02
pn 268675 1.29847565E+01 -1.49754167E+00 1.63233124E+02
pn 268681 1.29171505E+01 -1.35521603E+00 1.64141998E+02
pn 268682 1.24785805E+01 -1.14829195E+00 1.64956757E+02
pn 268677 1.22228508E+01 -1.51070738E+00 1.65030640E+02
pn 268676 1.27207470E+01 -1.58901775E+00 1.64186920E+02
pn 268681 1.29380655E+01 -1.35374475E+00 1.64144547E+02
pn 268823 1.18350296E+01 -9.73727763E-01 1.65650345E+02
pn 268828 1.20345135E+01 -6.69959843E-01 1.65620575E+02
pn 268824 1.18069820E+01 -7.53981948E-01 1.66597931E+02
pn 268829 1.19604235E+01 -4.64708269E-01 1.66512985E+02
pn 268825 1.16328535E+01 -4.35528100E-01 1.67460876E+02
pn 268830 1.17365952E+01 -1.44847453E-01 1.67367065E+02
```

```
pn 268826 1.14921741E+01 -7.31954351E-02 1.68274658E+02
pn 268827 1.13953066E+01 2.90854335E-01 1.69167236E+02
pn 268826 1.15211506E+01 -6.71316162E-02 1.68263458E+02
pn 268832 1.14200449E+01 5.14677644E-01 1.69109467E+02
pn 268796 1.12293797E+01 -5.95494688E-01 1.68738281E+02
c 5 bad: 241579 241604 241629 244579 244604 ;
pn 264776 7.88003159E+00 -2.21698332E+00 4.81332588E+01
pn 264775 7.93546581E+00 -2.13404942E+00 4.72258873E+01
pn 264776 7.88469267E+00 -2.24285603E+00 4.81325493E+01
pn 264774 7.97505283E+00 -2.00943470E+00 4.63340721E+01
pn 264777 7.78602982E+00 -2.29780221E+00 4.90022354E+01
pn 264777 7.80833435E+00 -2.32982326E+00 4.90041542E+01
pn 264776 7.87727070E+00 -2.26106954E+00 4.81305046E+01
pn 264923 7.78760672E+00 -2.35625362E+00 4.99007721E+01
pn 264923 7.76035309E+00 -2.41062164E+00 4.98938599E+01
pn 264893 7.47019005E+00 -2.57235098E+00 4.98765793E+01
pn 264928 7.88220024E+00 -2.25746036E+00 4.98877296E+01
pn 264781 7.99095345E+00 -2.12130976E+00 4.81145897E+01
pn 264782 7.91587543E+00 -2.19954896E+00 4.89997902E+01
pn 268375 1.03757763E+01 4.31796201E-02 1.53845230E+02
pn 268376 1.07581558E+01 2.17384845E-01 1.54742874E+02
pn 268381 1.06993732E+01 4.96803194E-01 1.54731033E+02
pn 268380 1.02873917E+01 3.15136105E-01 1.53822205E+02
c fixed.
c 254499 es, no changes
c 259249 es, tg says 6 bad
pn 283035 1.08731213E+01 3.87101698E+00 1.63129837E+02
pn 283040 1.07804604E+01 4.01717138E+00 1.63243668E+02
pn 283045 1.07094278E+01 4.19778490E+00 1.63345352E+02
pn 283050 1.06005306E+01 4.36576271E+00 1.63451950E+02
pn 283052 1.07908392E+01 4.80048466E+00 1.65442596E+02
pn 283027 1.04088478E+01 4.95401621E+00 1.65290817E+02
pn 283047 1.09077444E+01 4.60574389E+00 1.65289505E+02
pn 283174 1.09628353E+01 5.37686491E+00 1.67007156E+02
pn 283175 1.11024046E+01 5.83065128E+00 1.67717224E+02
pn 283032 1.09526491E+01 4.24341822E+00 1.64687607E+02
pn 283052 1.08760767E+01 4.72936773E+00 1.65458420E+02
pn 283173 1.08680153E+01 4.98340750E+00 1.66240356E+02
pn 283174 1.10437117E+01 5.38084793E+00 1.66976120E+02
pn 283176 1.12828226E+01 6.21532631E+00 1.68444107E+02
pn 283175 1.11857224E+01 5.83045387E+00 1.67687836E+02
pn 283176 1.13362656E+01 6.24488354E+00 1.68407364E+02
pn 283051 1.07709475E+01 4.50586987E+00 1.64488861E+02
pn 283052 1.09381533E+01 4.71301508E+00 1.65440155E+02
pn 283173 1.09727097E+01 4.96856260E+00 1.66189728E+02
pn 283174 1.11420889E+01 5.34984493E+00 1.66937637E+02
pn 283175 1.12705555E+01 5.78877735E+00 1.67662613E+02
pn 283168 1.09935818E+01 4.85548210E+00 1.66097275E+02
pn 283169 1.10631533E+01 5.20959520E+00 1.66848053E+02
pn 278398 1.11148739E+01 4.40846157E+00 1.65448486E+02
pn 278277 1.09722872E+01 4.11566973E+00 1.64510406E+02
pn 278398 1.11072140E+01 4.34507322E+00 1.65474747E+02
pn 283153 1.11251907E+01 4.54227924E+00 1.65591599E+02
```

```
pn 283153 1.11108818E+01 4.51135635E+00 1.65609940E+02
pn 283037 1.09578791E+01 4.35625505E+00 1.64895569E+02
pn 283032 1.09816399E+01 4.27775002E+00 1.64670700E+02
pn 283042 1.09655771E+01 4.49660587E+00 1.65089569E+02
pn 283037 1.09642487E+01 4.37311268E+00 1.64887039E+02
pn 283158 1.11054850E+01 4.66455173E+00 1.65784531E+02
pn 283168 1.10012608E+01 4.88579369E+00 1.66080139E+02
pn 283047 1.09342508E+01 4.61648989E+00 1.65276306E+02
pn 278277 1.10026808E+01 4.11219215E+00 1.64503021E+02
pn 278398 1.11339703E+01 4.37053633E+00 1.65454285E+02
c ansys says 5 bad: 259079 259089 259094 259119 259173 ;
pn 278398 1.11339703E+01 4.37053633E+00 1.65454285E+02
pn 283148 1.03032579E+01 5.23280334E+00 1.66062958E+02
pn 283149 1.03969212E+01 5.59598207E+00 1.66819916E+02
pn 283052 1.09294024E+01 4.78154325E+00 1.65413116E+02
pn 283047 1.09609585E+01 4.65380669E+00 1.65253784E+02
pn 283046 1.08478718E+01 4.43042564E+00 1.64380264E+02
pn 283042 1.09760265E+01 4.52598667E+00 1.65074463E+02
pn 283037 1.09765053E+01 4.38960552E+00 1.64876984E+02
pn 283036 1.09321423E+01 4.16187859E+00 1.63911713E+02
pn 283040 1.07993908E+01 4.06156397E+00 1.63220062E+02
pn 283046 1.08570757E+01 4.48161554E+00 1.64356171E+02
pn 283045 1.07115726E+01 4.22361946E+00 1.63333817E+02
pn 283041 1.09665537E+01 4.37608576E+00 1.64283707E+02
pn 283051 1.07801237E+01 4.56308365E+00 1.64462219E+02
pn 283035 1.08817692E+01 3.91866970E+00 1.63107391E+02
pn 283052 1.09138231E+01 4.81434488E+00 1.65405426E+02
pn 283047 1.09606266E+01 4.69201422E+00 1.65241364E+02
pn 283042 1.09753056E+01 4.54440498E+00 1.65068573E+02
pn 283037 1.09845610E+01 4.40969992E+00 1.64868835E+02
pn 283040 1.07962465E+01 4.10127354E+00 1.63207687E+02
pn 283035 1.08690147E+01 3.98962712E+00 1.63086685E+02
pn 283036 1.09533834E+01 4.18626022E+00 1.63899597E+02
pn 283030 1.09298124E+01 3.83252096E+00 1.62981628E+02
pn 283030 1.09445477E+01 3.85759878E+00 1.62970566E+02
pn 278276 1.10038109E+01 3.92990947E+00 1.63676224E+02
pn 278275 1.10336609E+01 3.72713780E+00 1.62864349E+02
pn 283031 1.09833593E+01 4.05455494E+00 1.63768921E+02
pn 278276 1.10264015E+01 3.94263983E+00 1.63669724E+02
c 1 bad
pn 283173 1.09797134E+01 5.03186655E+00 1.66151428E+02
pn 283174 1.11176853E+01 5.39111853E+00 1.66921738E+02
c fixed;
c 263999 es, tg says 6 bad
pn 284565 7.03445530E+00 1.84747922E+00 4.70917206E+01
pn 284564 7.03461599E+00 1.86294794E+00 4.62011719E+01
pn 284566 7.06189442E+00 1.75421989E+00 4.79997864E+01
pn 284561 7.23933077E+00 1.60484064E+00 4.80210571E+01
pn 284570 6.86600161E+00 1.90088522E+00 4.71002655E+01
pn 287826 1.01079798E+01 5.54557800E+00 1.64533478E+02
pn 287827 1.03220682E+01 5.85849857E+00 1.65502640E+02
pn 287825 1.00604610E+01 5.26791811E+00 1.63548630E+02
pn 287824 1.00512199E+01 5.17142296E+00 1.62530014E+02
```

```
pn 287826 1.02088366E+01 5.52959633E+00 1.64512512E+02
pn 287821 1.02918520E+01 5.25464487E+00 1.64551346E+02
pn 287820 1.01412926E+01 5.02543926E+00 1.63573029E+02
pn 287815 1.02371397E+01 4.82964087E+00 1.63563675E+02
pn 287810 1.03493814E+01 4.69342804E+00 1.63522232E+02
pn 287805 1.04298782E+01 4.55699635E+00 1.63489853E+02
pn 287806 1.06582012E+01 4.73188972E+00 1.64472702E+02
pn 287811 1.05071030E+01 4.89288998E+00 1.64511200E+02
pn 287816 1.04140816E+01 5.06179428E+00 1.64531357E+02
pn 287822 1.04975796E+01 5.56109715E+00 1.65527985E+02
pn 283050 1.05958624E+01 4.42193890E+00 1.63427307E+02
pn 283052 1.09382162E+01 4.85136890E+00 1.65381470E+02
pn 287807 1.08686857E+01 4.97525787E+00 1.65479355E+02
pn 287805 1.04589758E+01 4.58063936E+00 1.63464523E+02
pn 287929 1.09293833E+01 5.63636732E+00 1.66970230E+02
pn 287928 1.07582283E+01 5.18841457E+00 1.66242920E+02
pn 287933 1.06543741E+01 5.38320351E+00 1.66264328E+02
pn 287938 1.05284948E+01 5.60562563E+00 1.66280502E+02
pn 287948 1.02928286E+01 6.05355120E+00 1.66298523E+02
pn 287943 1.04209652E+01 5.81970263E+00 1.66292953E+02
pn 287928 1.07741737E+01 5.22841263E+00 1.66211090E+02
pn 287929 1.09398336E+01 5.65333223E+00 1.66955338E+02
pn 287943 1.04326696E+01 5.85269117E+00 1.66267258E+02
pn 287938 1.05485048E+01 5.62823725E+00 1.66258331E+02
pn 287933 1.06629591E+01 5.40572405E+00 1.66246552E+02
pn 283168 1.10132418E+01 4.91901731E+00 1.66054184E+02
pn 284569 6.87239170E+00 1.97602248E+00 4.61938057E+01
pn 284574 6.68877125E+00 2.09482789E+00 4.61798706E+01
pn 284575 6.69044304E+00 2.05298948E+00 4.70780029E+01
pn 284576 6.72203302E+00 2.03260922E+00 4.79808617E+01
pn 284577 6.72911453E+00 1.96414375E+00 4.88820992E+01
c tg's happy
c ansys says 19 bad:259349 259374 259399 259424 259474 259499 259524
260569
c 260594 261249 261274 263699 263724 263749 263774 263814
c 263819 263834 263839 ;
pn 283326 7.29489470E+00 8.33739662E+00 3.42806339E+00
pn 283325 7.14607191E+00 8.23816586E+00 2.54379129E+00
pn 283296 7.13390827E+00 8.66103840E+00 3.47561669E+00
pn 283295 6.96524191E+00 8.58550358E+00 2.58403826E+00
pn 283326 7.31971550E+00 8.34427547E+00 3.44163227E+00
pn 283326 7.36176491E+00 8.37279129E+00 3.46939588E+00
pn 283325 7.17582130E+00 8.32090664E+00 2.56545186E+00
pn 283296 7.09787798E+00 8.63231182E+00 3.45169067E+00
pn 283295 6.95000076E+00 8.54397964E+00 2.57297063E+00
pn 283327 7.31743813E+00 8.33582783E+00 4.32631588E+00
pn 283448 6.91460037E+00 8.12918091E+00 5.29740047E+00
pn 283449 6.33309221E+00 7.74053907E+00 6.12435532E+00
pn 283450 5.90468597E+00 7.51684713E+00 7.08281183E+00
pn 283451 5.48772955E+00 7.26649714E+00 8.04296207E+00
pn 283452 5.11393547E+00 7.08615637E+00 9.00912952E+00
pn 283573 5.06238127E+00 6.80864096E+00 9.89680004E+00
pn 283574 5.02929926E+00 6.55300045E+00 1.07887039E+01
```

```
pn 284570 6.88388538E+00 1.94069564E+00 4.71427994E+01
pn 284565 7.05506849E+00 1.84459913E+00 4.71318855E+01
pn 284566 7.08069372E+00 1.78694487E+00 4.80324745E+01
pn 284565 7.06776857E+00 1.87383294E+00 4.71550751E+01
pn 285202 6.68814278E+00 1.50044513E+00 7.11901093E+01
pn 285201 6.67642069E+00 1.50194860E+00 7.03020554E+01
pn 285323 6.68767881E+00 1.51371229E+00 7.20776138E+01
pn 285324 6.70042753E+00 1.51183736E+00 7.29813232E+01
pn 287699 9.60774899E+00 5.77104712E+00 1.57781906E+02
pn 287700 9.86539745E+00 5.57410240E+00 1.58720383E+02
pn 287701 1.02027264E+01 5.36416578E+00 1.59665466E+02
pn 287702 1.04872580E+01 5.20130730E+00 1.60593765E+02
pn 287823 1.03910484E+01 5.23454332E+00 1.61624939E+02
pn 287823 1.04162369E+01 5.24474812E+00 1.61640427E+02
pn 287809 1.03679256E+01 4.69503450E+00 1.62525787E+02
pn 287814 1.02592678E+01 4.81838942E+00 1.62548660E+02
pn 287815 1.02658720E+01 4.85051250E+00 1.63582321E+02
pn 287810 1.03653526E+01 4.70242643E+00 1.63532333E+02
pn 287814 1.02807226E+01 4.83351660E+00 1.62559982E+02
pn 287804 1.04845181E+01 4.56474733E+00 1.62503143E+02
pn 287809 1.03804998E+01 4.70292330E+00 1.62532333E+02
pn 287815 1.02841387E+01 4.88432455E+00 1.63592285E+02
pn 287820 1.01606045E+01 5.04289770E+00 1.63581482E+02
pn 287805 1.04826593E+01 4.59857655E+00 1.63471237E+02
pn 287810 1.03900175E+01 4.72692251E+00 1.63539825E+02
pn 287811 1.05482235E+01 4.89097500E+00 1.64519989E+02
pn 287816 1.04357376E+01 5.06746578E+00 1.64536575E+02
pn 287810 1.03867483E+01 4.76460552E+00 1.63531067E+02
pn 287815 1.02752428E+01 4.91075611E+00 1.63589737E+02
pn 287816 1.04440603E+01 5.09807253E+00 1.64523529E+02
pn 287811 1.05650091E+01 4.93427467E+00 1.64498795E+02
pn 287820 1.01988411E+01 5.06682062E+00 1.63554108E+02
pn 287819 1.01527920E+01 4.97387314E+00 1.62543182E+02
pn 287815 1.02919626E+01 4.91612959E+00 1.63579224E+02
c 6 bad now: 260594 260619 263794 263819 263844 263869 ;
pn 284570 6.91054964E+00 1.96024692E+00 4.71202164E+01
pn 284571 6.94494200E+00 1.89094234E+00 4.79944496E+01
pn 284571 6.93512678E+00 1.88273776E+00 4.80095329E+01
pn 284572 6.94116211E+00 1.81854022E+00 4.88956985E+01
pn 284567 7.11421633E+00 1.70279419E+00 4.89116364E+01
pn 284566 7.08092833E+00 1.78880739E+00 4.80209999E+01
pn 284572 6.94914913E+00 1.83150744E+00 4.88911400E+01
pn 284571 6.93211794E+00 1.90845358E+00 4.79897270E+01
pn 287819 1.01946220E+01 4.98512125E+00 1.62540375E+02
pn 287814 1.03209867E+01 4.84706259E+00 1.62555328E+02
pn 287809 1.04053926E+01 4.71174669E+00 1.62529175E+02
pn 287818 1.04738083E+01 5.09617424E+00 1.61602081E+02
pn 287824 1.00982428E+01 5.17199659E+00 1.62535507E+02
pn 287824 1.01395502E+01 5.17715931E+00 1.62537003E+02
pn 287819 1.02121811E+01 4.99880505E+00 1.62532822E+02
pn 287819 1.02303534E+01 5.00972509E+00 1.62527313E+02
pn 287814 1.03391581E+01 4.85467482E+00 1.62552139E+02
pn 287815 1.03152828E+01 4.91977406E+00 1.63578873E+02
```

```
pn 287819 1.02397614E+01 5.01651335E+00 1.62523376E+02
pn 287820 1.02108421E+01 5.06926584E+00 1.63553558E+02
pn 287821 1.03460417E+01 5.28409815E+00 1.64522720E+02
pn 287816 1.04605255E+01 5.11543608E+00 1.64508224E+02
pn 287817 1.06243610E+01 5.33676815E+00 1.65522659E+02
c 263849 bad
pn 287825 1.01030588E+01 5.26373577E+00 1.63547821E+02
pn 287820 1.02310753E+01 5.06765461E+00 1.63552933E+02
pn 287821 1.03627949E+01 5.28863811E+00 1.64517563E+02


c -----------------------
delem lb 164630;

measure jacobian
info
write
```